Small Structures

small structures

www.small-structures.com

REVIEW OPEN ACCESS

Ions as Architects of DNA Nanostructures: Mechanisms, Simulations, and Technological Frontiers

Sergiy Perepelytsya[1,2] | Dmytro Piatnytskyi[1] | Tetiana Bubon[1,3] | Narcis Cibotariu[4] | Aatto Laaksonen[4,5,6,7] | Francesca Mocci[8]

[1]Bogolyubov Institute for Theoretical Physics of the National Academy of Sciences of Ukraine, Kyiv, Ukraine | [2]Kyiv Academic University, Kyiv, Ukraine | [3]Molecular Biology and Nanotechnology Laboratory (MolBNL@UniTS), DEA, University of Trieste, Trieste, Italy | [4]Centre of Advanced Research in Bionanoconjugates and Biopolymers, "Petru Poni" Institute of Macromolecular Chemistry of Romanian Academy, Iasi, Romania | [5]Department of Chemistry, Division of Physical Chemistry, Arrhenius Laboratory, Stockholm University, Stockholm, Sweden | [6]State Key Laboratory of Materials-Oriented and Chemical Engineering, Nanjing Tech University, Nanjing, P. R. China | [7]Department of Engineering Sciences and Mathematics, Division of Energy Science, Luleå University of Technology, Luleå, Sweden | [8]Department of Chemical and Geological Sciences, University of Cagliari, Cagliari, Italy

Correspondence: Sergiy Perepelytsya (perepelytsya@bitp.kyiv.ua) | Aatto Laaksonen (aatto.laaksonen@su.se) | Francesca Mocci (fmocci@unica.it)

Received: 31 October 2025 | **Revised:** 19 January 2026 | **Accepted:** 26 January 2026

Keywords: DNA nanostructure | DNAzymes | metallized DNA | multiscale modeling | nanopores

ABSTRACT

DNA, the most iconic molecular architecture, is not only the carrier of genetic information but also a programmable, biocompatible scaffold for nanoscale design. Its structural and physicochemical versatility makes it uniquely suited for self-assembly, biomedical applications, and the development of dynamic devices and advanced materials. A key determinant of DNA behavior across organizational levels is its interaction with ions, which governs hydration, stability, and compaction from the molecular to the supramolecular scale. Beyond their biological roles, ion-DNA interactions underpin a variety of technologies: in nanostructure assembly, cations stabilize DNA origami and multihelix constructs; in biosensing, ions enable aptamer folding, DNAzyme catalysis, and metal-mediated base pairing; in nanomedicine, polyvalent cations drive DNA condensation into polyplexes for gene delivery and stabilize nanorobots for logic-gated release; and in nanoelectronics and molecular computing, ions enhance DNA conductivity and act as molecular inputs in ion-responsive logic gates. Ion-induced condensation, a form of nanoscale confinement driven by electrostatics, remains a central phenomenon, linking biological function to material design. This review emphasizes the technological potential of ion-driven DNA nanomechanics, integrating experimental evidence with multiscale modeling, and highlights the emerging predictive role of computational tools in guiding the design of next-generation DNA-based nanomaterials.

1 | Introduction

More than 70 years after its discovery [1–4], the DNA double helix remains an emblematic molecular architecture, bridging biology and nanoscience. While the central biological role of DNA in encoding and transmitting genetic information is well established, DNA is increasingly recognized as a structurally and functionally designable bionanoscale material. Its unique physicochemical features support programmability and largely predictable self-assembly [5–7], enable biomedical applications [8, 9], drive the design of dynamic nanodevices [10, 11], and inspire innovative material applications [12–14].

At different organizational levels, from electronic and atomic to nano and mesoscale, DNA exhibits distinct structural and dynamic characteristics. These can range from local base-stacking and ion hydration effects [15–17] to persistence length and large-scale compaction [18, 19], offering a multiscale platform

for applications in nanotechnology, materials design, and bioelectronics. Importantly, while each level presents features exploitable for different applications, confinement effects are particularly intricate at the nanoscale, where both structural and electrostatic properties of DNA govern its response to ions and hydration environments [20–25]. Confinement can arise in a variety of environments: nanopores [26], surface-supported assemblies [27], DNA origami constructs [28], and, most prominently, ion-induced condensation [29]. Beyond condensation, ion–DNA interactions are architects of a wide spectrum of nanotechnological applications. The range of DNA-based applications enabled by ion–DNA interactions, and the underlying multiscale mechanisms that support them, is summarized schematically in Figure 1.

In structure-based DNA nanotechnology, DNA origami folding and stability rely on cation-mediated screening of backbone repulsion. Mg^{2+} is the canonical stabilizing cation, although in some cases, high Na^{+} concentrations can substitute it to enable magnesium-free conditions [30, 31]. A careful design of the ionic environment is thus a prerequisite for reliable assembly and long-term stability of DNA nanostructures, intended for biomedical or nanofabrication applications.

In biosensing, nucleic acid aptamers and DNAzymes require specific ions for folding or catalytic activity. For instance, G-quadruplex aptamers fold only in the presence of K^{+} or Na^{+}, while metal-mediated base pairs such as C–Ag–C or T–Hg–T enable selective ion sensing [32, 33]. These examples demonstrate how ions stabilize nucleic acid structures while acting as conditional structural and recognition elements in functional devices.

In nanomedicine, polyvalent cations and polycations (spermidine^{3+}, spermine^{4+}) compact DNA and RNA into polyplexes, protecting them from degradation and facilitating cellular uptake [34, 35]. Similarly, ion-stabilized DNA nanostructures have been engineered as nanorobots for logic-gated cargo delivery, where structural integrity is maintained until triggered release [31]. Ion-induced compaction is therefore central to gene delivery systems as well as to the emerging field of logic-gated DNA nanodevices.

In nanoelectronics and molecular computing, ions modulate DNA conductivity and act as molecular inputs. The complexes of metal ions with DNA have established a new field of research related to metallized DNA ("M-DNA"), where the ions impart new electronic properties to the system [36]. Ni^{2+}-bound DNA enhances charge transport that can be used in energy devices [37], while Gd^{3+}, Ag^{+}, or Hg^{2+} can switch DNA conformations and thereby serve as logical inputs in strand-displacement circuits [32]. Together, these examples highlight that ions are not merely species for electrostatic screening but active enablers of structural stability, recognition, catalysis, and signal transduction in DNA-based nanotechnology.

Ion-mediated DNA condensation is a phenomenon due to nanoscale confinement driven by complex electrostatics. Counterions screen the strong negative charge of the DNA backbone and concurrently modulate hydration and interhelical interactions [22, 38–42], thereby directing the transition from extended to compact states. These processes are essential for genome packaging in vivo [43] and serve as design principles for DNA-based nanostructures in vitro [17, 44].

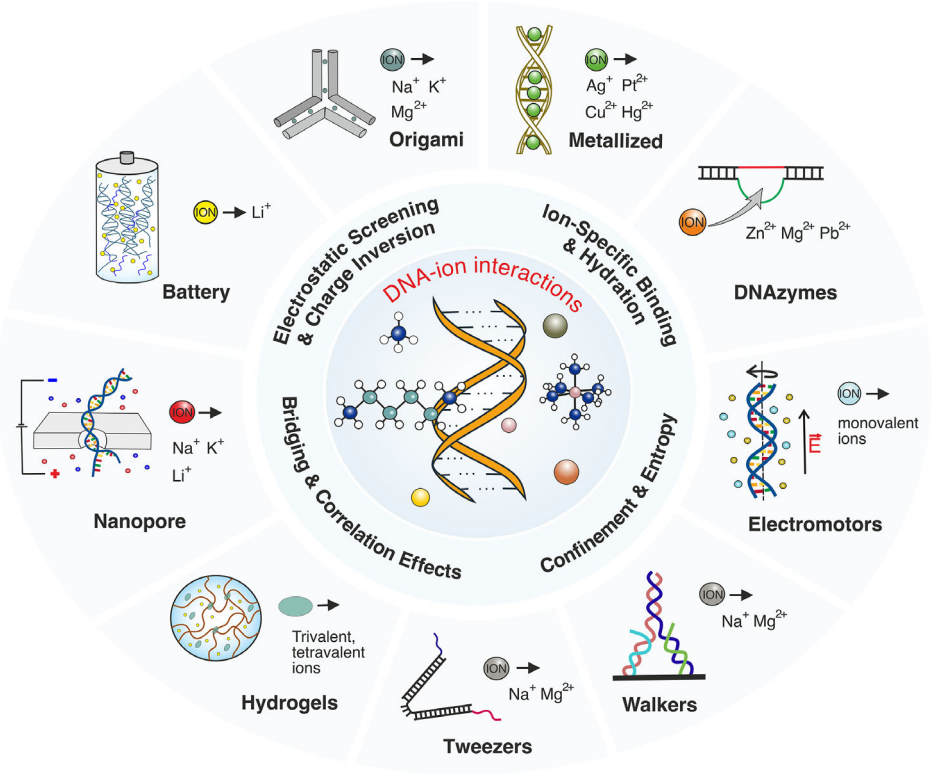

FIGURE 1 | Schematic overview of ion-DNA interactions across length scales. Ions modulate DNA structure from local hydration and groove binding to large-scale condensation and nanostructure assembly, enabling applications ranging from DNA origami and metallized nanowires to biosensing and nanomedicine.

A very recent review [45] has summarized the biological aspects of ion-driven DNA condensation, combining experimental evidence and computational models and showing how ion specificity, pH and dielectric effects, and charge inversion govern processes from chromatin folding to viral genome packaging. While ion-induced DNA condensation has long been studied for its biological implications, here we emphasize its role as a controllable confinement mechanism with direct technological relevance. By examining both theoretical and computational studies across scales, from atomistic to coarse-grained models, and selected experimental studies, we show how ions act as active determinants of structural organization beyond simple DNA charge neutralization. These insights are crucial for translating DNA condensation principles into nanoscale applications, including conductive nanowires, energy-storage devices, nanopores, and programmable DNA-based carriers.

Recent reviews have addressed the physics of DNA self-assembly, with Cumberworth and Reinhardt [5] providing an in-depth analysis of origami, bricks, and related nanostructures. Their emphasis is on cooperativity, nucleation barriers, and free-energy landscapes obtained from simulations, but ionic effects and the role of counterions are not explicitly addressed. In our current review, we intend to show that the ionic environment is not merely a background medium but a central regulator of DNA behavior under confinement and during its condensation in technological applications. We will focus on ion-driven DNA condensation as a model confined molecular system, highlighting the structural principles and simulation strategies that enable nanoscale design. By integrating results from experimental studies with multiscale modeling studies [23, 46, 47], we aim to bridge fundamental understanding with technological prospects and position DNA–ion systems as versatile building blocks for future bio-nanomaterials [36, 48]. We emphasize the essential role of computational tools, from atomistic molecular dynamics to coarse-grained and continuum models, in revealing and designing ion-mediated confinement. Looking ahead, these tools are expected to have a transformative role in viewing ions as active regulators of DNA behavior and to guide the creation of next-generation DNA-based nanomaterials.

2 | The Structure and Dynamics of the DNA Double Helix Hydration Shell

The DNA double helix consists of two antiparallel strands stabilized by base stacking and hydrogen bonding. Its surface is not uniform: two grooves of different widths and atomic composition are separated by the sugar–phosphate backbone, which carries the negative charges (Figure 2a). In the nucleus, the backbone negative charges are neutralized by counterions, which can be metal ions (e.g., Mg^{2+}, K^{+}, and Na^{+}) or molecular ions such as polyamines (e.g., putrescine^{2+}, spermidine^{3+}, and spermine^{4+}). These electrostatic and topological features make DNA an ion-responsive nanostructure rather than a passive biopolymer.

The anionic backbone attracts positively charged ions along with water molecules, forming a structured solvating ionic atmosphere that is an integral part of the double helix [15, 16, 49–52] and being crucial for stabilizing the DNA double helix, as demonstrated in pioneering studies [1–4]. Changes in the hydration state can induce conformational transitions in the DNA double helix [53]. The canonical *B*-DNA form is stabilized by approximately 40 water molecules per base pair, whereas under reduced hydration, the shorter *A*-DNA form is favored [52, 54, 55]. Besides relative humidity, the *B*–*A* transition depends on the nucleotide sequence [55, 56], type [54, 57, 58] and concentration of the salts [59, 60]. Experimental studies [54, 61] have further shown that larger ionic radii generally correlate with reduced hydration requirements for the stabilization of the double helix.

As solvation affects DNA structure, so DNA in turn affects the organization of the surrounding solvent. Using dielectric spectroscopy and molecular dynamics (MD) simulations, Singh et al. [62] showed that DNA influences the orientational dynamics of water

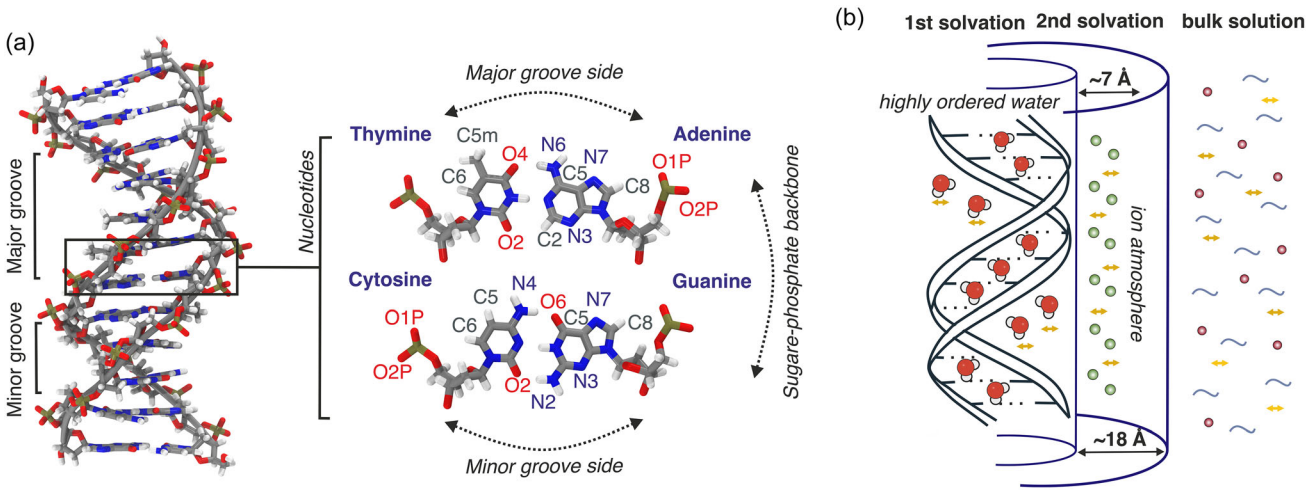

FIGURE 2 | (a) DNA double helix fragment with major and minor grooves indicated. The zoomed-in view highlights adenine–thymine and guanine–cytosine base pairs. Selected atoms are labeled to indicate preferential ion-binding sites, including phosphate oxygens and base heteroatoms. Atoms are color-coded as follows: carbon (gray), nitrogen (blue), oxygen (red), phosphorus (orange), and hydrogen (white). (b) Schematic representation of the DNA hydration shell based on computational and experimental data. Highly ordered water molecules (red) occupy the first solvation layer, while ions (green) form an ion atmosphere around the double helix, approximately 7 Å thick. The ordered water structure extends up to 18 Å from the DNA surface. Yellow arrows indicate the dynamical behavior of the solvation shell.

up to ≈18 Å from its surface. Water and ions form a hydration shell around DNA that comprises multiple layers, distinguishable by the spatial distributions and residence times of water molecules and ions around the double helix (see Figure 2b). The outermost layer exhibits bulk-like behavior [62, 63]. Closer to the DNA, the second solvation layer is formed by loosely bound water molecules that do not directly interact with the macromolecular surface but still exhibit structural order and slowed dynamics due to long-range electrostatic interactions induced by DNA [62, 64]. Within this region, ion accumulation is also observed as a ∼7 Å thick shell surrounding the double helix. Ion accumulation was predicted theoretically in early studies [65, 66] and later confirmed experimentally using small-angle X-ray scattering [67–69], buffer equilibration with atomic emission spectroscopy [70], as well as MD simulations [71, 72].

The innermost, first solvation layer consists of water molecules and ions directly interacting with the DNA surface (i.e., with the oxygen or nitrogen atoms of phosphate groups and nucleobases), which exhibit structural and dynamical properties that differ markedly from those of bulk solution. The particular structural pattern of ions [73, 74] and water molecules [49, 75–77] is influenced by the nucleotide sequence, while groove width also plays a role [78]. X-ray [79, 80], NMR [81–83], chiral nonlinear spectroscopy [84], Monte Carlo [85], and MD studies [73, 75, 77, 78] have shown that in the minor groove water molecules can bridge bases on opposite strands, forming an ordered "spine of hydration"—a dynamic, chiral structure induced by the confined groove. Recent work combining chiral vibrational spectroscopy and MD simulations [64] further demonstrates that water ordering also occurs in the major groove and around the phosphate groups.

Near the DNA surface, water dynamics slow down nearly fivefold compared to bulk [86, 87].The slowest molecules can be found in the most confined regions [77], where water can reside for over 200 ps [81, 88–90]. Water reorientation and hydrogen-bond rearrangements occur on picosecond timescales, extending up to ∼100 ps in confined regions, especially in the minor groove [91–93].

Similarly to water molecules, counterions associate with phosphate oxygens and the nitrogen or oxygen atoms of the bases, with preferential binding at the N7 site in the major groove [16, 94–96] (see Figure 2a). Certain cations, such as Cs^+ [97], Rb^+ [80], and Na^+ [74], can also occupy the hydration spine of the minor groove without disturbing its structure. MD simulations further revealed that the distributions and binding patterns of mono- and divalent counterions differ markedly between DNA and RNA [98].

The hydration behavior of counterions governs their interaction with DNA and their effect on water structure. They are classified as kosmotropes or chaotropes depending on their ability to structure water [99–101]. Kosmotropes (Na^+, Li^+, Ca^{2+}, and Mg^{2+}) bind water strongly and stabilize the hydrogen-bond network, whereas chaotropes (K^+, Rb^+, Cs^+, and NH_4^+) weaken it. MD studies show longer water residence times around kosmotropes [102], influenced by ion position near DNA [103]. Thus, kosmotropes interact mainly through their hydration shells, while weakly hydrated chaotropes can penetrate DNA grooves [25, 103, 104]. Both MD simulations [15, 25, 104, 105], including microsecond-scale studies [106–108], and experimental techniques (see, for example, NMR studies on Na^+> [109, 110]) further show that counterion residence times at DNA binding sites span

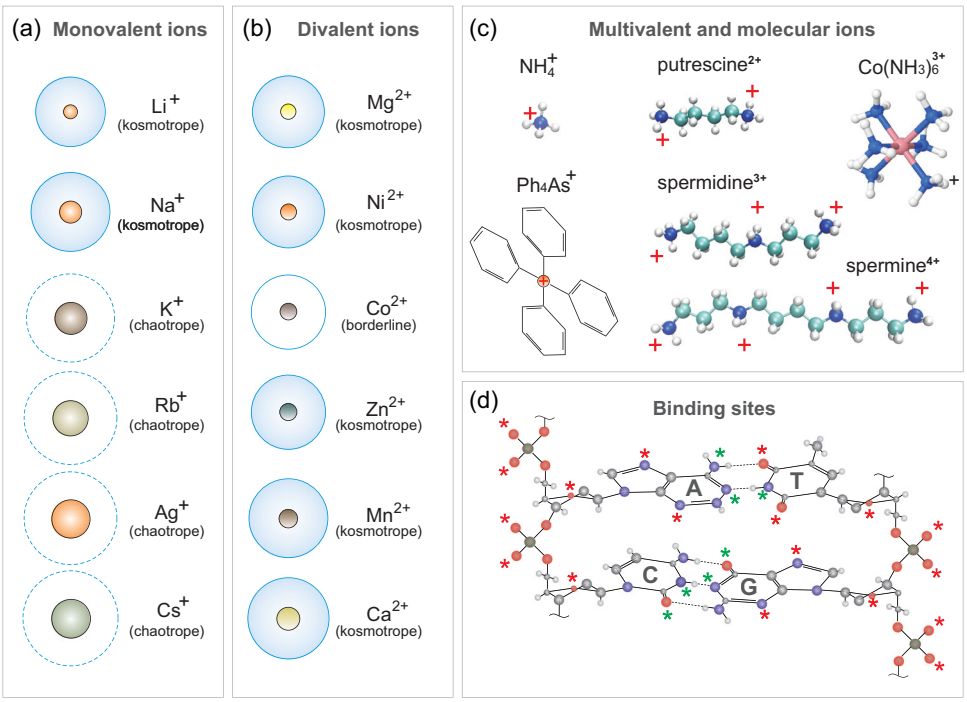

FIGURE 3 | Typical examples of DNA counterions, including condensation agents. Hydration shells are represented by circles: a solid light-blue circle with gradient fill for kosmotropic ions, a dashed circle for chaotropic ions, and a solid light-blue empty circle for the ion with borderline hydration character. (a) Monovalent ions. (b) Divalent ions. (c) Multivalent and molecular ions. (d) Typical binding sites of counterions on DNA nucleotides (based on refs. [50, 95]). Red asterisks denote characteristic binding sites common to all kinds of metal ions, while green asterisks indicate sites specific to divalent ions.

from tens of picoseconds to several nanoseconds, depending on the DNA sequence, compartment, and ion type.

Together, water and counterion interactions govern the structural integrity of the DNA double helix, differing between the grooves and backbone. These interactions underlie ion-mediated DNA organization, compaction, and stability, which are fundamental to nanotechnology applications ranging from programmable assemblies to DNA-based devices.

3 | DNA Condensation

DNA condensation is a well-established phenomenon observed in numerous experiments and strongly influenced by the counterions surrounding the DNA double helix. The process may follow distinct pathways depending on the charge, size, and hydration properties of the ions, as well as on the DNA concentration, nucleotide sequence, and other molecular or environmental factors. It occurs both in vivo and in vitro and underlies a wide range of applications from gene delivery to nanomaterials design. Several comprehensive reviews have addressed this topic, ranging from classical works of Bloomfield [20, 111] to more recent analyses [45, 112, 113]. In this section, we discuss the ionic specificity of DNA condensation and how ion-specific effects can be exploited in various technological applications.

Experimental studies show that DNA condenses at sufficiently high ion concentrations [20]. This effect strengthens with increasing ion charge. Typically, condensation occurs with ions of charge 3+ or higher, can occur under some conditions with divalent ions, but does not occur with monovalent ions. In practice, all charged species in solution influence the condensation of DNA. Common condensing agents include organic polycations such as spermidine^{3+} and spermine^{4+} or inorganic complexes like $[Co(NH_3)_6]^{3+}$ (Figure 3).

At the microscopic level, counterions interact with specific binding sites on DNA, including the oxygen atoms of the phosphate groups, as well as oxygen and nitrogen atoms in the minor and major grooves of the DNA double helix. These characteristic binding sites are indicated by asterisks in Figure 3d.

DNA condensation can proceed through several pathways, classified as all-or-none compaction, progressive compaction, adsorption, and wrapping around a core particle [113]. In the all-or-none mechanism, DNA molecules collapse into a compact form without intermediate states; as a result, some chains remain elongated, while others are fully collapsed. In progressive compaction, all DNA chains gradually adopt the compact form. Both modes involve DNA–DNA contacts mediated by counterions. The third pathway occurs when DNA interacts with a charged nanoparticle, such as a nucleosome core particle containing histone proteins.

Depending on specific conditions, such as the type and concentration of the condensing agent and other environmental factors, DNA condensation can give rise to diverse morphologies, including globular, rod-like, and toroidal forms. To elucidate the mechanisms underlying these structural transitions, the following subsections examine the effects of ions with different valencies: multivalent, divalent, and monovalent. The section concludes with an overview of the physical models developed to describe the fundamental principles governing DNA condensation.

3.1 | Effect of Multivalent Ions and Polycations

DNA condensation induced by multivalent ions and polycations can be described as a coil-globule transition. Fluorescence microscopy studies of individual bacteriophage T4dC DNA molecules (166 kbp) revealed that this transition occurs abruptly and discretely, following an "all-or-none" mechanism rather than a gradual process as inferred from bulk measurements [114, 115]. At a critical concentration of a condensing agent such as spermidine^{3+} or spermine^{4+}, DNA molecules switch sharply from an extended coil to a compact globule. Increasing the polyamine charge by one unit lowers the threshold concentration for condensation by roughly an order of magnitude, from about 1 to 0.01 mM.

Deng and Bloomfield [116] compared the effects of three trivalent cobalt-amine complexes on DNA condensation using light scattering and electron microscopy. The studied complexes, hexammine $[Co(NH_3)_6]^{3+}$ (Cohex), tris(ethylenediamine) cobalt(III)

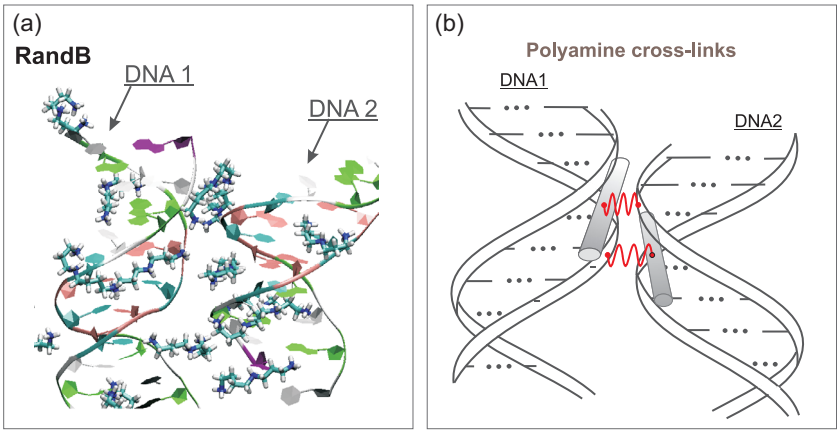

FIGURE 4 | Polyamine-mediated cross-links between DNA molecules. (a) Snapshot of a complex formed by two DNA oligomers with the nucleotide sequence d(CGCGATATCGCGCGAATTCGCG). This system is referred to as R and B in ref. [118]. (b) Schematic representation of the complex, highlighting how polyamines are coordinated by the phosphate groups of different DNA strands, schematically represented by red springs. Adapted with permission [118]. Copyright 2022, Springer Nature Switzerland AG.

(Coen), and cobalt(III) sepulchrate (Cosep), share similar coordination geometries but differ in size and hydrophobicity, in the order Cosep > Coen > Cohex. All three condense DNA effectively at sufficient concentrations; however, Cosep was roughly twice as efficient as Cohex or Coen in inducing DNA precipitation. The condensation of DNA by $[Co(NH_3)_6]^{3+}$ was also studied by Conwell et al. [117] who investigated how intrinsic DNA curvature and ionic strength influence the morphology of DNA condensates. Two linear DNA fragments were used: a 3 kb plasmid (2961 bp) without curvature and Atract60 (3681 bp), a DNA fragment containing phased A-tracts that generate a sequence-directed curved region, which serves as a static nucleation loop for condensation. The loop size, determined by the intrinsic curvature of the DNA, set the toroid diameter, whereas the toroid thickness depended solely on salt concentration (NaCl or $MgCl^2$). This decoupling of nucleation and growth demonstrates their independence and provides a powerful framework for controlling nanoscale DNA architectures.

DNA–DNA contact formation mediated by elongated polyamine ions, an essential step preceding full condensation, has been extensively studied both theoretically and experimentally [17, 118]. Yoo et al. [17] investigated how DNA sequence and methylation influence inter-duplex attraction in the presence of spermine^{4+} using all-atom MD simulations and single-molecule fluorescence resonance energy transfer (FRET) experiments. Methyl groups on thymine or methylated cytosine sterically hinder spermine^{4+} binding to the major groove (especially at purine N_7), forcing relocation toward the backbone and interhelical regions, where bridging between duplexes enhances attraction. Increasing NaCl concentration reduces spermine^{4+} binding and weakens inter-duplex attraction, highlighting the competitive role of monovalent ions. Similar to spermine^{4+}, the tricationic polyamine spermidine^{3+} also promotes DNA–DNA association by linking adjacent helices, as shown by MD simulations from our group [118, 119]. This polyamine can localize in the minor groove of one DNA molecule while simultaneously interacting with the phosphate groups of another (Figure 4a). Through these interactions, spermidine^{3+} forms cross-links between macromolecules (Figure 4b). Conformational flexibility

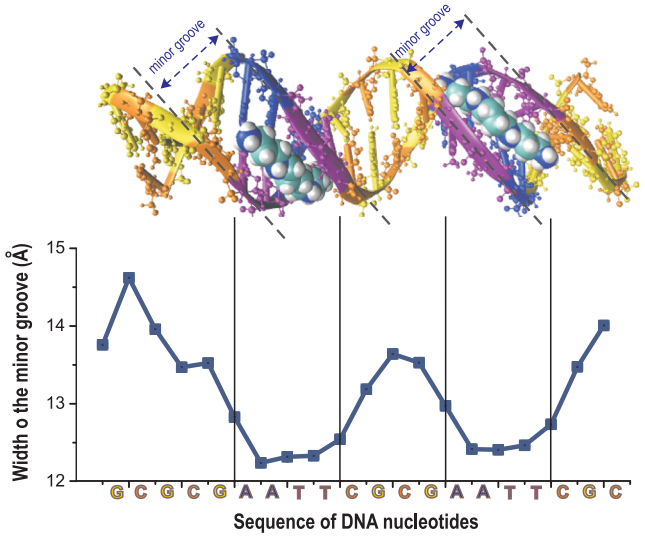

FIGURE 6 | Positioning of spermidine^{3+} in the minor groove of an A-tract region. The upper panel shows a snapshot of the spermidine–DNA complex, while the lower panel depicts the dependence of the minor groove width on the nucleotide sequence. The figure is based on data from ref. [40].

plays a crucial role in this process [120, 121]. Within DNA–DNA contacts, the polyamine can adopt a strongly bent conformation, in which its three amino groups interact with DNA phosphate groups on the minor groove side (Figure 5a). The dihedral angles accessible to the polyamine backbone resemble those in cyclohexane and cycloheptane (Figure 5b).

DNA condensation can exhibit sequence specificity because polyamine positioning along the double helix depends on the nucleotide sequence [40, 121]. MD simulations have shown that polyamines preferentially occupy the narrowest region of the double helix, the minor groove, where their localization reflects sequence-dependent variations in groove width [40]. As a result, polyamines show a clear propensity for A-tract regions, where the minor groove is particularly narrow (Figure 6). The formation of anomalous bent conformations of spermine^{4+} is likewise

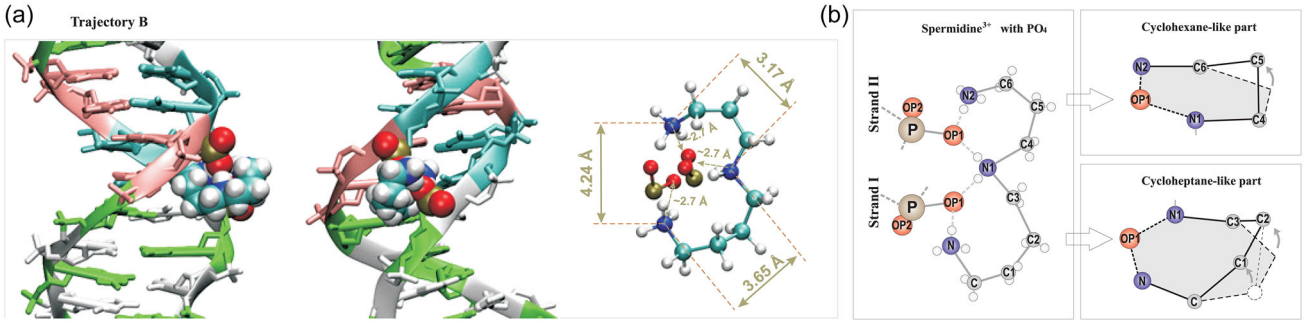

FIGURE 5 | Structure of the anomalous bent conformation of spermidine^{3+} in complex with a DNA oligomer with the nucleotide sequence d(CGCGAATTCGCGCGAATTCGCG). (a) Snapshot of a spermidine–DNA complex, with the polyamine localized in the minor groove in the AATT nucleotide region, linking two phosphate groups of opposite strands. The structures on the left and in the middle depict the DNA double helix with the polyamine molecule from different perspectives. Detailed views of spermidine^{3+} are shown on the right. (b) Representative conformations of spermidine^{3+} in the anomalous bent state. The left panel illustrates the association of bent spermidine^{3+} with oxygen atoms of DNA phosphate groups. The upper right panel shows the (N1-C4-C5-C6-N2) segment of spermidine^{3+}, forming a six-membered cyclic motif that includes the OP1 oxygen atom of a DNA phosphate group. The lower right panel shows the coordination involving the (N-C-C1-C2-C3-N1) segment of spermidine^{3+} forming a seven-membered ring with the OP1 phosphate oxygen. Adapted with permission [121]. Copyright 2024, AIP Publishing.

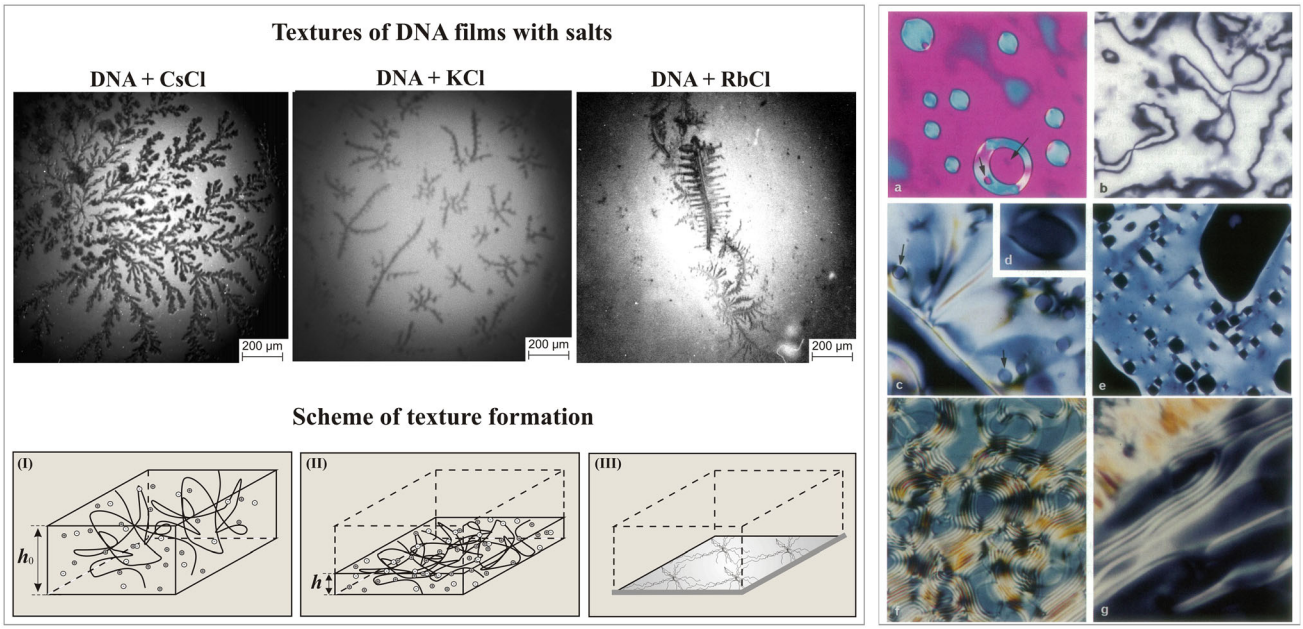

FIGURE 7 | DNA textures and liquid crystalline phases formed under the influence of counterions. **Left panel (top):** Textures of DNA films formed with CsCl (30 mM), KCl (5 mM), and RbCl (5 mM) excess salts in the initial solution (DNA concentration in initial solution: 0.2 mg/mL). **Left panel (bottom):** Schematic illustrating (I) initial saturated solution of DNA, (II) saturated DNA solution, (III) dried DNA film. Adapted with permission [122]. Copyright 2013, Wiley Periodicals, Inc. **Right panel:** Polarizing microscopy images showing the textures of the large-pitch cholesteric phase formed by spermidine^{3+} -condensed DNA. (a) Cholesteric droplets coexisting with a dilute isotropic phase; droplets may trap bubbles (arrows) (16 mM NaCl, 4 mM spermidine^{3+}). (b) Nematic textures characterized by black brush defects (10.7 mM NaCl, 7.9 mM spermidine^{3+}). (c) Cholesteric texture with a large-pitch and a few embedded isotropic droplets (arrows). (d) Tear-shaped defect line indicative of cholesteric organization. (e) Likely cholesteric birefringent texture with many isotropic bubbles (10.7 mM NaCl, 7.9 mM spermidine^{3+}). (f,g) Fingerprint textures characteristic of the cholesteric phase, observed under different thermal and ionic conditions: (f) 25 mM NaCl, 30 mM spermidine^{3+} and (g) 5.7 mM NaCl, 10 mM $MgCl_2$, 7.8 mM spermidine^{3+}. Adapted with permission [123]. Copyright 1996, The Biophysical Society. Published by Elsevier Inc.

favored in specific sequences [121]. These sequence-dependent interactions play a crucial role in regulating the formation of polyamine-mediated DNA–DNA cross-links and, consequently, in controlling DNA aggregation processes that can be exploited for diverse technological applications.

Through their interactions with DNA, counterions can induce the formation of large DNA aggregates and ordered structures (Figure 7). These organized DNA–counterion assemblies have been observed both as surface textures formed after solvent evaporation [122, 124, 125] and as liquid–crystalline phases [123, 126]. For alkali metal ions, evaporation of the solution produces fractal-like surface patterns that arise from salt crystallization on DNA and the formation of DNA–salt complexes (Figure 7). The presence of DNA strongly enhances salt crystallization compared to pure salt solutions. The tendency of excess salt to form crystalline structures decreases in the following order: KCl > NaCl > RbCl > CsCl > LiCl [122]. Multivalent ions can also induce structural ordering of short DNA fragments into distinct liquid–crystalline phases. For instance, the polyamine spermidine^{3+} promotes two structurally distinct DNA mesophases: cholesteric and columnar hexagonal [123]. The phase behavior depends critically on spermidine and salt concentrations, as well as on the length of the DNA fragment. As an illustration, see the textures of the cholesteric phase of DNA with spermidine^{3+} (Figure 7 right panel). A distinct type of liquid crystalline organization has been observed for short DNA fragments that assemble into columnar structures [126]. MD simulations later showed that the formation of these columnar structures arises from interactions between the terminal base pairs of the double helix [118, 127]. The ability of counterions to induce such ordered DNA architectures can be exploited in technological applications.

3.2 | Effect of Divalent Ions

The effects of divalent ions on DNA condensation are less pronounced than those of multivalent counterions and depend strongly on the specific ion involved. Raman studies have shown that transition metal ions (Mn^{2+}, Co^{2+}, Ni^{2+}, Cu^{2+}, Pd^{2+}, and Cd^{2+}) perturb the double helix structure through strong interactions between cations and nucleotide base atoms [128]. DNA aggregates form upon heating to temperatures near the melting temperature and subsequently dissociate [129]. This aggregation behavior can be explained by the formation of ion-mediated cross-links that arise after partial DNA melting, as described in the model proposed by Shibata and Schurr [130].

The formation of DNA–DNA contacts mediated by Mn^{2+} ions is much more pronounced compared to Mg^{2+} ions [131]. The different efficiencies of these ions as condensation agents are attributed to the specific interactions with the DNA double helix. X-ray analysis of DNA in the presence of Mg^{2+} shows that these ions bind primarily to the phosphate groups of the backbone, with water molecules from the ion's hydration shell playing an essential role [80]. In contrast, NMR experiments show that Mn^{2+} ions bind to atoms of the nucleobases from the minor groove side

[132]. The formation of DNA–DNA contacts induced by divalent metal ions has been observed in rheology experiments on λ-DNA solutions [44]. In these experiments, monovalent cations were found to slightly enhance viscoelasticity, whereas divalent cations such as Mg^{2+} caused more complex structural changes by promoting DNA–DNA crosslinks.

The nucleotide sequence is a key factor in DNA condensation induced by divalent metal ions. Sequence-dependent condensation of DNA has been observed with Ni^{2+} ions [133]. In particular, GC-rich motifs exhibit DNA condensation at millimolar ion concentrations, whereas AT-rich sequences do not condense even at ten times higher ion concentrations. This behavior is explained by the *B-Z* transition of the GC nucleotide sequence, which facilitates the localization of counterions in configurations favorable for the formation of DNA–DNA contacts. More generally, DNA condensation under these conditions can be described within the framework of the electrostatic "zipper" model by Kornyshev and Leikin [134].

Not all divalent ions are capable to induce DNA aggregation. Vibrational Raman spectroscopic studies of DNA in the presence of Zn^{2+} show no aggregation [135]. In general, the ability of divalent metal ions to promote DNA aggregation decreases in the following order: $Cd^{2+} > Ni^{2+} > Co^{2+} > Mn^{2+} \sim Ca^{2+} > Mg^{2+}$ [129].

3.3 | Effect of Monovalent Ions

In contrast to multivalent counterions, monovalent ions interact only weakly with the DNA backbone and do not induce condensation. Their limited electrostatic correlations are insufficient to reverse the DNA charge; consequently, charge inversion and aggregation observed with polyamines such as spermidine^{3+} are absent [111]

Among monovalent ions, Li^+ interacts most strongly with the phosphate groups of the DNA backbone, with interaction strengths reported to be significantly stronger than those of other monovalent ions [22, 98, 104]. This behavior arises from the unique hydration properties of Li^+, which stabilize its association with the oxygen atoms of the phosphate groups [104]. The formation of such ion-phosphate complexes contributes to the development of gel-like structures in DNA solutions at high LiCl concentrations, where ion-mediated DNA–DNA contacts can occur [136, 137]. DNA condensation induced by monovalent ions has also been reported for organic tetraphenylchloridearsine ions [138], whose hydrophobic tetrahedral structure promotes DNA aggregation even at very low concentrations. However, whether monovalent ions alone can induce DNA condensation remains controversial.

3.4 | Effect of Organic Salts and Small-Molecule Drugs

Organic salts (including ionic liquids and cationic surfactants), as well as small-molecule drugs, can modulate DNA compaction, aggregation, and mechanical response through a combination of mechanisms that involve not only electrostatic interactions with charged functional groups but also hydrophobic and/or aromatic moieties and directional hydrogen bonding. A representative example is provided by ionic liquids (ILs), whose tunable cation-anion chemistry can stabilize duplex DNA, modify hydration structure, and reshape DNA mechanical properties. These effects depend sensitively on alkyl-chain length, aromaticity, and ion pairing. A comprehensive review by Egorova et al. [139] summarizes how IL micro-heterogeneity and specific ion-groove interactions control nucleic-acid stabilization. These mechanistic insights also underpin emerging applications in nucleic-acid handling and delivery. Single-molecule and bulk measurements further show that imidazolium-based ILs can measurably alter dsDNA elasticity and conformational transitions, consistent with a mixed electrostatic-hydrophobic binding scenario coupled with solvent reorganization [140]. Cationic surfactants and related amphiphilic organic salts constitute another important class of compounds capable of inducing DNA collapse, with a pronounced dependence on hydrophobic chain length and cooperative surfactant aggregation on the DNA surface. Single-molecule optical-tweezer experiments demonstrated clear signatures of surfactant-induced DNA compaction when hydrophobic tails exceed a critical length, consistent with the formation of a condensed DNA-surfactant phase [141]. Related single-molecule force spectroscopy studies further showed that DNA compaction by monovalent cationic surfactants can be driven predominantly by cooperative hydrophobic aggregation of bound molecules, rather than by classical multivalent charge neutralization [142] Small-molecule drugs can also modulate DNA condensation indirectly by altering DNA structure, mechanics, and intermolecular recognition. Drug-DNA interactions can be cooperative and environment-dependent, such that ligand binding modifies DNA–DNA association propensities without relying solely on classical multivalent 'condensing counterions' [143]. In this context, Lima et al. [144] demonstrated that the intercalating anticancer drug mitoxantrone induces DNA condensation only above a threshold concentration, coinciding with the onset of strongly cooperative binding and a collapse of DNA mechanical stiffness. These results indicate that condensation emerges from collective, higher-order effects of ligand binding rather than from simple charge neutralization by multivalent ions. Related biophysical studies on protamine-induced DNA condensation further demonstrate that small-molecule DNA binders can also modulate condensation pathways in a binding-mode-dependent manner. In particular, intercalators and minor-groove binders were shown to suppress DNA condensation through distinct mechanisms: intercalators directly compete with condensing agents, whereas minor-groove binders act allosterically by altering DNA stiffness and groove geometry [145]. More generally, different classes of DNA binders can induce changes in groove geometry, hydration, and local electrostatics, often in a sequence-dependent manner, which in turn reweight DNA–DNA interactions and the surrounding ion atmosphere. High-resolution structural surveys document such ligand-induced DNA deformations, including groove widening, bending, base flip-out, and hydration rearrangements, depending on binding mode and sequence context [146], while recent structure-based and structure-property studies highlight how specific chemical features and conformational flexibility of minor-groove binders tune binding modes, specificity, and functional performances [147, 148]. Beyond canonical binding, small-molecule DNA binders can programmably regulate DNA reaction pathways by cooperatively modulating DNA structure and accessibility, supporting the idea that small molecules can exert indirect, higher-order control over DNA–DNA interactions and nucleicacid behavior at mesoscopic scales [149]. Consistent with this picture, a recent review [45]

explicitly emphasizes hydrophobic contributions from organic cations as key drivers of DNA compaction and charge regulation, underscoring why organic salts and amphiphilic drugs can produce condensation phenomenology that differs qualitatively from that observed in purely inorganic electrolytes.

3.5 | Models of DNA Condensation

Several widely used theoretical models describe DNA condensation. Among them, Ray and Manning investigated how two negatively charged rod-like polyions, such as DNA or similar polyelectrolytes, can attract each other despite their like charges [150]. In their model, the rods are treated as rigid, infinitely long, and uniformly charged (Figure 8a). Positive counterions condense onto the rods according to Manning's counterion condensation theory [153]. When the rods approach each other closely, some of the condensed counterions can be shared between them, generating an attractive force that overcomes electrostatic repulsion within a limited separation range. The model predicts that this attraction can exceed the thermal energy in the presence of multivalent ions, whereas for monovalent ions, it remains very weak. It should be noted that this model accounts only for electrostatic interactions, while hydration and other ion-specific effects may also play important roles in DNA condensation.

Rouzina and Bloomfield developed a model describing two macroion surfaces with identical high surface charge immersed in an electrolyte containing multivalent counterions [151]. The counterions are divided into two populations: adsorbed ions that form a mobile quasi-2D layer near the surfaces and a diffuse ion cloud farther away in the bulk solution (Figure 8b). The model demonstrates that electrostatic correlation among counterions can lead to attraction between like-charged surfaces, with the pseudo-2D layer of adsorbed ions being particularly effective in generating this attraction. This model helps explain why DNA condenses in the presence of multivalent ions.

An elegant model proposed by Shklovskii describes DNA condensation as driven by the formation of a Wigner crystal phase [152]. In this theory, DNA macromolecules are treated as infinitely long, uniformly charged rods surrounded by counterions. The central idea is that counterions condense on the rods and form an ordered lattice of charges, a Wigner crystal, that mediates attractive interactions between them. This ordering is governed by a single dimensionless parameter that combines charge density, ion spacing, and geometry. For DNA, the ordering effectively reduces to one dimension along the helix. The model predicts regimes in which attraction becomes energetically favorable, depending on ion valence, surface charge density, and geometry.It also shows how the counterion ordering can overcome the repulsion predicted by mean-field theories. The concept of counterion ordering has also been extended to studies modeling DNA with counterions as an ionic lattice [24, 41, 154–158], enabling the description of ion–phosphate vibrations observed in the low-frequency spectral range (Figure 8c). These approaches, which conceptualize DNA with its counterions as an ordered system, provide a mechanistic and unifying framework for understanding the phenomenon of DNA condensation.

Kornyshev and Leikin [134] introduced a model describing the formation of stabilizing complexes between two DNA molecules. The core concept is the electrostatic zipper motif. In this model, DNA helices having a helical charge distribution arising from phosphates and counterions bound in grooves can approach each other in specific orientations and separations such that the charges along the grooves of one helix align with oppositely charged groups on the other (Figure 8d). When counterions bind in the grooves in particular configurations, they create an axial charge separation in which positive charges distributed along the axis through bound ions can "fasten" the two helices together by maximizing opposite-charge contact. In this analogy, the grooves act as the "teeth" in a zipper; when they interlock in favorable orientation, attraction is enhanced and repulsion minimized. The predictions of this theory quantitatively agree with many experimental observations.

4 | Modeling Challenges and Computational Advances

Modeling nucleic acid–ion interactions is a challenging task in computational chemistry due to the complex, multiscale nature

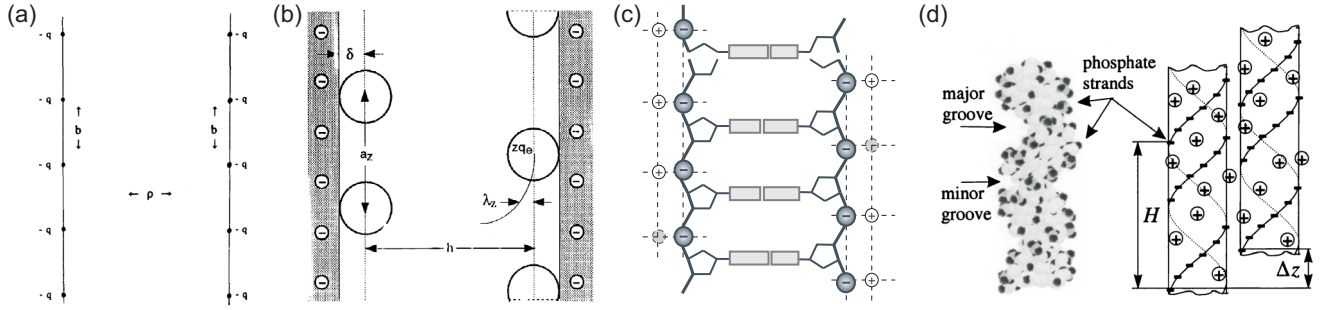

FIGURE 8 | Models of DNA–DNA attraction. (a) A model based on the simple polyelectrolyte approach: two chains of charges q in parallel orientation with separation distance ρ. Adapted with permission [150]. Copyright 1994, American Chemical Society. (b) A model of surface–surface interaction between charged planes. σ is the charge density, h is the separation distance, and z is the valency of counterions. Adapted with permission [151]. Copyright 1996, American Chemical Society. (c) Models of ionic ordering: schematic representation of counterion arrangement around DNA according to the Wigner crystal model [152] and the ion-phosphate lattice model [24]. (d) Electrostatic zipper "motif" model [134]. The structure of canonical *B*-DNA is shown on the left. Simplified representation of attracting DNA helices is shown on the right: negatively charged phosphate groups of the macromolecule backbone and positively charged counterions localized in the grooves of the double helix are arranged next to each other, creating a "zipper" of electrostatic attraction between macromolecules. Adapted with permission [134]. Copyright 1999, American Physical Society.

of these interactions. Some key challenges are discussed in the following.

4.1 | Force Field Limitations

Standard biomolecular force fields, which assume fixed atomic charges and pairwise-additive interactions, may not always be able to accurately reproduce metal ion binding affinities and geometries. While fixed-charge force fields reliably reproduce global DNA structure in simple electrolyte environments, their limitations can affect functional nanostructures. For instance, specific ion-DNA interactions can cause clustering of local ionic concentration in the region where DNA molecules make direct contact [159]. Inaccurate ion coordination to certain DNA sites leads to discrepancies with experimentally observed ion selectivity [72], and overestimated binding to phosphates [160] further exemplifies these shortcomings. These fixed-charge limitations have clear implications for the modeling of systems such as DNA origami, DNAzymes, or metallized DNA. Metal cations can exhibit diverse coordination numbers and geometries, and induce polarization of nearby atoms, effects that simple nonpolarizable models cannot capture well. For example, divalent ions such as Mg^{2+} or Zn^{2+} may coordinate directly to nucleic acid functional groups or to water molecules in the first hydration shell. A fixed-charge force field with a point-charge ion may either over-stabilize or under-stabilize such contacts. This limitation means that simulations can have difficulty distinguishing a fine ion specificity. For example, explaining why K^+ and Na^+ have different stabilizing effects on a G-quadruplex [161, 162] or predicting the structural effects of replacing one ion with another. Benchmarking studies and critical assessments of ion force fields have shown that ion-DNA interactions are highly sensitive to ion parameterization [163, 164]. Large-scale atomistic simulations of DNA condensates have demonstrated that quantitative agreement with experimentally measured DNA–DNA forces requires careful calibration of ion-phosphate interactions; simulations employing unrefined ion parameters favor a direct ion-bridging mechanism, whereas calibrated models support a noncontact ion-mediated condensation mechanism [160]. More sophisticated ion models incorporating a 12-6-4 Lennard-Jones potential have been proposed to partially account for charge-induced polarization effects and have been subjected to preliminary tests on Mg^{2+}-DNA systems, showing improved local ion-phosphate coordination relative to standard force-field parameters [164]. However, such approaches have not yet been adopted for large-scale DNA assemblies or collective ionic environments.

4.2 | Ion Hydration and Dynamics

Correctly modeling the hydration shell of ions is critical for accurate DNA simulations. Ions such as Mg^{2+} carry a tightly bound first shell of water molecules that mediate interactions with DNA. Experimental properties such as catalytic rates, folding yields, and mechanical stiffness are often ultimately governed by subtle differences in ion hydration structure and water-exchange dynamics, which control water residence times, orientational ordering, and the effective electrostatic environment surrounding DNA [62, 102]. Conventional fixed-charge force fields may inadequately capture ion hydration, binding energetics, and residence times, leading to inaccuracies in ion localization and intermolecular forces that hinder quantitative comparison with experimentally measured structural and mechanical properties in ion-responsive DNA nanostructures [106, 160, 164]. In simulations, if an ion's hydration free energy or exchange kinetics are not well described, the residence times and strength of DNA–ion contacts will be inaccurate. Moreover, many-body effects, such as ions polarizing water, which in turn influences DNA, mean that any purely additive model can misinterpret how an ion "sees" the nucleic acid. Polarizable force fields provide a state-of-the-art solution. For instance, the AMOEBA and Drude oscillator models include inducible dipoles, allowing the ion's electric field to polarize the DNA and water molecules and vice versa. These advanced force fields have been developed for nucleic acids and their ions and validated in long simulations of DNA and RNA that show improved agreement with experimental observables [165]. By accounting for electronic polarization, such models may better reproduce ion residence times and coordination geometries around nucleic acids than conventional force fields.

4.3 | Sampling and Ion Atmosphere

The ion atmosphere around DNA and RNA, a diffuse cloud comprising hundreds of ions even for short oligonucleotides, is challenging to sample computationally. Ions may temporarily bind in the grooves or at specific sites. Capturing the equilibrium distribution of multiple ions requires extensive sampling. Several studies show that ion distributions, especially near subtle sequence-dependent features such as AT-rich versus GC-rich regions or narrow minor grooves, converge very slowly in simulations [106]. Enhancing sampling via techniques like replica exchange, grand-canonical Monte Carlo moves for ions, or long time-scale MD simulations is often necessary to achieve converged ion populations around nucleic acids. Insufficient sampling can lead to artifacts, e.g., a simulation might get a spuriously "stuck" ion in a site, skewing the results. Thus, computational models must carefully address the stochastic, dynamic nature of ion association with nucleic acids.

4.4 | Reactive Chemistry and QM/MM

In nucleic acid catalysts such as ribozymes and DNAzymes, metal ions often participate directly in phosphodiester bond cleavage, acting beyond simple electrostatic screening and rendering purely classical molecular dynamics intrinsically insufficient. In such cases, quantum mechanics/molecular mechanics (QM/MM) methods provide a natural framework to describe the reactive chemistry. A localized region containing the reacting groups and the catalytic metal ion is treated quantum mechanically, typically using density functional theory (DFT), while the remainder of the system is described by a classical force field. This framework, originally formulated by Warshel and Levitt [166] and later systematized for biomolecular systems [167], enables an explicit description of polarization, charge transfer, and electronic rearrangements associated with metal-assisted catalysis in nucleic acids [168]. QM/MM therefore enables simulation of bond-breaking and bond-forming events and metal-ion-assisted catalytic mechanisms in nucleic acids, including

RNA-cleaving DNAzymes [169]. For example, QM/MM simulations have been used to resolve metal-assisted phosphoryl transfer mechanisms in nucleic-acid chemistry, as demonstrated in studies of human DNA polymerase λ [170]. In that work, Mg^{2+} and Mn^{2+} ions play direct catalytic roles that cannot be captured by classical molecular dynamics. In a DNAzyme-specific context, Aranda et al. [171] combined classical MD and QM/MM free-energy simulations to resolve the full catalytic mechanism of the 9DB1 DNAzyme, showing that explicit treatment of Mg^{2+} ions is essential to reproduce experimentally observed RNA ligation activity. A key challenge in such simulations is the choice of an accurate quantum description, as different DFT functionals can yield substantially different reaction energetics. Nevertheless, QM/MM, when complemented by *ab initio* fragment calculations and DFT benchmarks on model complexes, provides critical insight into the reactive roles of ions bound to nucleic acids.

4.5 | Multiscale Approaches

The behavior of nucleic acids in ionic environments spans multiple spatial and temporal scales, from the femtosecond fluctuations of hydration water to mesoscale DNA condensation and chromatin organization. Capturing this hierarchy requires multiscale modeling, where atomistic accuracy is systematically transferred to coarse-grained (CG) and continuum descriptions. Among the most physically grounded techniques developed for this purpose is the inverse Monte Carlo (IMC) method introduced by Lyubartsev and Laaksonen [172] and further advanced in collaborative works with Nordenskiöld and Korolev. The IMC approach inverts the radial distribution functions (RDFs) obtained from fully atomistic molecular dynamics or Monte Carlo simulations to derive effective pairwise interaction potentials between coarse-grained sites. These potentials are iteratively refined until the CG model reproduces the target RDFs with statistical fidelity, ensuring thermodynamic consistency between scales. Within the broader theoretical context of predictive coarse-graining and multiscale modeling [173, 174], these approaches provide a quantitative link between microscopic ion-DNA interactions and experimentally measurable macroscopic properties.

The IMC method has proven particularly powerful for modeling DNA–ion systems, where explicit solvent and ion correlations play essential roles. Lyubartsev and Nordenskiöld [175, 176] demonstrated that CG models derived via IMC reproduce the experimentally observed counterion condensation and DNA–DNA attraction mediated by multivalent cations. Later, Korolev et al. [177–180] extended the framework to describe the sequence dependence of DNA flexibility, DNA aggregation induced by multivalent and molecular ions, and electrostatic interactions in chromatin fibers. These studies established a bridge between atomistic electrostatics and mesoscale DNA mechanics, allowing quantitative exploration of how specific ionic conditions translate into macroscopic condensation forces.

Recent developments have combined IMC-derived potentials with coarse-grained molecular dynamics, Brownian dynamics, and Poisson–Boltzmann or density-functional models, enabling direct simulation of DNA arrays, chromatin compaction, and polyelectrolyte complexation under experimentally relevant salt concentrations. This multiscale paradigm provides not only computational efficiency but also transferability across ionic conditions and molecular topologies, which is difficult to achieve with purely empirical CG models.

By integrating atomistic accuracy with mesoscale statistics, multiscale approaches such as IMC constitute a cornerstone of contemporary computational biophysics. They make it possible to interpret the microscopic origin of ion-mediated forces and predict emergent behaviors such as bundle formation, elasticity changes, and phase transitions. As such, these models complement the higher-resolution methods described in Sections 4.1–4.4, forming a coherent computational hierarchy that connects electronic-scale polarization to mesoscopic DNA organization —an essential framework for understanding and designing DNA-based nanomaterials.

In summary, modeling nucleic acid–ion interactions requires balancing electrostatic accuracy, ion specificity, and adequate sampling. Progress is being made through improved force fields (including polarizable and refined ion models) [165] and hybrid quantum-classical techniques for reactivity. These computational advances, often validated against experimental data and high-level quantum calculations, are gradually overcoming the limitations of earlier models. As a result, simulations are becoming increasingly reliable in capturing how ions stabilize DNA/RNA structures, modulate their flexibility, and mediate the nanotechnological functions described above. In a broader sense, multiscale modeling serves as a conceptual bridge linking chemistry, physics, and materials science, allowing quantitative predictions that span from molecular interactions to experimentally measurable macroscopic properties. This synergy of experiment and computation is driving a deeper understanding of nucleic acid–ion systems, which is essential for rational design in DNA nanotechnology, biosensor development, and molecular device engineering.

5 | Confined DNA as a Platform for Materials Design

5.1 | Metallized DNA

DNA metallization is an important technological application of DNA–ion interactions under confinement [181]. In this process, DNA acts not only as a biological polyelectrolyte but also as a molecular scaffold for binding and organizing metallic ions, such as Ag^{+}, Cu^{2+}, Au^{3+}, and Ni^{2+}, which can then be reduced to form ordered metallic structures along or within the DNA [182, 183]. The resulting hybrid architectures retain the programmability of nucleic acids while gaining the conductivity, magnetism, and catalytic activity typical of metals. Such systems exhibit unique physicochemical properties and are promising for nanoscale electronic and photonic applications. Comprehensive reviews on this topic are available (e.g [36, 183, 184]). A form of DNA metallization involves the formation of metal-mediated base pairs, in which a metal ion bridges two nucleobases as a coordination center. Complexes of this type, typically involving heavy metals such as Ag^{+}, Pt^{2+}, Au^{3+}, and Hg^{2+}, display strong relativistic effects that alter their bonding and electronic structure. In this section, we examine the key structural and spectroscopic features of such metallized DNA systems and how metal incorporation between nucleotides influences their stability, conductivity, and functional behavior.

In pioneering work, the structural and physical characteristics of Cu^{2+}-mediated DNA complexes demonstrated that DNA can act both as a scaffold and as a coordinating ligand. Atwell et al. [185] reported the first high-resolution crystal structure of a DNA duplex containing a Cu^{2+}-mediated base pair, where two artificial ligand bases coordinate a Cu^{2+} ion to form a metallo "base pair". The metal ion bridges the ligand bases, stabilizing a non-canonical base-pair geometry and inducing a local *Z*-DNA conformation. The duplex can accommodate metal-mediated pairing without losing helical integrity, remaining structurally compatible with both *B*- and *Z*-forms.

Building upon this concept, Tanaka et al. [186] achieved the self-assembly of discrete 1D metal arrays within artificial DNA duplexes (Figure 9). Oligonucleotides containing hydroxypyridone bases coordinated Cu^{2+} ions along the helical axis, producing a right-handed helix with an average Cu^{2+}–Cu^{2+} spacing of ~3.7 Å. Magnetic characterization revealed ferromagnetic coupling between adjacent unpaired d-electrons of Cu^{2+}, effectively transforming the duplex into a molecular magnetic chain.

In a subsequent study, Tanaka et al. [187] extended this approach to achieve programmable self-assembly of metal ions within DNA duplexes, showing that the number, type, and arrangement of metal ions can be precisely controlled by the DNA sequence design. Spectroscopic analyses (UV, CD, ESI-MS, and EPR) confirmed that the Cu^{2+} and Ag^{2+} ions incorporated inside the DNA double helix between the nucleotide bases can form a highly ordered heterogeneous structure maintaining intermetallic distances conducive to electronic and magnetic coupling. Collectively, these studies established the structural framework and physical principles of Cu^{2+}-mediated DNA metallization, revealing that DNA can act not only as a passive template but as an integral component of hybrid molecular systems exhibiting metallic, magnetic, or conductive properties.

Silver atoms and clusters form highly stable and structurally unique complexes with DNA, yielding hybrid materials with potential electronic and photonic functionality. Buceta et al. [188] electrochemically generated ligand-free Ag_2 and Ag_3 clusters and characterized their interactions with DNA. Thermodynamic, kinetic, and QM/MM analyses revealed that Ag_3 clusters intercalate between base pairs, locally distorting the double helix

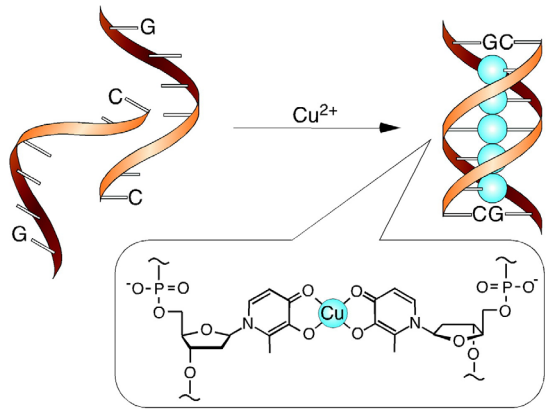

FIGURE 9 | Scheme illustrating the metallization of the artificial DNA by Cu^{2+} ions coordinated to hydroxypyridone nucleobases inside the double helix. Reproduced with permission [186]. Copyright 2003, The American Association for the Advancement of Science.

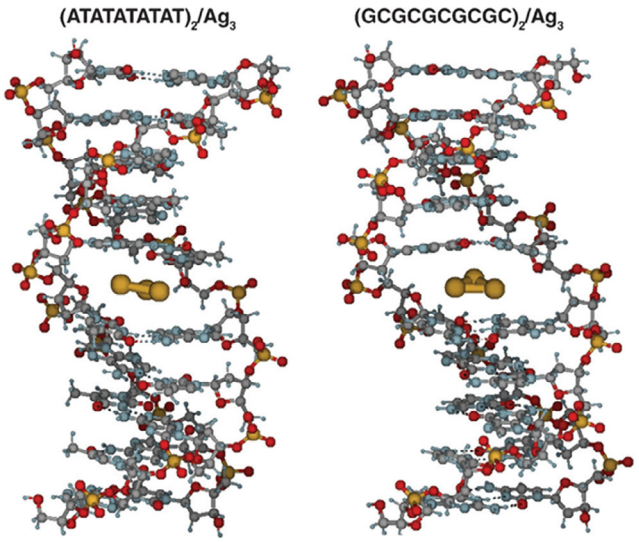

FIGURE 10 | Intercalation of Ag_3 clusters between base pairs of $d(ATATATATAT)_2$ and $d(GCGCGCGCGC)_2$ DNA duplexes [188]. The structures were obtained using QM/MM calculations. Reproduced with permission [188]. Copyright 2015, WILEY-VCH Verlag GmbH & Co. KGaA, Weinheim.

(Figure 10). The resulting Ag_3–DNA complexes exhibit extraordinary kinetic stability, with lifetimes two to three orders of magnitude longer than those of classical organic intercalators such as ethidium bromide and proflavine. QM/MM modeling clarified the energetics underlying this long-lived binding, explaining the exceptional stability observed experimentally. These findings demonstrated that small silver clusters behave as active intercalating species rather than passive counterions, capable of modulating DNA conformation and electronic characteristics.

Besides the intercalative binding observed for Ag_3 clusters, Ag^+ ions can engage in distinct coordination modes with DNA, leading to well-defined metal-mediated base pairs. Kondo et al. [189] provided crystallographic and spectroscopic evidence for Ag^+-mediated base pairing where Ag^+ bridges opposing nucleotide bases, replacing conventional hydrogen bonds while maintaining the helical framework (Figure 11). X-ray, NMR, and mass spectrometry revealed selective binding at cytosine–cytosine mismatches, generating ordered 1D arrays of Ag^+ along the helical axis. These metallo-base pairs confer enhanced rigidity and altered electronic characteristics compared to canonical Watson-Crick duplexes.

A technological development was introduced by Vecchioni et al. [190], who embedded metal-mediated base pairs (mmDNA) into 3D DNA nanostructures. Ag^+ and Hg^{2+} ions were incorporated between engineered pyrimidine–pyrimidine mismatches to produce programmable mmDNA helices assembled into crystals via tensegrity triangle motifs. X-ray diffraction revealed two coordination modes (N3-dominant centrosymmetric pairing and major-groove binding) tunable through chemical modification at the 5-position of the bases. Electronic structure calculations showed that mmDNA introduce additional LUMO levels, imparting electronic properties favorable for molecular electronics. Notably, the formation of mmDNA-containing crystals up to 500 μm in size illustrates that DNA scaffolds can guide both chemical precision and structural order.

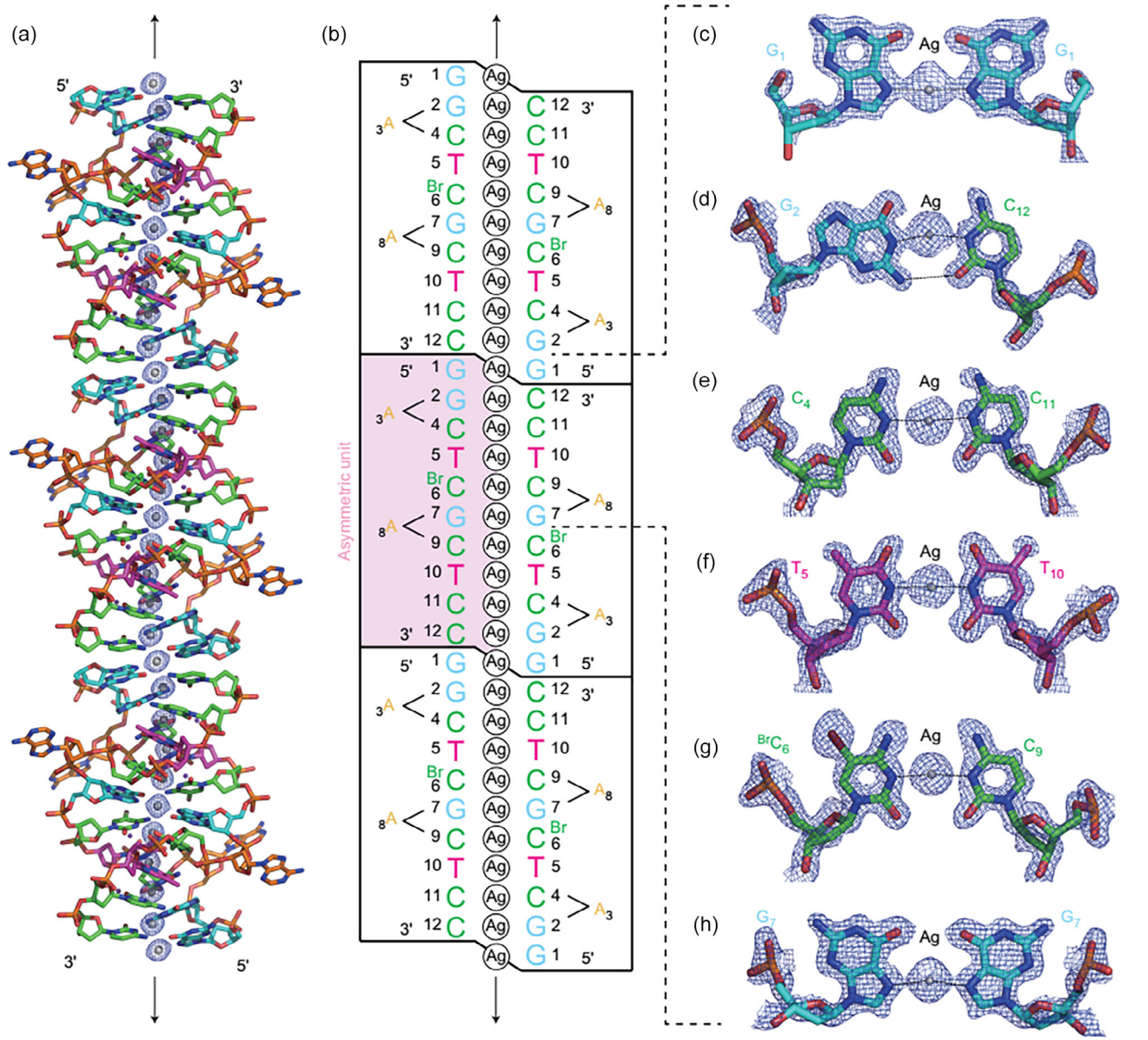

FIGURE 11 | Structure of DNA metallized with Ag^+ ions. (a) Crystal structure of the DNA double helix with Ag^+ ions inside. Coloring scheme: nucleosides G—blue, C—green, T—pink, A—orange; atoms N—blue, O—red, P—orange, Ag—silver. Hydrogen atoms are not shown for clarity. (b) The secondary structure of an extended nanowire, illustrated by three representative dodecamer duplexes. (c–h) Detailed structure of Ag^+-mediated base pairs. Reproduced with permission [189]. Copyright 2017, Springer Nature Limited.

These studies demonstrate that DNA can act as both a scaffold and an active component in the formation of metallized structures, accommodating a wide variety of metal ions (Cu^{2+}, Ag^+, and Hg^{2+}) and intercalating clusters. Copper-mediated base pairs show that DNA can host discrete metal arrays, forming linear chains capable of electronic and magnetic coupling, while retaining helical integrity and allowing programmable assembly [185–187]. Silver atoms and clusters, on the other hand, can intercalate into the duplex or coordinate the nucleotides inside the base pairs, stabilizing DNA and conferring unique electronic and structural properties [188, 189]. The integration of metal-mediated base pairs into 3D DNA nanostructures further illustrates the versatility of DNA as a template, enabling the design of highly ordered, programmable, and electronically functional materials [190]. These results highlight that metal ions in DNA are not merely passive counterions but can serve as intrinsic structural and functional units, directly influencing duplex geometry, stability, electronic states, and potential nanotechnological applications. Overall, metallized DNA represents a robust platform for combining molecular architecture with electronic, magnetic, and photonic functionalities, bridging the gap between biological macromolecules and functional nanomaterials.

5.2 | DNA Nanowire and Stretched π-Stacked Configurations

As discussed in Section 5.1, metallized DNA demonstrates how metal ions can provide the double helix with conductive and magnetic properties. An equally intriguing route explores

whether DNA itself, in modified or mechanically stretched forms, can act as an intrinsic molecular wire. MD simulations by Lohikoski et al. [191] revealed that when double-stranded DNA is elongated to roughly twice its native length under torsion-free conditions, the canonical base-pair hydrogen bonds break and the molecule reorganizes into a remarkable base-stacked zipper-like structure. In this conformation, the nucleobases become tilted and stacked directly on top of one another along the major-groove side, forming a continuous π-stack stabilized by hydration and counter-ion interactions. The authors showed that water and nearby ions are essential for maintaining this stretched configuration, preventing strand separation and minimizing electrostatic repulsion between phosphate groups. This simulation, later correlated with single-molecule stretching experiments, introduced a new structural motif, often referred to as "zip-DNA" or "π-stacked stretched DNA", that opened a conceptual route toward DNA-based nanoelectronics.

Subsequent theoretical and computational studies have extended this idea to explore the electronic properties of the stretched π-stacked state. Balaeff et al. [192] demonstrated via steered molecular dynamics that tension-induced base interdigitation between opposite strands forms a single column of overlapping π-orbitals capable of supporting long-range charge migration. Density-functional and tight-binding calculations indicated that such all-purine "zip-DNA" exhibits significantly enhanced electronic coupling compared with *B*-DNA, suggesting that mechanical deformation could convert an insulating biopolymer into a semiconducting or quasi-metallic nanowire. Sathe et al. [193] further examined stretched DNA confined in graphene nanopores and predicted characteristic shifts in transverse-current spectra that could be used to identify the stretched configuration experimentally. Complementary work by Bruot et al. [194] provided direct evidence of piezoresistivity in DNA, showing that elongation strengthens nearest-neighbor π-stacking and increases conductance consistently with the structural and theoretical predictions.

An essential factor governing electron transport in these stretched configurations is the ionic environment. Ions in close vicinity to the π-stacked backbone play a dual role: they stabilize the conformation by screening the strong phosphate repulsion, and they electrostatically gate the π-stacked conduction channels. Both simulations and experiments indicate that altering cation identity and concentration (e.g., $Na^+ \rightarrow K^+ \rightarrow Mg^{2+}$) shifts energy-level alignment between neighboring bases and modifies the charge–transfer rate. Hydration layers and bound counterions thus act as dynamic tuners of DNA conductance, while excessive ionic strength can, conversely, disrupt the delicate stacking geometry. These findings collectively emphasize that electronic transport through DNA is not solely a property of its base sequence or mechanical state but arises from a synergistic interplay between molecular structure, solvent, and ionic atmosphere. The stretched π-stacked state therefore represents a distinct paradigm for DNA-based electronics, one in which mechanical strain and ionic control together create conductive pathways without requiring metallization.

The question of electrical conductance in DNA has attracted sustained attention since the earliest days following the discovery of the double-helical structure [195]. To date, experimental studies have demonstrated that the intrinsic electrical conductivity of DNA is typically very low, with measured currents in the nanoampere range under most experimental conditions [196–199]. To measure the electrical properties of DNA, a field-effect transistor-based device can be used. Importantly, DNA conductivity is not a universal material constant but instead depends sensitively on a wide range of factors, such as temperature, base-pair composition, and sequence, structural integrity of the double helix, hydration level, and the presence and type of surrounding metal ions.

A variety of physical models have been proposed to describe charge transport in DNA. At present, two main mechanisms are widely considered to govern intrinsic charge transport: on the one hand, thermally activated hopping of charge carriers (electrons or holes) between neighboring nucleobases, facilitated by π-π stacking interactions along the helix, and on the other hand, quantum tunneling, which becomes relevant at shorter distances or in well-ordered DNA segments [200]. In recent years, these models have been complemented by advanced computational studies employing hybrid quantum-classical simulations, which allow for a more realistic description of electronic states coupled to the molecular dynamics of the DNA backbone and surrounding solvent [201, 202]. In addition, machine-learning techniques have been introduced as powerful tools to explore complex structure-property relationships and to accelerate the prediction of charge-transport parameters in large DNA datasets [203].

When compared to conventional metals, the intrinsic electrical conductivity of DNA is several orders of magnitude lower and may even approach that of an insulating material [197]. From this perspective, the intrinsically low electronic conductivity of native DNA prevents its direct use as an efficient nanoscale wire. One strategy to overcome this limitation is DNA metallization, discussed in Section 5.1, where metal-like conduction pathways can be formed along the double helix through controlled ion incorporation. This ion-engineering approach has emerged as a distinct and active research direction. At the same time, it is important to note that electrical transport in DNA-based systems arises not only from electronic conduction along the DNA but also from the motion of counterions surrounding the macromolecule. In this conductivity mechanism, ions are explicitly involved in charge transport through their motion within the DNA-electrolyte environment. This type of transport already underpins the operation of several bioelectronic and nanofluidic devices. A detailed discussion of DNA-based devices exploiting ionic conductivity is presented in Section 5.3.

5.3 | DNA Battery

The DNA macromolecule can be used as an electrolyte for the construction of energy devices [136, 137, 204, 205]. Gel electrolytes from various polymers are commonly used in batteries and supercapacitors, offering sustainable and high-performance charging-discharging processes. However, the existing gel-based electrolytes often suffer from limited flexibility, instability, crystallinity, lower electrochemical performance, short lifetimes, toxicity, and complex synthesis. To overcome these limitations, Mitta et al. [136] introduced a pure DNA gel as a new electrolyte material for the construction of a supercapacitor. DNA, a naturally abundant biopolymer, is biodegradable, nontoxic, nonflammable, ion-compatible, and mechanically flexible. The gel forms a stable amorphous, porous network facilitating ion transport. Leveraging its intrinsic properties, the authors fabricated and

demonstrated a flexible supercapacitor powered by a DNA gel electrolyte (D-gel-SC).

The DNA gel was synthesized from salmon-sperm DNA dissolved in water with excess lithium chloride (LiCl). Heating to 90°C dissociates double-stranded DNA into single-stranded, which then physically entangle upon cooling, forming a stable amorphous gel without the need for toxic crosslinkers. Unlike commonly used PVA (polyvinyl alcohol) or PVA/DNA gels, pure DNA gel maintains a stable amorphous phase after temperature changes (Figure 12a).

A range of experimental techniques, including differential scanning calorimetry (DSC) (Figure 12b,c), wide angle X-ray scattering (WAXS) (Figure 12d), scanning electron microscopy (SEM) (Figure 12e), and Raman and Fourier transform infrared (FTIR) spectroscopies (Figure 12f), were used to study the properties of the DNA-gel in great details [136]. The results reveal the amorphous nature of the DNA-gel with a porous network that supports ion diffusion. Analysis of the solvation structure of the DNA gel shows that Li^+ ions bind preferentially to the oxygen atoms of the phosphate groups. This provided evidence of preferential interactions between phosphate groups of the DNA gel network chains and Li^+ ions, which resulted in high ionic conductivity. This amorphous, porous, and ion-friendly structure makes such DNA gel ideal for use as an electrolyte. The mechanical properties of the DNA gel electrolyte, important for the construction of batteries and supercapacitors, were shown to depend on concentrations, reaction conditions, and reaction time. The DNA gel exhibited favorable mechanical properties: no cracks were observed after elongation, and energy was dissipated effectively at the entanglements. The use of higher ion concentration and DNA with high polymer chain density allowed the formation of hydrogel networks with many physical entanglements and metal-ion complexes.

Electrochemical performance of DNA gel was also tested by placing it into symmetric supercapacitors (D-gel-SC) with activated carbon electrodes. When compared directly to liquid electrolytes and PVA gels, the DNA gel showed superior capacitance, faster ion transport, and lower resistance. The D-gel-SC was successfully used to power a green LED for more than 6 min after just 20 s of charging. The device maintained performance under bending and folding, demonstrating its potential for flexible and wearable electronics. Tests in extreme environments showed the device could operate from 0°C (in ice) up to 75°C without significant performance loss, highlighting its robustness.

To enhance mechanical strength, Mitta et al. [137] introduced DNA hybrid hydrogels incorporating natural polysaccharides (agarose, alginate, and lignin) and the chemical crosslinker poly (ethylene glycol) dimethacrylate (PEGDA). DNA gel electrolytes were prepared with LiCl concentrations ranging from 10 to 800 mM, and their ionic conductivity, ion transport behavior, and Li–DNA interactions were evaluated using electrochemical impedance spectroscopy (EIS) and temperature-dependent conductivity measurements. Conductivity increased with LiCl concentration up to ∼200 mM and then decreased at higher concentrations due to ion aggregation. The study of the mechanical properties of DNA hybrid gels without and with PEGDA crosslinkers showed that the tensile strength of DNA hybrid gels depends on the choice of polysaccharides and their combinations, as well as on DNA concentration. Adding PEGDA crosslinkers substantially improved mechanical strength.

FT-IR and Raman spectroscopy showed that, as in pristine DNA systems, Li^+ ions bind strongly to the oxygen atoms of the phosphate groups of the double helix. The presence of PEGDA induces two additional peaks in the vibrational spectra, indicating the formation of crosslinks between DNA. The interaction between negatively charged groups in polymers and solvated metal ions can modulate the solvation structure, which in turn promotes ion migration and facilitates effective ion transfer.

The hybrid gel electrolytes were integrated into supercapacitor devices and tested in realistic settings: powering LED lights and small vehicles, operating toy cars, fans, and digital clocks, even supporting flexible solar cell setups. Exceptional flexibility and strength of DNA hybrid gels support robust device interfaces.

Biopolymer-based hydrogel electrolytes can be sustainable alternatives to conventional liquid electrolytes in energy storage devices [206–209]. Systems based on cellulose, chitosan, alginate, gelatin [210], and other natural polymers have demonstrated good flexibility, safety, and interfacial contact with electrodes, at the same time enabling ion transport through hydrated polymer networks [206–208]. In these materials, ion conduction is typically governed by solvation and hopping mechanisms facilitated by hydroxyl or amine functional groups within largely random polymer networks. In contrast, DNA gel electrolytes possess a uniquely high and regular linear charge density arising from the phosphate backbone, providing well-defined and strongly interacting coordination sites for metal ions. Moreover, the molecular structure of DNA is intrinsically ordered and programmable, allowing control over chain length, sequence, and hybridization, which offers additional tunability of the gel structure and ion-transport environment. These characteristics distinguish DNA-based gel electrolytes from other biopolymer hydrogels and highlight their potential as a structurally and chemically versatile electrolyte platform for energy storage applications.

Conventional liquid electrolytes used in lithium-ion batteries exhibit high ionic conductivities of approximately1–10 mS/cm at room temperature but suffer from flammability, leakage, and interfacial instability [211, 212]. Synthetic polymer gel electrolytes improve safety and mechanical stability; however, their ionic conductivities are typically lower, in the range of 0.1–1 mS/cm, due to restricted polymer segmental motion [211, 213]. Biopolymer-based hydrogel electrolytes, including cellulose-, chitosan-, and alginate-based systems, can reach ionic conductivities of approximately 1–100 mS/cm in aqueous or highly solvated environments, although their performance is often limited by environmental sensitivity and scalability challenges [209, 214]. DNA hydrogel electrolytes occupy an intermediate position, typically exhibiting ionic conductivities of approximately 0.1–10 mS/cm (73.27 mS/cm in [137]), depending on hydration level, salt concentration, and counterion identity [136, 137]. While their conductivities remain lower and less stable than those of liquid electrolytes, DNA hydrogels offer distinct advantages in safety, mechanical integrity, and conformal electrode–electrolyte contact. Current limitations include sensitivity to environmental conditions, long-term conductivity stability, and scalability of DNA-based materials. Recent studies demonstrate that ion engineering (through controlled selection of counterions, salt concentration, and multivalent ion coordination) can partially mitigate these bottlenecks by enhancing charge carrier density, stabilizing the hydrogel network, and reducing ion pairing via specific interactions with the DNA phosphate backbone [136, 137].

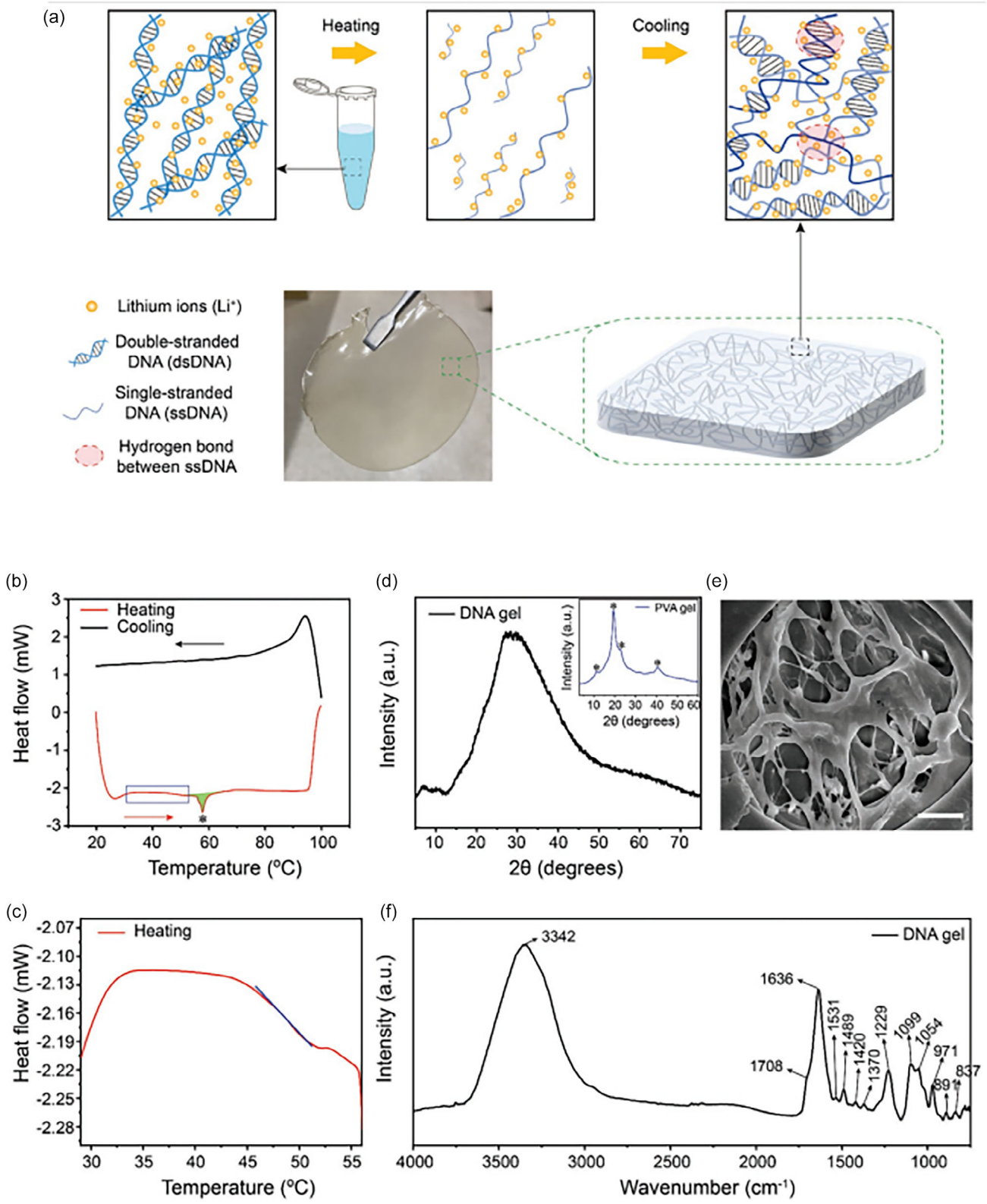

FIGURE 12 | Physicochemical characteristics of DNA-based gel electrolyte. (a) Preparation of DNA gel electrolyte. The photographic image of free-standing (left) and a schematic illustration of the 3D polymeric network (right) of the DNA gel electrolyte are shown in the bottom row. (b) DSC heating and cooling curves of DNA gel. (c) Enlarged view of the portion of the heating curve highlighted in (b) by a blue rectangular box, demonstrating the glass transition temperature indicated by a blue line. (d,e) WAXS spectra and SEM morphologies of DNA gel. The inset in (d) shows the WAXS spectrum of PVA gel. The scale bar in (e) is 10 μm. (f) FTIR spectra of DNA gel. Reproduced under the terms of the CC-BY-NC-ND license [136]. Copyright 2022, Progeneer Incorporation. Advanced Materials Interfaces published by Wiley-VCH GmbH.

From a scalability perspective, conventional liquid electrolytes remain the most industrially viable due to established manufacturing and low-cost raw materials [211, 212]. Synthetic polymer gels are moderately scalable but require controlled casting and cross-linking processes [140, 211]. Biopolymer hydrogels, including cellulose- and chitosan-based systems, are renewable but face challenges in uniform gel formation and consistent mechanical properties at scale [209, 214]. DNA hydrogel electrolytes currently have the lowest scalability due to cost, extraction/purification complexity, and difficulties in producing uniform gels at high throughput [136, 137], although advances in synthetic DNA and gel fabrication may partially address these constraints.

Kumar et al. [205] constructed energy cells based on a composite material combining DNA-CTMA (deoxyribonucleic acid complexed with cetyltrimethylammonium) and PVDF (polyvinylidene fluoride) as a host matrix and separator for lithium battery electrolytes containing LiAsF6. Comprehensive characterization using impedance spectroscopy, TGA, FTIR, and mechanical tests demonstrated that DNA–CTMA/PVDF films exhibit Arrhenius-type ionic conductivity, behaving as solid electrolytes at low temperatures (<15°C) and as gel-like electrolytes at higher temperatures (>15°C), with thinner films showing superior conductivity. The composite also displayed excellent thermal stability, as the degradation temperature remained nearly unchanged upon electrolyte addition, and FTIR spectra revealed Li^+ coordination with C = O groups of DNA–CTMA, suggesting its role in ion transport. The inclusion of DNA significantly enhanced flexibility, elasticity, and resistance to folding or stretching compared to pure PVDF films. DNA–CTMA/PVDF–LiAsF6 composite shows promise as a flexible and thermally stable electrolyte or separator for Li-ion batteries, though further optimization and full-cell testing are needed for practical applications.

Hur et al. [204] developed a novel approach in which the polyelectrolyte multilayers (PEM) DNA hydrogels (Dgel) were used to construct supercapacitors based on a DNA hydrogel scaffold coated via layer-by-layer assembly of conductive polyelectrolytes (PEDOT:PSS (poly (3,4-ethylenedioxythiophene): poly(styrenesulfonate)) and PDADMAC (polydiallydimethylammonium chloride)). These devices are designed for direct operation in physiological fluids without cytotoxic effects and improved cycling stability compared to conventional supercapacitors. The PEM-Dgel supercapacitors were tested in phosphate-buffered saline (PBS), artificial urine, and cell culture medium, mimicking physiological conditions. Cyclic voltammetry results showed that the devices maintain stable and symmetric behavior across varying scan rates, demonstrating reliable capacitive performance. The multilayer PEM coatings exhibit strong durability, with higher layer counts providing better capacitance retention over repeated cycles. The devices perform consistently in physiological environments such as PBS, artificial urine, and cell culture medium, confirming their robustness and biocompatibility. Incorporation of manganese oxide further enhances their energy storage capacity. Importantly, cell culture tests reveal minimal cytotoxicity, confirming the suitability of these supercapacitors for biomedical implant applications. Moreover, their structural and functional properties suggest strong potential for seamless integration into fluid-rich tissues or organs, including vascular, ocular, and bladder environments.

5.4 | DNA in Nanopore

Understanding the behavior of DNA in nanopores is of high relevance for physics, biology, and nanotechnology. It is not only a way to understand DNA behavior under extreme confinement, but it also has important implications that drive innovations in genome sequencing, biosensing, and nanoscale devices.

Experimental and computational research on DNA in nanopores reveal how the ionic environment, together with other variables such as temperature and geometry, governs the behavior of this charged biopolymer in a confined environment. Indeed, the ionic environment is not just a background condition, but a central regulator of DNA behavior under confinement. Already in early atomistic simulations of DNA inside protein pores such as α-hemolysin [215], Na^+ and Cl^- ions were observed to be the

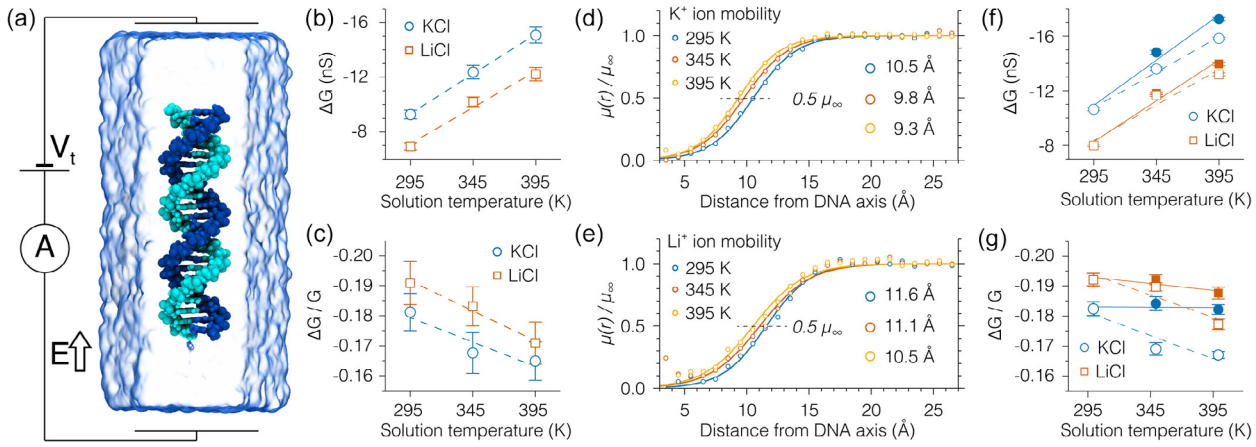

FIGURE 13 | MD simulations of temperature effects on ionic current blockade for the DNA with Li^+ and K^+. (a) Simulation setup with a 22-bp DNA double helix in electrolyte under a constant electric field (35 mV/nm); harmonic restraints prevent DNA drift. (b,c) Temperature dependence of absolute and relative conductance blockades. (d,e) Radial profiles of normalized ion mobility relative to bulk values ($r > R^* = 22$ Å); solid lines show smooth-step fits. Absolute (f) and relative (g) conductance blockades computed from ion density and mobility profiles. Open symbols correspond to MD data; filled symbols show results assuming temperature-independent ion mobility. Lines are linear fits. Reproduced with permission [217]. Copyright 2016, American Chemical Society.

carriers of the measurable current and reporters of conformational changes in single-stranded DNA. Experiments in solid-state pores [216] reinforced this picture by showing that capture statistics depend on ionic strength, with K^+ and Cl^- controlling how DNA enters the pore. Later, hybrid plasmonic pores [217] highlighted how the identity of the counterion matters: Li^+ reduces the effective DNA charge more strongly than K^+, thereby slowing translocation, while simulations revealed how heating and ion mobility alter capture dynamics (Figure 13). Experiments with asymmetric conical pores [218] confirmed that geometry and ions combine to dictate kinetics, with high concentrations of Li^+ enabling slower and more resolvable events, critical for sequencing.

A parallel line of development has focused on DNA-based nanopores. DNA origami structures acting as hybrid gatekeepers [219, 220] rely on Mg^{2+} to stabilize their geometry, while monovalent ions fine-tune their conductance and dwell times. Shi et al. [221] designed DNA origami turbines that autonomously rotate upon docking into solid-state nanopores, powered by ion gradients (Na^+/Cl^-) or transmembrane voltages, with Mg^{2+} stabilizing the origami structure. Interestingly, the ions drive hydrodynamic water flow through nanopores, which directly rotate the DNA blades, and high salt conditions reverse the rotation direction by altering ion distributions and solvent flow patterns.

DNA nanopores have been broadly applied in functional contexts. A recent review [222] provides a detailed overview of DNA-nanopore design strategies and their diverse biosensing and transport applications, offering broader context for these developments. Among these studies, Xing et al. [223] demonstrated that rationally designed DNA nanopores with tunable geometry enable direct, label-free electrical detection of large biomolecules, including proteins, and can be integrated with portable devices such as the MinION platform. Similarly, Peng et al. [224] showed that DNA nanopores can link lipid vesicles to form controlled molecular pathways for the transport of small molecules, while leakage is minimized through the use of removable DNA nanocaps.

Theoretical and computational models of these systems, from coarse-grained Brownian dynamics to continuum electrostatics, have been essential in rationalizing experimental observations, for example by linking ion permeation through origami plates to leakage currents or by predicting voltage-dependent deformations. Reviews on solid-state pores [5, 225] have emphasized that surface counterions within the electrical double layer govern selectivity, electroosmotic flow, and even reverse electrodialysis phenomena, underscoring how ions turn nanopores into active nanofluidic devices rather than passive channels. Zeng and coworkers [226] demonstrated that DNA can be compacted inside sub-attoliter cavities only in the presence of high Li^+ concentrations, directly linking counterion-mediated charge neutralization to the onset of current fluctuations. Simulations of 2D materials such as graphene and MoS_2 pores [227] also show that ion specificity and pore–DNA interactions define signal resolution at the single-nucleotide scale.

Taken together, these studies highlight a consistent theme: ions actively regulate DNA capture, translocation speed, compaction, and the resulting ionic current signals in nanopores. Experimental evidence provides measurable signatures, while theoretical and computational approaches are indispensable to interpret those signals in terms of molecular structure and electrostatics. This synergy has not only deepened our understanding of polymer physics under nanoscale confinement but has also paved the way for transformative applications in DNA sequencing, biosensing, and nanofluidic energy harvesting.

5.5 | DNA Tweezers

DNA tweezers are programmable, dynamic nanodevices that are typically made from two or more rigid double-stranded DNA segments that are connected by a flexible hinge that can switch reversibly between open and closed states [33, 228]. Their movement is based on strand displacement reactions mediated by short complementary sequences (toeholds) and does not require enzymes [33, 229]. The structure was first described in 2000 by Bernard Yurke and his collaborators, representing one of the first demonstrations of a molecular mechanism powered by DNA "fuel" [228]. Although they are not naturally occurring, these nanodevices represent valuable models for studying programmable molecular interactions and for developing biosensors [230], molecular logic systems as well as platforms to control enzymatic reactions [230–232].

The literature that simulates explicitly Yurke-type tweezers is surprisingly limited. There are essentially few works that actually model tweezer devices and explicitly or implicitly deal with ions, while the rest are "related" studies (hinges/joints, arm actuators) that are not tweezers in the strict sense but use the same simulation frameworks and the same assumptions about ions.

Early work from Ouldridge et al. [233] introduced a sequence-independent CG model of DNA, later known as oxDNA [234],

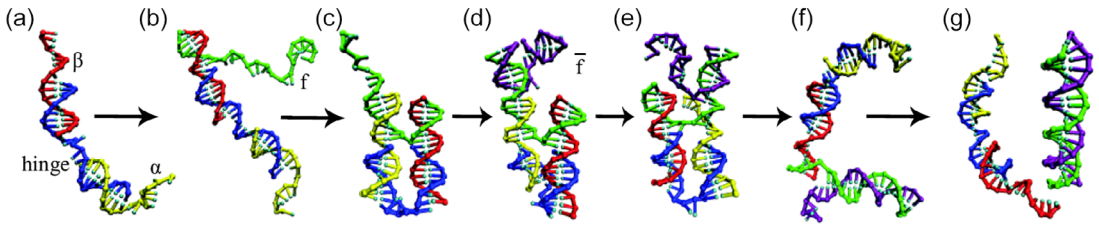

FIGURE 14 | Simulation snapshots showing the sequential operation of DNA tweezers. (a) Tweezers in the open state. (b) Introduction of fuel strand (f) leading to hybridization with one arm (β). (c) Fuel f hybridizes with the second arm (α), resulting in tweezer closure. (d) Antifuel strand $\bar{f}$ attaches to the toehold region of the f. (e) $\bar{f}$ initiates strand displacement of the first arm. (f) Reopening of the tweezers occurs as the first arm is released, while displacement of the second arm proceeds. (g) Complete hybridization between f and $\bar{f}$ yields the waste duplex. Reproduced with permission [233]. Copyright 2010, American Physical Society.

in which each nucleotide is treated as a rigid body with one backbone site and anisotropic interaction sites representing base repulsion, stacking and hydrogen bonding directions. These interaction potentials collectively produce the *B*-DNA helix structure, stabilize the duplex and contribute to the dangling-end effects, while finitely extensible nonlinear elastic (FENE) springs connect the backbone sites. All bases are treated identically, major and minor grooves are neglected, and the parameters were adjusted based on experimental data obtained for just one salt of concentration of 500 mM Na^+, a regime in which the Debye screening length is short (∼4.5 Å). Despite this simplification, the model quantitatively reproduces duplex melting, single-strand stacking, and hairpin transitions, and it captures the (weak) salt dependence consistent with experiments for a range of concentrations of monovalent ions (e.g., 50–120 mM Na^+), though it does not take into account the specificity of ions or divalent ions like Mg^{2+}.

To demonstrate the utility of this CG approach for DNA tweezers, the authors simulated a single device with one fuel (f) and antifuel ($\overline{f}$) strand in a periodic cell using unbiased sampling at 300 K. The tweezers consist of three strands forming two 10-bp duplex arms connected by a 4-base single-stranded hinge, each bearing 8-base overhangs. A 24-base f strand complementary to both overhangs closes the tweezers, while a complementary $\overline{f}$ strand initiates toehold-mediated strand displacement to reopen them. Using umbrella sampling and weighted histogram analysis method (WHAM), the authors constructed the full free-energy landscape for one operational cycle at 300 K, which is depicted in Figure 14.

The results showed that the duplex formation is highly cooperative, whereas the strand-displacement steps are nearly flat in free energy. A small ∼3 kT barrier was observed during the first displacement due to transient hairpin formation in the antifuel and steric restrictions in the tweezers' geometry, leading to slower kinetics for this step compared with the second displacement. Removing the hairpin-forming bases or reducing steric clashes eliminated the barrier. Thus, this study demonstrates for the first time that a CG model can describe the entire operational cycle of a DNA nanomachine and also how mechanical motion is directly related to the thermodynamic aspects of strand exchange under implicit ion conditions.

Dhakal et al. [235], on the other hand, combined experimental techniques and explicit-ion MD to dissect the structural determinants of tweezer actuation. In particular, they studied the Holliday-junction hinge, known to adopt one of two principal forms of coaxial stacking, iso-I and iso-II, whose equilibrium is strongly influenced by the ionic conditions (e.g., Mg^{2+}). These cations shield the negative charges on the phosphate groups of the DNA backbone, thereby stabilizing the more compact stacked configurations. Using single-molecule FRET, AFM, and MD with explicit Na^+ and Mg^{2+} ions, the authors were able to demonstrate that the incomplete closure of the tweezers was a consequence of flexible thymine spacers in the actuator and junction sequences that, under Mg^{2+} conditions, favored the less compact iso-II state. Using shorter lengths for the actuator linkers and a stronger hairpin stem resulted in an improved closing mechanism, while the substitution of all junctions with the Seeman J1 sequence [236] produced a more planar and homogeneous device since the J1 sequence creates a more favorable Mg^{2+} stabilized iso-I junction state than the junction states created by the original sequence. These optimized constructs were shown to greatly increase enzymatic activity when implemented in nanoreactors, proving that Mg^{2+} ion-mediated control over the stacking of junctions is crucial for both reliability and efficiency in mechanical properties. Dhakal et al. [235] related sequence-specific junction modification and ionic regulation to functional behavior in DNA machines by demonstrating how simulations involving explicit ions can complement the previously existing implicit-ion CG model.

Sedeh et al. [237] developed a multiscale Brownian dynamics framework that integrates finite-element (FE) mechanics with implicit-solvent dynamics to model large nucleic-acid assemblies far beyond atomistic timescales. The DNA duplexes were treated as elastic beams with empirical stretching, bending, and twisting stiffness, and the hydrodynamic drag was distributed via a Rotne-Prager tensor. Three systems were analyzed: a DNA tweezer with 204 base pairs, a nine-layer DNA ring origami with 3600 base pairs, and a pointer-shaped DNA origami figure with more than 7000 base pairs. The DNA tweezer was modeled with both Brownian dynamics and MD to validate the Brownian dynamics framework, while the ring and pointer origami structures were simulated using only Brownian dynamics to test the ability of the approach to analyze larger structures. All-atom MD simulations of the DNA tweezer were performed only for the DNA tweezer in explicit water (TIP3P) with Mg^{2+} and Cl^- ions to neutralize charges and reproduce an ionic environment of 12.5 mM Mg^{2+}, Distributions of local dihedral angles (J_{twist}) of four-way junctions obtained from the MD data were used to provide ground-state angles for the Brownian dynamics models. A quantitative correspondence between MD and Brownian dynamics was established to map atomic coordinates to translational and rotational degrees of freedom for every base pair. The results indicate that the Brownian dynamics simulations using a CG representation successfully captured the major motion of DNA assemblies, as observed by the all-atom MD simulations. CG simulations also found similar major modes of the DNA tweezer, specifically the cooperative motion of arm scissoring. Relaxation rates and fluctuation patterns calculated using Brownian dynamics were similar to those using MD; therefore, the reduced model used to perform these simulations was able to reproduce key mechanical and dynamical properties of this system. To conclude, the Brownian dynamics approach presented by Sedeh et al. [237] has proven to be an effective method for simulating the out-of-equilibrium conformational dynamics of very large nucleic acid assemblies while maintaining consistency with atomistic results. The Brownian dynamics methodology has been shown to be capable of accurately modeling the large-scale and collective motion of large DNA based structures, and therefore it presents itself as a viable tool for studying the dynamic behavior of structures made of nucleic acids in nucleic acid nanotechnology.

All of these research efforts on DNA tweezers have led to considerable advances in understanding and simulating the structure of DNA at the nanoscale, combining experimental techniques with simulations ranging from CG to atomistic models, accompanied by simulations of Brownian dynamics. These studies clearly demonstrate that DNA tweezers are not just models but represent a basis for building functional nanomachines capable of implementing well-defined processes, with potential applications in biotechnology and molecular nanorobotics.

5.6 | DNA as an Electromotor

The possibility of using DNA as an electromotor is related to the properties of charged, chiral molecules that could, in principle, couple electrical or electrochemical energy to motion [221, 238]. For a conventional macroscopic electromotor, this process depends on electromagnetic induction, where an electric current interacts with a magnetic field to generate torque. However, for nanoscales, the underlying physics is quite different, such that instead of requiring magnetic fields for the production of torque, the process depends instead on electrostatic and hydrodynamic forces between the charged molecular surfaces and its ionic environment [239–241]. In this case, the term electromotor is used by analogy to define any nanoscale system that is capable of transducing electrical input into directed mechanical rotation via electrochemical coupling. This system will require the presence of a stationary body, the stator, a movable one, the rotor, and a mechanism for coupling energy from the applied potential or ionic flux into mechanical work. The inherent chirality of DNA creates a breaking of the spatial symmetry, making it possible for directed rotation instead of Brownian motion to occur. In the following, we will review articles that are subject to this understanding of the meaning of electromotor.

For example, Maffeo et al. [238] demonstrated via extensive all-atom MD simulations how DNA (or RNA) duplexes respond while subjected to an electric field applied along its axis: they behave as nanoscale electromotors. 16-base-pair duplexes of *B*-DNA (right-handed), *L*-DNA (left-handed), and *A*-form RNA were equilibrated in 1 M KCl using the CHARMM36 force field with CUFIX ion corrections and TIP3P water. When applied the electric fields up to 100 mV/nm, the DNA/RNA duplex will experience a unidirectional torque at a speed of 10_9 rotations per minute dependent on the handedness of the helix. In the absence of the field, the rotation was random, determined only by Brownian motion. The authors identified electro-osmosis as the primary force behind the generation of the hydrodynamic torque experienced by the DNA/RNA duplex, which occurs as follows. The ionic species (K^+ and Cl^-) move significantly faster than the solvent (water), but when analyzing the angular-momentum flux it appears that about 80% of the torque experienced by the DNA/RNA duplex is generated by the movement of the solvent (water).

The protocol for measuring the torque generated by the DNA/RNA duplex is shown in Figure 15.

To measure the torque generated by the DNA/RNA duplex, one end of the duplex was connected to itself through the use of a harmonic restraint connecting the phosphorous atoms, making the DNA/RNA duplex appear infinitely long. In addition, Figure 15 (panels 15b–15f) show that the torque measured decreases linearly with increasing electric field strength and that the torque generated is directly proportional to the axial water velocity (panel 15h), demonstrating that the rotation of the DNA/RNA duplex is generated by the hydrodynamic coupling between the DNA/RNA duplex and the solvent (water) and not by the direct effect of the electric field on the backbone. In addition, the authors performed additional simulations where the DNA/RNA duplex was subjected to pressure-driven flow in the absence of an electric field and found the same level of torque as seen in the previous studies. These studies provide further evidence that the observed torque is a result of the fluid dynamic coupling between the DNA/RNA duplex and the solvent (water). Additionally, left-handed *L*-DNA rotates in the opposite direction of right-handed *B*-DNA, and *A*-form RNA exhibits similar field-torque scaling. Furthermore, the authors also simulated how DNA behaves when inserted into charged carbon nanopores and observed the same principle generating mechanical torque on attached nanostructures, indicating potential applications in the development of nanoscale electromechanical systems. The authors predict that the torques will be within the range that could be detected in nanopore experiments. In summary, the authors have demonstrated that DNA can function as a purely physical, electro-osmotic turbine that can convert electric-field

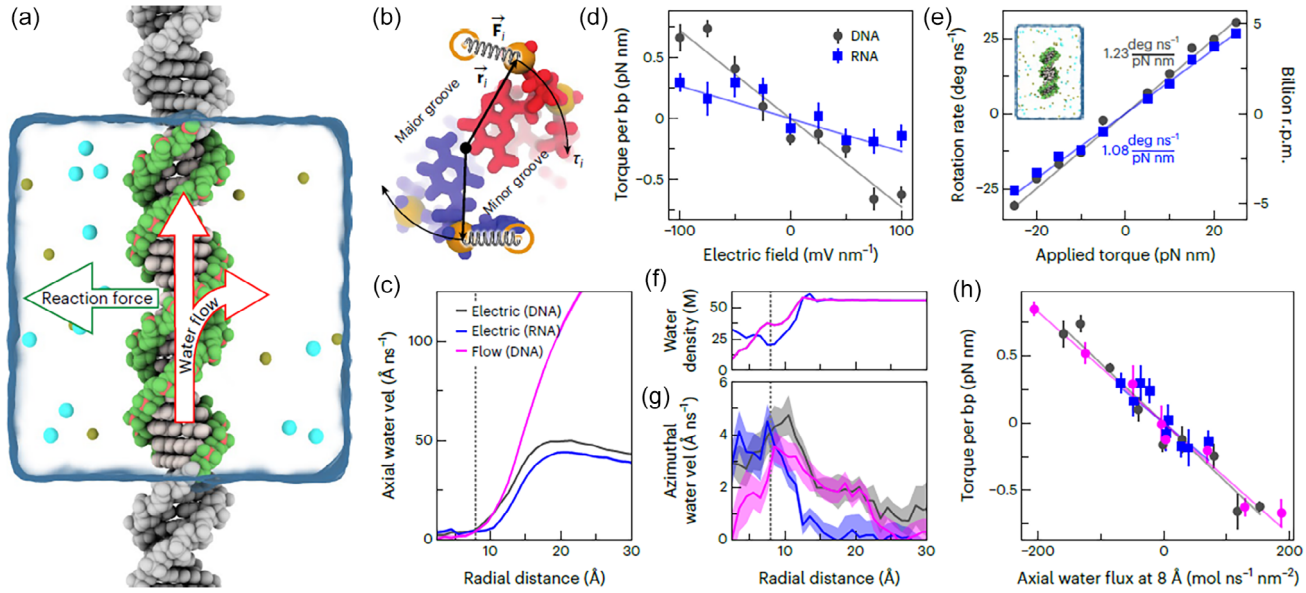

FIGURE 15 | Illustration of torque generation mechanism. (a) Simulation setup of an infinite DNA duplex. (b) Torque-measurement scheme. (c–e) Field-dependent torque and rotation dynamics. (f–h) Hydrodynamic profiles showing how water motion transfers angular momentum. Reproduced with permission [238]. Copyright 2022, Springer Nature Limited.

energy into rotary motion via the coupling of ions and solvents, thus providing a minimal model for chiral electromechanical transduction at the nanoscale. Implicit-solvent simulations, in which DNA was treated as a rigid body and ions as discrete particles governed by precomputed mean-force potentials [72], reproduced the all-atom results, indicating that torque generation is dominated by ion-driven hydrodynamics.

The same research group constructed chiral DNA origami turbines that can dock inside solid-state nanopores, spinning using transmembrane electrochemical potentials [221]. With single-molecule fluorescent imaging and cryo-electron microscopy, Shi et al. were able to demonstrate the ability for continuous unidirectional rotation, controlled by the handedness of the chiral turbines. The motors were driven either by salt concentration gradients or by applied voltages. Theoretical simulations for the motors using Poisson-Nernst-Planck-Stokes equations, along with molecular simulations in explicit water and ions analyzed the process by which the anisotropy in electrophoretic mobility and electroosmotic flow could produce rotors. The simulations showed that varying the strength of the electrolyte has a considerable effect on the aforementioned anisotropy, causing it to reverse direction. The chiral DNA turbines were also found to reach speeds of up to 10 rot/sec, requiring rotational torques that were rated in the range of tens of pN·nm, thereby confirming the electrohydrodynamic model.

The DNA origami rotary ratchet motor by Pumm et al. [242] is a synthetic molecular machine, where the direction of the rotor's movement is determined through the interaction of the nonequilibrium coupling between an alternating electric field and an asymmetric free-energy landscape. Simulations were done using the model of a Brownian particle moving within a time-dependent potential for the rotor, which showed that the directional bias for the rotor comes from field modulated energy barriers, not a constant mechanical torque. Alternating electric fields were used to induce oscillatory ion flow around the charged DNA structure, which biased the rotational diffusion of the DNA to create net unidirectional movement, while at equilibrium, there was no net movement due to the randomness of the motion. The experimental results for the rotational statistics of the DNA correlated with both Brownian dynamics simulations and fluctuation theorem relations and supported the ratchet based mechanism of motion. Additionally, a torsional spring version of this device was shown to store elastic energy through the action of the springs, resulting in a mechanical work output.

5.7 | DNA Origami

The concept of DNA origami dates back to Nadrian Seeman's "immobile junctions" [7], which laid the groundwork for building nanoscale frameworks from DNA strands. The field matured significantly with Paul Rothemund's introduction of DNA origami [6], the technique of folding a long single-stranded DNA scaffold into defined shapes using hundreds of complementary "staple" strands. Various architectural strategies include 2D planar origami (rectangles, triangles, and even artistic shapes such as maps and dolphins), 3D lattices such as honeycomb and square geometries, and curved and wireframe models, which reduce cation requirements and enhance biocompatibility. The hierarchical assembly (the combination of multiple DNA origami units into larger, functional complexes) represents a key direction for creating biologically relevant systems. Numerous features and properties of DNA origami are discussed in recent reviews [14], [243].

The use of DNA origami in biology and nanotechnology enables the precise nanoscale organization of biomolecules, facilitating studies of protein interactions, enzyme cascades, and cellular architectures. By patterning ligands or antigens with nanometer precision, DNA origami can modulate cellular signaling and immune responses [243]. Moreover, it serves as a versatile template for the organization of metals, semiconductors, and nanoparticles, advancing applications in plasmonics and photonic circuits. Of particular importance is the interaction of metal ions and clusters with the DNA framework incorporated into origami structures, as it governs their stability, electronic properties, and overall organization. In this section, we will highlight recent results concerning the interactions between metals and DNA origami, which play a crucial role in determining their structural integrity and functional potential.

In DNA origami, experimental folding efficiency, rigidity, and long-term stability depend on ion valence, concentration, and hydration properties. Fixed-charge force fields successfully reproduce global origami geometry but may underestimate ion-specific effects that influence helix–helix interactions and local stiffness. The use of computationally expensive polarizable force fields is hindered, however, by the large size of DNA origami systems. Atomistic simulations employing refined ion parameters have improved agreement with experimental measurements of DNA mechanical response and ion localization, enabling quantitative reproduction of ion-dependent stiffness changes [244], while more recent experimental and modeling studies of DNA origami demonstrate that folding efficiency and structural stability vary with Mg^{2+} concentration and mixed-salt conditions [245]. Some coarse-grained and continuum approaches, such as the oxDNA framework as applied and refined for DNA origami by Snodin et al., treat ions as effective electrostatic fields rather than explicit chemical species, yet still provide predictive insight into DNA origami architecture by capturing global rigidity, helix–helix spacing, and design-relevant mechanical constraints at the origami scale [246]. These ion-dependent mechanical properties are directly relevant for applications of DNA origami as functional nanodevices, where rigidity, helix–helix spacing, and local flexibility determine structural integrity under mechanical stress and operating conditions. In this context, multiscale modeling enables the selection of ionic environments that support robust device performance.

Yoo and coworkers [244] performed the first all-atom MD simulations of complete DNA origami structures. Three models of DNA origami were considered: HC (honeycomb) lattice—a straight 6×3 pleated DNA bundle; SQ (square) lattice—a straight 4×4 pleated DNA bundle; HC-90°–a 6×3 pleated structure with a programmed 90° bend. Each structure was immersed in a 10 mM $MgCl_2$ solution, as magnesium ions are known to neutralize DNA's negative charge and stabilize multihelix assemblies. The results show that across all three systems, the simulated DNA origami objects retained their overall designed shapes throughout the MD runs. However, local deviations from idealized geometries were found. These deviations arose from steric crowding, electrostatic repulsion, and solvent-mediated interactions. Magnesium ions (Mg^{2+}) are distributed nonuniformly within the origami bundles, clustering near phosphate backbones to neutralize DNA's

negative charge. Their average distance from phosphorus atoms was ∼5.4 Å and their diffusion coefficients were significantly reduced inside the origami structures compared to the bulk solution, highlighting the restricted ion mobility within the dense

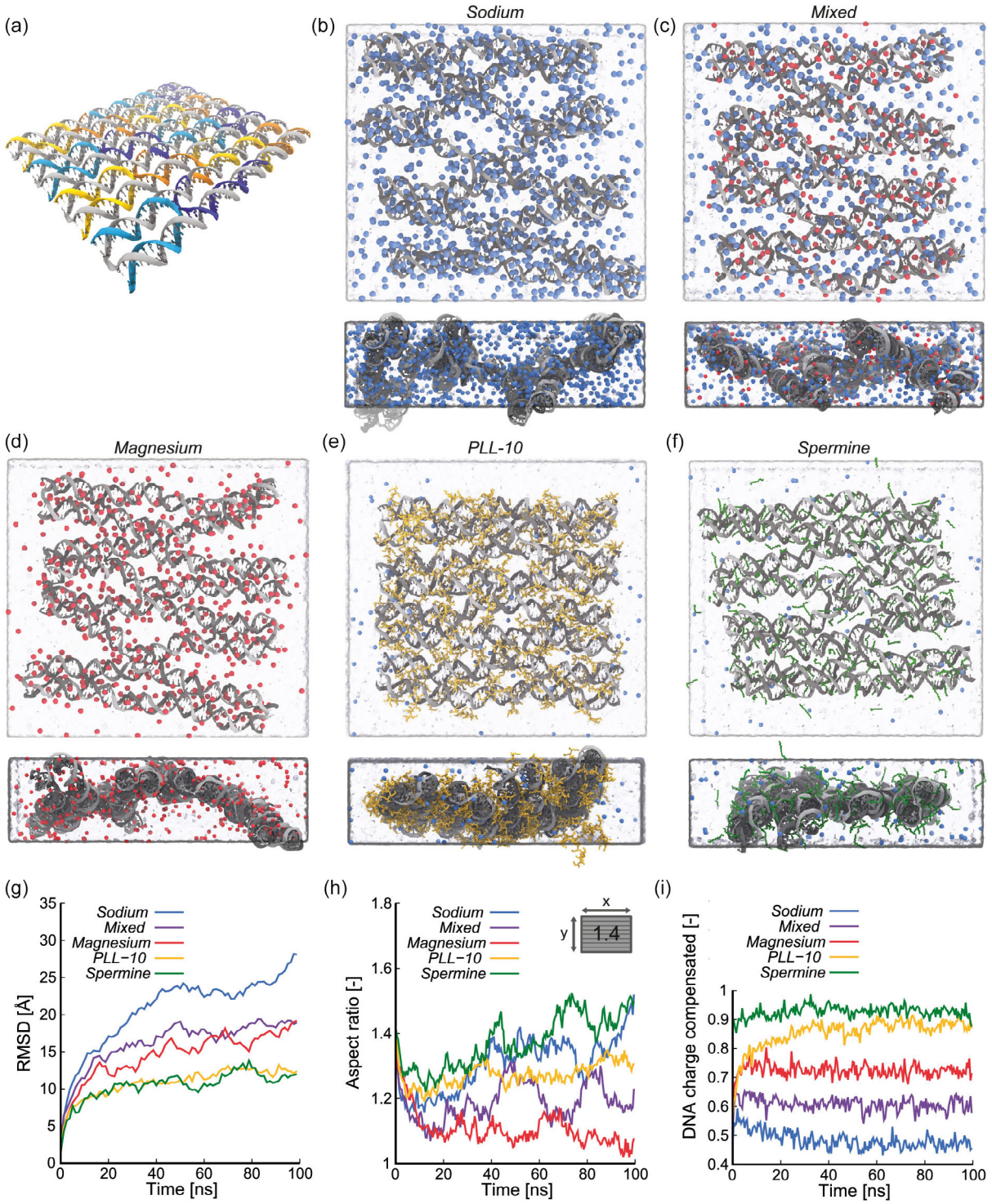

FIGURE 16 | Influence of various counterions on DNA origami studied by atomistic MD simulations [245]. (a) Simulated rectangular DNA origami structure. The scaffold and staple strands are shown in gray and in color, respectively. (b-f) Top and side views of the DNA origami systems with sodium, mixed, magnesium, *PLL-10*, and spermine counterions at the end of the simulation trajectories. Coloring scheme: DNA origami—in gray; water—in light blue; the counterions Na^{+}—blue; Mg^{2+}—red; K_{10}—yellow; spermine^{4+}—green. (g) Time dependence of the root–mean–square deviation (RMSD) of the DNA double helix backbone atoms with respect to their initial positions. (h) Time dependence of the length-to-width aspect ratio of the DNA origami; the initial aspect ratio is shown in the inset. (i) Time dependence of the fraction of the DNA macromolecule's electrostatic charge neutralized by counterions. Counterions are considered to belong to the DNA atmosphere if they are within 5 Å of any DNA atom for all counterion types. Reproduced under the terms of the CC-BY-NC-ND license [245]. Copyright 2019, American Chemical Society.

DNA lattice. This work provided unprecedented insight into conformation, dynamics, and local mechanical properties of DNA origami objects in solution, offering a microscopic complement to experimental studies. Their findings show that DNA origami is not a static lattice but a dynamic, fluctuating system, whose stability arises from a balance of electrostatics, sterics, and solvation effects.

Roodhuizen et al. [245] studied the molecular-level mechanisms by which different cations stabilize (or destabilize) a representative DNA origami nanostructure, using atomistic MD simulations for a 512-base-pair DNA origami rectangle immersed in explicit water with different ionic environments: Mg^{2+}, Na^{+}, K_{10} (decameric oligolysine – *PLL-10*), and spermine^{4+}, and combinations of these species and concentrations (Figure 16a–f). The results show that monovalent-only (Na^{+}) environments exhibited large deviations from the designed origami geometry, indicating that Na^{+} alone poorly stabilizes the compact multihelix architecture on the simulated timescale. Mg^{2+}, spermine^{4+} and K_{10} stabilized the structure (Figure 16g,h). These cations preserved global shape and limited helix repulsion mainly due to effective electrostatic screening of the DNA phosphate groups (Figure 16i). Mg^{2+} frequently localized in close coordination to phosphate groups and in grooves, forming well-defined inner-sphere and outer-sphere complexes that screen local charge. Multivalent polyamines (spermine) and oligolysines tended to connect helices by simultaneous contacts to phosphates on adjacent helices, acting as inter-helix crosslinks. Thus the work [245] delivers a careful, insightful atomistic study that advances mechanistic understanding of how different counterions stabilize DNA origami.

Another important step in the computational analysis of DNA nanotechnology was made in [246]. The oxDNA coarse-grained model is used to analyze the properties of archetypal 2D and 3D DNA origami. The results are compared with the experimental data, including cryo-EM and SAXS, to validate the model's predictive capabilities. The oxDNA model [234, 247, 248] is particularly promising because it represents DNA at the nucleotide level, with well balanced resolution and computational efficiency. The oxDNA2 model was used, which is an improved version of the oxDNA model. Simulations were performed in 0.5 M NaCl salt solution and conducted on both isolated motifs (Holliday junctions) and complete origami structures (2D and 3D designs). The results showed that oxDNA favors a left-handed junction geometry, whereas experimental studies indicate a right-handed preference. While this represents a limitation of the model, the authors argue that it does not significantly hinder the ability of oxDNA to capture origami structure. In practice, junctions in origami are constrained near anti-parallel geometries, meaning the deviations in chirality produce similar levels of stress in both model and experiment. Importantly, oxDNA simulations reproduced key features such as helix bending away from junctions, a phenomenon central to the so-called "weave" pattern observed in origami structures.

The article [249] presents a pioneering approach to the design of dynamic DNA nanostructures whose assembly and disassembly can be reversibly controlled by metal ions. The study integrates G-quadruplex motifs into DNA origami tiles, creating ion-responsive nanomaterials that undergo conformational changes depending on environmental conditions. G-quadruplexes are four-stranded DNA structures formed from guanine-rich sequences. In the presence of monovalent ions such as potassium (K^{+}) or sodium (Na^{+}), guanine bases associate through Hoogsteen hydrogen bonding to form G-quartets, which stack to build G-quadruplexes. The stability and topology of these structures depend strongly on the ion type and concentration, with K^{+} typically producing more stable complexes than Na^{+}. The research [249] demonstrated the reversible, ion-dependent self-assembly of DNA origami dimers mediated by G-quadruplex interactions. Their experiments showed that potassium ions induce folding of the G-quadruplexes, leading to structural disassembly, while ion removal reverses the process. This mechanism introduces a controllable and repeatable form of dynamic behavior in DNA nanostructures, which is an essential feature for designing intelligent nanomaterials capable of multiple operational states. Furthermore, when the number of G-quadruplex-forming sequences was reduced from four to one, the binding affinity decreased significantly. Dimers containing only one G-quadruplex showed minimal responsiveness to K^{+}, emphasizing that multiple sticky ends are necessary to balance structural stability and responsiveness. To the best of our knowledge, no computational modeling studies of G-quadruplex-containing DNA origami systems have been reported to date. We anticipate that such modeling will require particularly careful treatment of ion-DNA interactions and solvent effects, given their critical role in determining G-quadruplex stability and responsiveness, as highlighted in previous studies [250, 251]. Hierarchical multiscale methods previously used for both duplex and quadruplex DNA structures [252–254] could take advantage of atomistic and even polarizable force field results at smaller scales, which have been shown to provide the most accurate description of G-quadruplex ion coordination [255], to inform parameterization strategies and retain ion-specific effects in simulations of large origami systems.

5.8 | DNA Hydrogel

DNA hydrogels provide a clear illustration of why predictive materials design in stimuli-responsive soft matter requires a multiscale modeling framework. Atomistic simulations are essential for resolving local ion binding, hydration structure, and specific ion-DNA interactions, but they are inherently insufficient to capture collective properties such as swelling, elasticity, and ion transport observed experimentally. These macroscopic responses emerge from mesoscale organization and network connectivity, which must be described using coarse-grained or continuum approaches. Such mesoscale models enable quantitative prediction of hydrogel structure and mechanical behavior [256, 257]. However, the explicit incorporation of experimentally observed [258] sensitivity to ionic strength, ion valence, and competitive binding effects remains an open challenge. As discussed in the preceding subsection on DNA origami, hierarchical multiscale strategies that combine atomistic and mesoscale descriptions offer a promising route to retain ion-specific effects in simulations of large DNA-based assemblies.

DNA hydrogels represent a versatile class of programmable, biocompatible, and ion- and stimuli-responsive biomaterials formed through the cross-linking of DNA strands into polymer networks that mimic the physical properties of natural tissues [259]. Various construction techniques, such as self-assembly based on sequence-specific hybridization, enzymatic cross-linking using ligases, hybridization chain reaction, and rolling circle amplification,

enable precise control over their structure and functionality [260]. Hybrid DNA hydrogels, which integrate natural or synthetic polymers, biomolecules, or nanomaterials with DNA, combine the advantages of multiple components to enhance mechanical stability, responsiveness, and biofunctionality [261]. Cross-linking can occur through chemical (covalent) or physical (noncovalent) interactions, with the chosen method determining the hydrogel's stability, mechanical properties, and environmental sensitivity [259]. The sequence programmability of DNA allows for the design of hydrogels with tunable stiffness, elasticity, and responsiveness to external stimuli such as pH, temperature, and ionic strength. These properties make DNA hydrogels particularly promising for biomedical applications, including controlled and targeted drug delivery, biosensing, tissue engineering, and cell culture [261]. By encapsulating therapeutic agents and releasing them in response to specific triggers, DNA hydrogels offer precise drug delivery systems, while their structural adaptability enables the creation of sensitive biosensors and injectable therapeutic matrices. Furthermore, their ability to mimic the extracellular matrix provides a favorable environment for cell attachment, proliferation, and differentiation, facilitating tissue regeneration and serving as advanced in vitro platforms for drug testing and discovery [260].

Li et al. [262] proposed a conceptual framework for the rational design of DNA hydrogels linking polymer-level physical descriptors to macroscopic material properties. Focusing on backbone rigidity and cross-linking kinetics as key determinants, the authors elucidate how molecular-level features govern mechanical stiffness, diffusion, swelling, and dynamic responsiveness. The review highlights that hydrogels with rigid dsDNA networks tend to exhibit greater stiffness and reduced swelling than flexible ssDNA networks, while flexibility enhances assembly efficiency and adaptability, underscoring the need for a balance between rigidity and functionality. The analysis of cross-linking kinetics reveals that long-lived covalent bonds yield robust yet less adaptable hydrogels, whereas transient supramolecular cross-links enable self-healing, shear-thinning, and stimuli-responsive behavior. From this synthesis, the concept of tuning cross-linker lifetime emerges as a crucial but often overlooked design principle. From these insights Li et al. outline how DNA hydrogels may be tailored for specific biomedical purposes: rigid scaffolds for bone or cartilage regeneration, permeable networks for cell culture, and dynamic matrices for controlled drug delivery and biosensing.

Ion-mediated DNA condensation effects are particularly evident in DNA hydrogels. Jeon et al. [258] demonstrate the use of polycations (especially spermine^{4+}) to condense DNA hydrogels, thereby making them highly resistant to enzymatic degradation. Subsequent addition of NaCl expands the hydrogel back to its original state, restoring degradability and enabling programmed release. This balance between condensation (protection) and expansion (release) provides a pathway for engineering DNA hydrogels as versatile, tunable molecular carriers. Spermine^{4+} was employed to condense the hydrogels through electrostatic interactions with DNA backbones. This condensation reduced hydrogel volume drastically, while protecting against nuclease degradation. To trigger expansion, Na^+ ions were then added. Because Na^+ competes with spermine^{4+} for DNA binding, it disrupts the spermine–DNA interaction, restoring the hydrogel's uncondensed structure. Repeated condensation-expansion cycles were achieved by alternately exposing hydrogels to spermine and NaCl, demonstrating reversible programmability. Hydrogels responded differently depending on cation valence. Tri- and tetravalent cations (spermidine^{3+}, cobalt hexammine^{3+}, spermine^{4+}) induced strong condensation at low concentrations, reducing hydrogel area by ~90%. Monovalent and divalent cations (Na^+, Mg^{2+}) were far less effective. This confirms that multivalent cations drive phase separation and condensation by binding strongly to DNA backbones. By adjusting the DNA cross-link length and ratio, the condensation kinetics can be controlled without altering the final condensation level [258]. Shorter cross-links produced slower condensation, offering a design variable for tuning DNA hydrogel response kinetics (see Figure 17). The expansion was tunable with salt concentration: higher NaCl induced faster expansion, while lower concentrations delayed it. Condensation and expansion cycles were repeatable, demonstrating a reversible and programmable system.

DNA-based hydrogels also offer important practical applications. The paper [263] presents a novel strategy for converting biomass-derived DNA directly into functional biodegradable materials—such as gels, membranes, and plastics, without first breaking DNA down into monomeric building blocks or conducting conventional polymer syntheses. The authors show that DNA harvested from biomass can be processed into diverse materials with useful and sometimes unexpected properties. They demonstrate large-scale processing, cost-effectiveness, and several

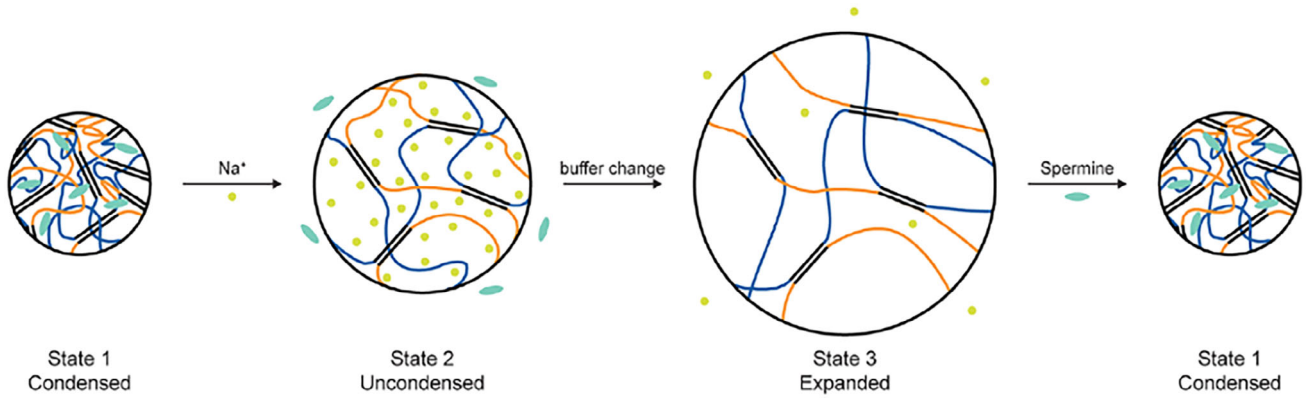

FIGURE 17 | Schematic illustrations of repetitive condensation and expansion of hydrogels under varying ionic conditions [258]. Adapted with permission [258]. Copyright 2024, American Chemical Society.

applications, including drug delivery, adhesion, composite materials, patterning, and even using DNA-based plastics for cell-free protein production. The overall goal is to reduce dependence on petrochemicals by offering an alternative based on renewable, degradable biomass. The authors aim to use DNA as-is (in sufficiently pure form) to make materials, by using physical processing (cross-linking, casting, shaping) to create gels, membranes and plastics. This could lower cost, energy, and synthetic complexity.

To elucidate the physical and chemical properties of DNA hydrogels, coarse-grained molecular dynamics simulations at different levels of molecular organization are widely used [256, 257]. Wang et al. [256] present a computational study that clarifies the structural determinants of DNA-cross-linked PEG hydrogels and their ability to function as drug carriers. The results demonstrate that 6-armed, high-molecular-weight PEG precursors at sufficiently high concentrations produce percolated networks with narrow pore distributions, enhancing drug retention. These findings not only deepen the fundamental understanding of hydrogel architecture but also provide a rational framework for designing DNA-responsive biomaterials for therapeutic applications. By combining coarse-grained MD simulations with structural and diffusion analyses, the authors bridge the gap between nanoscale hydrogel morphology and macroscopic drug delivery performance. The work highlights the promise of DNA-mediated hydrogels as customizable, biocompatible carriers in advanced drug delivery systems. The study by Xing et al. [257] demonstrates that coarse-grained modeling can successfully capture the structural and mechanical properties of DNA hydrogels. The model reproduces melting transitions, reveals 3D structural features, and predicts linear elasticity consistent with experimental trends. Importantly, it highlights how the programmability of DNA interactions can be exploited to control hydrogel mechanics in ways not possible with conventional polymers. Despite limitations in capturing dissipative rheology, the model sets the stage for future studies of responsive, hierarchical, and multifunctional DNA hydrogels. In these works [256, 257] counterions were not modeled explicitly and their role was effectively implicit, entering through coarse-grained interactions.

5.9 | DNA Walker

DNA walkers are DNA-based molecular machines that move stepwise along a track through the programmable formation and disruption of base pairs. At their core, the DNA walkers use toehold-mediated strand displacement [264, 265] to attach and detach their "feet" from specific footholds on a track, allowing forward movement directed by fuel strands, enzymes, or differences in binding energy [266–268]. The ability to engineer the kinetic and mechanical properties of these nanoscale machines has led to applications in signal amplification, cargo transport [264], and even nascent nanorobotics [266]. However, because DNA is a polyelectrolyte, the electrostatic repulsion among phosphates and the screening by monovalent or divalent ions strongly influence both the thermodynamics and the kinetics of these systems. Experimental walkers typically operate in buffers with high concentrations of Na^+ or Mg^{2+} ions to stabilize duplexes and origami structures. Computational models used to design and optimize DNA walkers must, therefore, capture the effects of ions on base pairing, stacking, and the mechanical elasticity of DNA. The earliest generation of coarse-grained models for DNA nanotechnology, such as the oxDNA model, treats each nucleotide as a rigid body with interaction sites representing the backbone, base stacking, and hydrogen bonding interactions. The parameterization of the average-base version of oxDNA was performed at high monovalent salt concentrations. The model used by Ouldridge and coworkers [269] was fitted to reproduce the melting temperatures and mechanical properties of average DNA sequences at a monovalent salt concentration of 0.5 M, so that electrostatic repulsion could be approximated by short-range excluded-volume interactions. This assumption allows the model to neglect explicit Coulombic interactions and treat repulsion through excluded volumes. The high-salt parameterization is justified because most DNA nanotechnology experiments are performed in buffers that suppress interstrand repulsion.

One of the earliest simulation studies to apply such a CG model to a DNA walker was conducted by Ouldridge et al. [269], who investigated the operation of a two-footed DNA walker designed to step along a reusable track. Virtual Move Monte Carlo (VMMC) simulation, Langevin dynamics, umbrella sampling, and forward flux sampling were performed in order to investigate the movement of the walker on tracks of different lengths and tensions. The results of the simulations showed that increasing the tension of the track caused an increase in the bias toward moving the walker one base pair at a time, reduced mis-binding of the walker to the track, and facilitated recovery of the walker when it moved past a certain point by creating fraying of the duplex. The study also examined the kinetics of release of the fuel and the displacement of the strands of DNA. It was found that the remaining pieces of fuel fragment influenced the path the walker took when it reattached to the track.

Several subsequent studies have adopted similar coarse-grained models using the framework of either oxDNA or oxDNA2, varying mainly in either geometry or integration with experiments, and without varying the ionic conditions. For example, a "burnt-bridges" model for a molecular walker has been used by Šulc et al. [270] to explore free energy landscapes for various distances between the stators, and for different lengths of the toehold domain, while Khara et al. [271] used a combination of single-molecule FRET and simulations using the framework of oxDNA in studying the kinetic properties of the molecular walking process on a DNA origami surface for various sizes and orientations. An example using chemomechanical coupling for an autonomous bipedal walking model has also been presented by Tee et al. [272], and for a circular origami surface for autonomous motion by Siti et al. [273], both using extensions of the framework for oxDNA. However, in each of these studies, the ionic conditions are also implicitly taken into account through the salt-concentration-dependent parameters used for the model, namely 0.5 M monovalent salt, without varying the ionic conditions. Other studies, such as Wang et al. [274] or Li et al. [275] and more recently Mou et al. [276] continued with implicit ion models of salt, even in more complex functional systems such as theranostic devices based on DNA walkers bound to nanoparticles. In the latter work, for example, kinetics was optimized with simulation-guided design, with ion interactions modeled implicitly with the oxDNA model parameterization.

In contrast to these CG approaches, Xu et al. [277] introduced a general analytical framework to describe the mechanics of bipedal DNA-based nanomotors. The motor is modeled as an

elastic dimer made up of two identical elastic legs that are coupled to a symmetric periodic potential, representing the molecular track. By coupling leg elasticity to phase-shifted periodic driving applied to each leg, the framework encapsulates transitions between metastable mechanical configurations involving single and double leg attachment. This analytical and numerical study demonstrated multiple regimes, including hand over hand, inch worm, and phase winding types of motion; it also demonstrated a "superlubric" regime at a phase locked state in which the effective friction experienced by the nanomotor is minimized. Additionally, Xu et al. [277] showed that the model reproduced the qualitative behaviors of synthetic and biological walkers, and that elasticity and phase coupling were necessary for the low-friction, low-dissipation operation of nanoscale transport.

A recent study by Ogieva et al. [278] investigated how geometric confinement of DNA tracks can accelerate walker motion. The authors combined CG oxDNA simulations with an analytical first-passage framework describing tethered binding in the reaction-limited regime. In this model, the walker-track pair is treated as a tethered reactive system diffusing on an effective angular-radial energy landscape, and the stepping rate is obtained using Szabo's relation for the effective surface rate constant. The authors examined two different geometrical constraints: (i) the double-stranded tails of the foothold bound to the walker, leading to a pseudo-rotationally constrained motion process for the walker in the substrate plane (pseudo-rotationally constrained system), and (ii) the embedding of the substrate path for the walking process in origami trenches, leading to lateral constraints for the walking process (lateral or trenches-constrained system). The simulation and kinetic analysis indicate that for pseudo-rotationally constrained systems, it is possible to observe a four-fold reduction in the average walking time, and for lateral (in trenches) constraints, it is possible to observe a three-fold reduction in the average walking time, along with an increase in its average lateral dimension leading to a partial loss in walking speedup, since its average height increases.

5.10 | DNAzymes

DNAzymes, or deoxyribozymes, are single-stranded DNA molecules that have enzymatic properties, first identified by in vitro selection in the mid-1990s [279, 280]. Although DNA has no confirmed naturally evolved enzymatic role [281], its capacity to fold into complex tertiary structures enables DNA to catalyze diverse reactions, from RNA cleavage and ligation to phosphorylation and peroxidase activity [282]. Among the numerous DNAzymes discovered, the RNA-cleaving 8–17 and 10–23 motifs remain the most extensively characterized, particularly as models for gene manipulation and biosensing [283, 284]. Both require divalent metal ions, notably Mg^{2+} and Pb^{2+}, to promote catalysis through electrostatic stabilization and activation of the scissile phosphate [280]. Because intracellular metal-ion concentrations are tightly regulated, understanding ion-enzyme interactions at the atomistic level is critical for improving DNAzyme function in vivo. Computational modeling has thus become indispensable for uncovering the structural dynamics and catalytic mechanisms of DNAzymes under varying ionic conditions, complementing the sparse experimental structures available.

DNAzymes provide a clear example in which advances in molecular modeling have helped reconcile discrepancies between structural interpretations and experimental observations. Early simulations based on fixed-charge force fields successfully captured global folding and prereactive conformational ensembles but were inherently unable to account for experimentally observed metal-ion specificity at the catalytic level or for chemical reaction rates. More recent studies combining explicit-ion molecular dynamics with high-resolution structural data have clarified how different metal ions organize the active site, stabilize catalytically competent geometries, and modulate hydrogen-bond networks, thereby resolving long-standing inconsistencies between folding and activity measurements [169, 285]. In parallel, multiscale simulations incorporating QM/MM approaches have provided a DNAzyme-specific view of how metal ions participate directly in catalysis, as demonstrated by Aranda et al., who resolved the full reaction mechanism of the 9DB1 DNAzyme and identified a two-metal-ion catalytic strategy [171]. At a more general level, mechanistic and computational reviews have emphasized that discrepancies in metal-ion selectivity cannot be fully rationalized without explicitly accounting for polarization effects and metal–ligand charge transfer within the catalytic core, highlighting fundamental limitations of fixed-charge force fields [168]. Early computational studies of DNAzymes began with Kenward and Dorfman [286] who performed the first CG Brownian dynamics simulations of the 10–23 DNAzyme to investigate its structural and conformational dynamics. Their model reproduced the experimentally measured end-to-end distance of the enzyme–substrate complex and was able to qualitatively explain the effects of recognition-arm length and point mutations. However, electrostatics and metal ions were not explicitly included, as the authors assumed that such effects play a secondary role in determining the DNAzyme's tertiary structure compared with base pairing, stacking, excluded volume, and chain semiflexibility. The study introduced a CG framework intended as a starting point for more detailed atomistic simulations of DNAzymes. A decade later, the field advanced dramatically with classical MD simulations being able to provide refined molecular insight into their catalytic behavior. Ekesan and York [169] investigated the 8–17 DNAzyme in explicit solvent using four idealized molecular states: the standard, general-base-deprotonated, activated precursor, and transition-state mimic, all of them representing conceptual points along the proposed RNA cleavage pathway. Simulations have shown how the changes in the system's state favor nucleophile activation and transition state formation. In the initial state, the system is in a prereactive configuration, stable but unproductive. As the general base is activated by deprotonation, the ionic environment (particularly Pb^{2+} and Na^{+} ions) contributes to the correct alignment and polarization of the groups involved in the reaction, facilitating the nucleophilic attack on the phosphodiester bond. In the transition state, metal ions play an essential role in stabilizing the accumulated negative charges, although no energetic barriers were calculated within classical MD. Therefore, simulations indicate that catalytic efficiency arises from cooperative interactions between electrostatic effects and the structural reorganization of the system. Importantly, the authors emphasize that these models are idealized constructs which may not correspond to real reaction intermediates and that the precise catalytic mechanism cannot be resolved at the classical MD level. The quantitative estimation of barrier energies or proton-transfer steps will be achieved via quantum or QM/MM simulations, as well as experimental verification of proposed binding modes of metal ions.

Ganguly et al. [287] employed MD and free energy simulations to explore a possible hydrogen-bond-mediated catalytic mechanism, termed tertiary γ-hydrogen-bond network (3° γ(HBN)) catalysis, in several RNA and DNA cleavage systems, including the Pb^{2+}-dependent 8–17 DNAzyme. The simulations suggest that divalent metal coordination to a nonbridging phosphate oxygen can reorganize the active-site hydrogen-bond network, suppressing unproductive O2′-phosphate interactions and favoring a productive O2′-guanine contact that could promote nucleophile activation. The effect was most pronounced in the 8–17 DNAzyme model. While these computational results highlight a potentially metal-tunable feature of nucleic acid catalysis, experimental validation is needed to assess whether 3° γ(HBN) interactions operate in real systems.

A completely different simulation-driven strategy for designing DNAzyme-based nanomachines for the detection of single-nucleotide variants was proposed by Zhang et al. [288]. The authors combined thermodynamic modeling and kinetic simulations to optimize the system before experiments. Using NUPACK and the SantaLucia internal-loop model, they calculated standard Gibbs free energies (ΔG) for DNA hybridization and adjusted toehold lengths so that the toehold-exchange reaction approached thermodynamic equilibrium ($\Delta G \approx 0$). Although there is no mention of how ionic effects were modeled, the authors imply that they were implicitly included through the thermodynamic parameters used by NUPACK. Reaction kinetics were modeled in MATLAB through ordinary differential equations solved with the ode23s stiff solver, allowing simulation of the strand displacement and noncovalent DNA catalysis reactions. These simulations mapped the trade-off between sensitivity and specificity, guided the adjustment of toehold domains and reactant ratios, and predicted dynamic trends later confirmed experimentally. Through this combined computational-experimental approach, the study demonstrates how the in silico modeling can help guide DNAzyme design, leading to the improvement of detection sensitivity and minimizing trial-and-error efforts in the design of DNA biosensors.

A combined experimental-theoretical approach was used by Borggräfe et al. [168] in order to investigate the structural dynamics of the precatalytic state of the 10–23 DNAzyme in complex with its RNA substrate. The experimental investigation was performed by employing high-resolution NMR-spectroscopic measurements, which were supported by MD simulations. In the simulations, Mg^{2+} ions were modeled as fully solvated and able to move freely, forming and breaking contacts with the nucleic acid instead of being fixed at specific sites. The simulations produced a detailed, experimentally verified model of the 10–23 DNAzyme:RNA complex under nearly physiological conditions, in which the substrate-binding arms are compact and well organized, while the catalytic loop stays flexible and samples conformations compatible with catalysis.

Three metal-binding sites (MBS I–III) were identified for their function in association with the 10–23 DNAzyme:RNA complex, each serving a distinct role: MBS I, at the junction between the DNAzyme's two substrate-binding arms, acts mainly as a structural scaffold. Metal ions here neutralize the strong negative

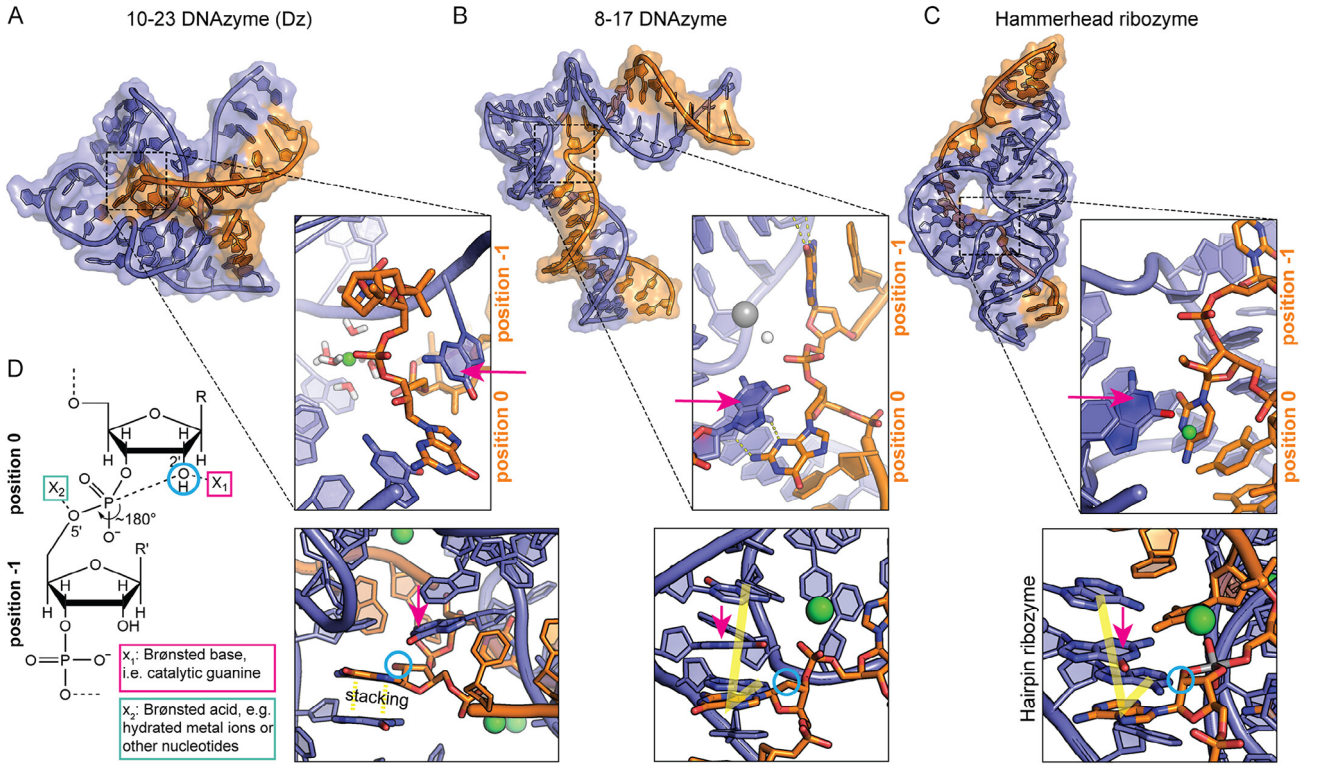

FIGURE 18 | Structural representations of RNA cleavage sites for (A) the 10–23 DNAzyme (PDB: 7PDU), (B) the 8–17 DNAzyme (PDB: 5XM8), (C) the hammerhead (top, PDB: 3ZP8) and hairpin (bottom, PDB: 1M5O) ribozymes. DNA strands are shown in blue, RNA substrates in orange, Mg^{2+} ions in green, and Pb^{2+} in gray, and (D) a schematic of the reactive linkage arranged for in-line attack, with catalytic acid/base sites marked. Reproduced under the terms of the CC-BY-NC license [168]. Copyright 2022, The Authors. The FEBS Journal published by John Wiley & Sons Ltd on behalf of Federation of European Biochemical Societies.

charges of the DNA backbones, allowing the molecule to fold into a compact active form. MBS II, closer to the 5′ end of the loop, is involved in activation: Mg^{2+}-induces folding and stacking between the substrate base rG_0 (the riboguanosine residue at the cleavage site) and G6 that positions the reactive bond for in-line cleavage. MBS III, near the loops 3′ end, has a catalytic role. Metal-ion coordination close to another guanine (G14) makes that base more effective at removing a proton from the RNA backbone at the reaction site, which is a key chemical step leading to bond cleavage. The MD simulations also showed that the RNA-substrate is bent, such that the O2′–P–O5′ linkage of rG_0, is positioned in a manner that facilitates an in-line attack. This configuration is shown in Figure 18D. Furthermore, the MD simulations demonstrated the presence of a stacking interaction between G6 and rG_0 that facilitates alignment of the reactive center (Figure 18A). In addition, the MD simulations revealed the existence of a π-π stacked interaction between G6 and rG_0, that favors the orientation of the reactive center and the formation of the in-line attack conformation. However, the 8–17 DNAzyme and the hairpin ribozyme (Figure 18B,C) use the L-platform strategy—its characteristic structure in which the catalytic guanine residue is found to be sandwiched between the neighboring bases of the catalyst and the substrate at the cleavage point. Taken together, the findings reported by Borggräfe et al. [168] underscore the structural diversity of catalytic DNA molecules, as well as the role of metal ion interactions in modulating this structural landscape.

Building on these structural and mechanistic insights, Nguyen et al. [289] applied the knowledge of metal-ion-induced conformational dynamics reported by Borggräfe et al. [168] to guide the chemical optimization of the 10–23 DNAzyme. Through iterative 'design-build-test-learn' cycles, the authors developed modified variants with enhanced catalytic efficiency and reduced Mg^{2+} dependence, demonstrating how structural understanding of ionic effects can inform the rational engineering of more active DNAzymes.

Complementary insights emerged from the work of Amini and Bashirbanaem [290], who used classical MD simulations to clarify the ambiguities in the reaction mechanism of the ligating DNAzyme 9DB1. Starting from the post-catalytic crystal structure of the DNAzyme 9DB1, they developed an alternative possible pre–catalytic complex and simulated various structural and sequence mutations to demonstrate how these mutations affect the arrangement within the catalytically important site. These simulations utilized both explicit solvation and a mixture of the cations Na^+ and Mg^{2+} in a mixed ion solution where the divalent cations were allowed to diffuse and move throughout the solution rather than being placed into predetermined locations. The results show that the divalent Mg^{2+} ions participate in the stabilization of the phosphate and nucleobase groups by means of an outer sphere electrostatic method, enabling the reactive geometry to be maintained, while the Na^+ ions provide general electrostatic screening and stabilize the base-pair product. The conformational changes noted are interpreted in relation to the experimental rate differences for the mutants constructed and support previous experimental conclusions regarding metal dependence. The authors highlighted that ignoring monovalent ions can lead to misinterpretation of catalytic geometries, underscoring the necessity of modeling mixed-ion systems when simulating DNAzyme catalysis.

Recent high-resolution studies have consolidated this mechanistic landscape. Wieruszewska et al. [285] used NMR spectroscopy to determine the solution structure of the canonical 8–17 DNAzyme bound to Zn^{2+} and compared it with the Pb^{2+}-bound crystal form. This solution structure was very similar to the Pb^{2+} structure (the RMSD between the two structures is $\approx$ 1.3 Å) which indicates Zn^{2+}, Mg^{2+}, Na^+, and even Pb^{2+} are all capable of populating a single compact tertiary fold of the DNAzyme rather than individual metal-specific folds. Subsequent NMR experiments with Mg^{2+} and Na^+ revealed that all these cations induce the same overall tertiary structure, though with differing population weights of the active state. As a result of this study, the authors were able to develop a unified model for the cleavage kinetics of the 8–17 DNAzyme, separating the effects of metal binding and folding from those involved in catalysis. Schmuck et al. [291] further emphasized that this discovery reframes the mechanistic paradigm: ion identity modulates dynamics and occupancy rather than gross folding topology. The use of NMR-derived restraints in MD ensemble refinement validated that Zn^{2+} and Na^+ reproduce the same conformational ensemble observed experimentally, illustrating the power of combined computational-experimental analysis.

Together, the works presented here illustrate the evolution of computational work on DNAzymes. As systems have gone from the simple coarse-graining of the underlying systems with implicit ionic screening to the current time when models include NMR restrained MD simulations and explicit treatment of ions, the field has advanced towards a clearer answer to the ongoing question of how metal ions control catalysis and structural stability. Divalent cations such as Mg^{2+}, Zn^{2+}, and Pb^{2+} act by directly interacting with the oxygen atoms of the phosphate groups leading to transition state stabilization and greater in-line attack probability, while monovalent ions such as Na^+ modulate the electrostatic landscape and aid in directing proper global folding. The interplay of the cationic species will serve to dictate the available conformational ensemble of the catalytically active core. With the continued improvement in the resolution of computational studies, such models can be formulated that will incorporate both the discrete binding event, as well as large scale electrostatic modulation, allowing two aspects of a molecular detail that are experimentally measurable in activity to be combined.

6 | Conclusions and Future Perspectives

Despite being the central molecule of life, DNA is increasingly recognized for its technological potential. This growing importance arises from its unique properties and its abundance in nature. The uniqueness of DNA lies in its ability to self-assemble through the complementarity of nucleotide bases and in the conformational flexibility of its structure, which can range from single- and double-stranded forms to more complex architectures such as G-quadruplexes, triplexes, H-motifs, and others. Among its distinctive characteristics, the polyelectrolyte nature of DNA, originating from the negatively charged phosphate groups of the double helix backbone, is particularly significant. This feature makes DNA-ion interactions, especially with metal and molecular counterions, a key factor underlying many of its structural and dynamical effects.

At the same time, ions themselves in biological systems are not passive electrolytes. Besides being critical for a multitude of vital functions, they are also active design variables. Ions stabilize DNA structure in vivo and also shape, gate, and power DNA nanostructures and devices in vitro and in technological settings. The ionic environment governs both structure and function from hydration-shell structuring and specific groove binding (Section 2), through ion-driven condensation as nanoscale confinement (Section 3), to modeling strategies that transmit atomistic ion physics up to mesoscales (Section 4), and finally to applications, metallized DNA, stretched π-stacked nanowires, nanopores, tweezers, hydrogels, electromotors, walkers, and DNAzymes (Section 5). What unifies them is their valence, identity, and hydration thermodynamics. Together with geometry and sequence of nucleotides in the DNA macromolecule, they determine the free-energy landscape on which DNA-nanotechnology operates.

Among the key properties of ions, valence is one of the most straightforward. Multivalent cations (e.g., polyamines, $[Co(NH_3)_6]^{3+}$) create strong inter-helix attractions that enable DNA condensation and the formation of ordered phases, while divalent ions (Mg^{2+}, Mn^{2+}) tune local mechanics, catalysis, and junction stability. Monovalent ions (Na^+, K^+) primarily determine electrostatic screening and act as coordination elements in structures such as G-quadruplexes. The charge and size of ions are directly related to their hydration, which is a property of paramount importance for structuring the DNA hydration shell and, consequently, for the mechanisms of water-mediated interactions. Kosmotropic ions (e.g., Mg^{2+}, Li^+), structuring water molecule around, interact via hydration shells, whereas chaotropic ions (e.g., K^+ and Cs^+), disordering structure of the hydration shell, penetrate the grooves of the DNA double helix more readily. Ion hydration patterns thus serve as design handles for fold stability, switching thresholds, and conductance. On the other hand, the structural features of the DNA macromolecule are equally essential for constructing molecular mechanisms at the nanoscale. In the most common *B*-form of the double helix, the structure of the macromolecule is modulated by the nucleotide sequence, influencing groove width, conformational flexibility, and the structure of the ion-hydration shell, which is an interrelated property. Base chemistry and methylation impose barriers to ion occupancy in the major and minor grooves, thereby affecting inter-duplex attraction, device hinge flexibility, and catalytic cores.

To describe the properties of DNA-ion systems as materials for nanotechnology, a bridge between experiments, theoretical models, and simulations is required. These simulations should be performed at different levels of molecular organization, including (i) quantum-chemical studies to elucidate the mechanisms of complex formation between metal ions or clusters and DNA; (ii) classical molecular dynamics (MD) with improved ion parameters and polarizable force fields, as well as QM/MM simulations, to capture hydration effects and the role of water molecules; (iii) Inverse Monte Carlo and related coarse-grained models to describe large-scale structures such as DNA gels; and (iv) continuum and Brownian dynamics, along with other theoretical approaches, to provide physical interpretation for experimental observations. On the experimental side, ASAXS/SAXS, NMR, chiral vibrational and sum-frequency spectroscopies, single-molecule pulling, and ionic-current readouts provide complementary constraints on ion distributions and dynamics. The near-term opportunity lies in developing data-assimilation workflows that fit coarse-grained potentials directly to measured structure factors and dynamical data, validate them against spectroscopic and single-molecule experiments, and iteratively refine designs until the targeted values (such as conductance, rate, and stability windows) are achieved.

These insights pave the way for ion-controlled DNA nanotechnologies, where ionic composition and dynamics are not merely background conditions but active design parameters. Important directions include:

1. Metallized DNA, involving the selective binding and reduction of metal ions (e.g., Ag^+ and Cu^{2+}) along the phosphate backbone or within base-pair stacks to form continuous conductive paths. This underpins DNA nanowires and stretched π-stacked configurations functioning as a quasi-1D electronic material for nanoelectronic applications.
2. DNA battery, in which ions such as Li^+ migrate through DNA hydrogels, forming ion-conducting channels analogous to those in solid electrolytes, offering routes toward biocompatible energy-storage systems.
3. DNA in nanopore systems, where DNA acts as a sensor, transducer, or selective filter. The ionic composition determines capture rates, translocation dynamics, and signal-to-noise ratios, while specific ions (e.g., Na^+, K^+) modulate electroosmotic flow and the hydration of pore walls.
4. DNA tweezers, switchable molecular devices that undergo conformational transitions upon external stimuli. They are highly sensitive to ionic strength and valence; multivalent ions or pH-dependent counterions can trigger folding or refolding, while metal-dependent aptamers enable selective actuation.
5. DNA-based electromotors, which exploit charge asymmetry or ion-driven conformational changes to generate mechanical motion. Ionic gradients can induce directional twisting or bending through local electric fields.
6. DNA origami, where thousands of staple strands fold a long scaffold strand into a predetermined shape. Ion valence and hydration strongly influence folding pathways and final stability: Mg^{2+} and Na^+ balance backbone repulsion differently, affecting yield and rigidity.
7. DNA hydrogels, formed through physical or chemical crosslinking of DNA strands. Their mechanical strength, swelling behavior, and ionic conductivity depend sensitively on ionic concentration and type, enabling applications in soft electronics and biosensing.
8. DNA walkers, nanoscale machines that move along predefined tracks via strand-displacement reactions or catalytic cycles. In experimental studies, ions act as electrostatic screening agents; therefore, this effect is accounted for by the implicit coarse-grained simulation model, which saves computational time.
9. DNAzymes, catalytic DNA sequences whose activity depends on specific coordinating metal ions (e.g., Mg^{2+}, Zn^{2+}, and Pb^{2+}). Their structural dynamics and reactivity are tightly coupled to ion coordination geometry and

hydration, making them central to sensing and signal transduction.

Together, these directions outline a coherent roadmap for ion-controlled DNA nanotechnology, where predictive modeling at different levels of DNA structure and experimental feedback converge to achieve programmable function, structural adaptability, and sustainable material design.

Author Contributions

D.P., N.C., and T.B. contributed to writing – original draft, writing – review and editing, visualization, validation, and resources. S.P., A.L., and F.M. contributed to supervision, conceptualization, writing – original draft, writing – review and editing, visualization, validation, and resources.

Acknowledgments

The authors thank COST Action CA21101 (COSY). A.L. and N.C. acknowledge financial support from European Union's Horizon Europe Research and Innovation Programme under grant agreement No 101086667, project BioMat4CAST (BioMat4CAST - "Petru Poni" Institute of Macromolecular Chemistry Multi-Scale in Silico Laboratory for Complex and Smart Biomaterials). S.P., D.P., and T.B. acknowledge the National Academy of Sciences of Ukraine for the partial support of the research (project No 0125U000263). S.P. and D.P. acknowledge SIMONS Foundation for the financial support (Grant SFI-PD-Ukraine-00014573). T.B. acknowledges financial support under the National Recovery and Resilience Plan, CAPTOR (Grant CUP: 20222BL5Y4). F.M. acknowledges financial support from Progetto Fondazione di Sardegna (Grant CUP: F72F20000230007).

Funding

This study was supported by COST Action CA21101 (COSY), European Union's Horizon Europe Research and Innovation Programme under grant agreement No 101086667, project BioMat4CAST, National Academy of Sciences of Ukraine (grant 0125U000263), SIMONS Foundation (Grant SFI-PD-Ukraine-00014573), National Recovery and Resilience Plan, CAPTOR (Grant CUP: 20222BL5Y4), and the Progetto Fondazione di Sardegna (grant F72F20000230007).

Conflicts of Interest

The authors declare no conflicts of interest.

Data Availability Statement

No original research data were generated or analyzed for this review article; it is based solely on previously published studies.

References

1. R. E. Franklin and R. G. Gosling, "Evidence for 2-Chain Helix in Crystalline Structure of Sodium Deoxyribonucleate," *Nature* 172, no. 4369 (1953): 156.

2. R. E. Franklin and R. G. Gosling, "Molecular Configuration in Sodium Thymonucleate," *Nature* 171. no. 4356 (1953): 740.

3. J. D. Watson and F. H. C. Crick, "Molecular Structure of Nucleic Acids: A Structure for Deoxyribose Nucleic Acid," *Nature* 171 (1953): 737.

4. M. H. F. Wilkins, A. R. Stokes, and H. R. Wilson, "Molecular Structure of Nucleic Acids: Molecular Structure of Deoxypentose Nucleic Acids," *Nature* 171 (1953): 738.

5. A. Cumberworth and A. Reinhardt, "Models and Simulations of Structural DNA Nanotechnology Reveal Fundamental Principles of Self-Assembly," *Chemical Society Reviews* 54 (2025): 2344.

6. P. W. K. Rothemund, "Folding DNA to Create Nanoscale Shapes and Patterns," *Nature* 440 (2006): 297.

7. N. C. Seeman, "Nucleic Acid Junctions and Lattices," *Journal of Theoretical Biology* 99 (1982): 237.

8. V. Linko and A. Keller, "Stability of DNA Origami Nanostructures in Physiological Media: The Role of Molecular Interactions," *Small* 19, no. 34 (2023): e2301935.

9. T. Tian, Y. Li, and Y. Lin, "Prospects and Challenges of Dynamic DNA Nanostructures in Biomedical Applications," *Bone Research* 10 (2022): 40.

10. A. R. Chandrasekaran, "Isothermal Assembly of DNA Nanostructures," *Chemical Communications* 61 (2025): 7983.

11. M. DeLuca, Z. Shi, C. E. Castro, and G. Arya, "Dynamic DNA Nanotechnology: Toward Functional Nanoscale Devices," *Nanoscale Horizons* 5 (2020): 182.

12. S. Kosara, R. Singh, and D. Bhatia, "Structural DNA Nanotechnology at the Nexus of Next-Generation Bio-Applications: Challenges and Perspectives," *Nanoscale Advances* 6, no. 2 (2024): 386.

13. V. Linko and H. Dietz, "The Enabled State of DNA Nanotechnology," *Current Opinion in Biotechnology* 24, no. 4 (2013): 555.

14. P. Zhan, A. Peil, Q. Jiang, et al., "Recent Advances in DNA Origami-Engineered Nanomaterials and Applications," *Chemical Reviews* 123 (2023): 3976.

15. F. Mocci and A. Laaksonen, "Insight into Nucleic Acid Counterion Interactions From inside Molecular Dynamics Simulations Is "Worth Its Salt," *Soft Matter* 8, no. 36 (2012): 9268.

16. W. Saenger, *Principles of Nucleic Acid Structure* (Springer New York, 1984).

17. J. Yoo, H. Kim, A. Aksimentiev, and T. Ha, "Direct Evidence for Sequence-Dependent Attraction between Double-Stranded DNA Controlled by Methylation," *Nature Communications* 7 (2016): 11045.

18. C. Bustamante, S. B. Smith, J. Liphardt, and D. Smith, "Single-Molecule Studies of DNA Mechanics," *Current Opinion in Structural Biology* 10, no. 3 (2000): 279.

19. P. J. Hagerman, "Flexibility of DNA," *Annual Review of Biophysics and Biophysical Chemistry* 17, no. 1 (1988): 265.

20. V. A. Bloomfield, "DNA Condensation by Multivalent Cations," *Biopolymers* 44, no. 3 (1997): 269.

21. T. Bubon, O. Zdorevskyi, and S. Perepelytsya, "Molecular Dynamics Study of Collective Water Vibrations in a DNA Hydration Shell," *European Biophysics Journal* 52, no. 1-2 (2023): 69.

22. T. Bubon and K. Azizi, "Effects of Alkali-Metal Counterions on the Vibrational Dynamics of the DNA Hydration Shell," *Journal of Physical Chemistry B* 129, no. 1 (2025): 28.

23. N. Korolev, L. Nordenskiöld, and A. P. Lyubartsev, Multiscale Coarse-Grained Modelling of Chromatin Components: DNA and the Nucleosome, *Advances in Colloid and Interface Science* 232 (2016): 36.

24. S. M. Perepelytsya and S. N. Volkov, "Counterion Vibrations in the DNA Low-Frequency Spectra," *European Physical Journal E* 24 (2007): 261.

25. S. Perepelytsya, "Hydration of Counterions Interacting with DNA Double Helix: A Molecular Dynamics Study," *Journal of Molecular Modeling* 24 (2018): 171.

26. J. Kasianowicz, E. Brandin, D. Branton, and D. Deamer, "Characterization of Individual Polynucleotide Molecules Using a Membrane Channel," *Proceedings of the National Academy of Sciences* 93, no. 24 (1996): 13770.

27. H. Hansma and D. Laney, "DNA Binding to Mica Correlates with Cationic Radius: Assay by Atomic Force Microscopy," *Biophysical Journal* 70, no. 4 (1996): 1933.

28. S. M. Douglas, H. Dietz, T. Liedl, B. Högberg, F. Graf, and W. M. Shih, "Self-Assembly of DNA into Nanoscale Three-Dimensional Shapes," *Nature* 459 (2009): 414.

29. J. Pelta, F. Livolant, and J.-L. Sikorav, "DNA Aggregation Induced by Polyamines and Cobalthexamine," *Journal of Biological Chemistry* 271 (1996): 5656.

30. C. Kielar, Y. Xin, B. Shen, et al., "On the Stability of DNA Origami Nanostructures in Low-Magnesium Buffers," *Angewandte Chemie* 130, no. 30 (2018): 9614.

31. T. G. Martin and H. Dietz, "Magnesium-Free Self-Assembly of Multi-Layer DNA Objects," *Nature Communications* 3, no. 1 (2012): 1103.

32. Y. Takezawa, K. Mori, W.-E. Huang, et al., "Metal-Mediated DNA Strand Displacement and Molecular Device Operations Based on Base-Pair Switching of 5-Hydroxyuracil Nucleobases," *Nature Communications* 14 (2023): 4759.

33. D. Y. Zhang and G. Seelig, "Dynamic DNA Nanotechnology Using Strand-Displacement Reactions," *Nature Chemistry* 3 (2011): 103.

34. M. Spotheim-Maurizot, S. Ruiz, R. Sabattier, and M. Charlier, "Radioprotection of DNA by Polyamines," *International Journal of Radiation Biology* 68, no. 5 (1995): 571.

35. D. Sy, S. Hugot, C. Savoye, S. Ruiz, M. Charlier, and M. Spotheim-Maurizot, "Radioprotection of DNA by Spermine: A Molecular Modelling Approach," *International Journal of Radiation Biology* 75, no. 8 (1999): 953.

36. Z. Chen, C. Liu, F. Cao, J. Ren, and X. Qu, "DNA Metallization: Principles, Methods, Structures, and Applications," *Chemical Society Reviews* 47 (2018): 4017.

37. D. J. Kim, M.-A. Woo, Y. L. Jung, et al., "DNA Metallization for High Performance Li-Ion Battery Anodes," *Nano Energy* 8 (2014): 17.

38. A. Y. Grosberg, T. T. Nguyen, and B. I. Shklovskii, "Colloquium : The Physics of Charge Inversion in Chemical and Biological Systems," *Reviews of Modern Physics* 74, no. 2 (2002): 329.

39. G. S. Manning, "Limiting Laws and Counterion Condensation in Polyelectrolyte Solutions I. Colligative Properties," *The Journal of Chemical Physics* 51, no. 3 (1969): 924.

40. S. Perepelytsya, J. Uličný, A. Laaksonen, and F. Mocci, "Pattern Preferences of DNA Nucleotide Motifs by Polyamines Putrescine^{2+}, Spermidine^{3+} and Spermine^{4+}," *Nucleic Acids Research* 47 (2019): 6084.

41. S. M. Perepelytsya and S. N. Volkov, "Intensities of DNA Ion-Phosphate Modes in the Low-Frequency Raman Spectra," *European Physical Journal E* 31 (2010): 201.

42. D. V. Piatnytskyi, O. O. Zdorevskyi, and S. N. Volkov, "Interaction of Hydrogen Peroxide Molecules with Non-Specific DNA Recognition Sites," *European Physical Journal D* 75 (2021): 24.

43. K. Luger, A. W. Mäder, R. K. Richmond, D. F. Sargent, and T. J. Richmond, "Crystal Structure of the Nucleosome Core Particle at 2.8 Åresolution," *Nature* 389, no. 6648 (1997): 251.

44. J. Harnett, S. Weir, and D. Michieletto, Effects of Monovalent and Divalent Cations on the Rheology of Entangled DNA, *Soft Matter* 20, no. 19 (2024): 3980.

45. K. B. Chhetri, A Review on Salt-Induced DNA Compaction and Charge Inversion, *Progress in Biophysics and Molecular Biology* 195 (2025): 15.

46. P. D. Dans, J. Walther, H. Gómez, and M. Orozco, "Multiscale Simulation of DNA," *Current Opinion in Structural Biology* 37 (2016): 29.

47. A. Savelyev and G. A. Papoian, "Chemically Accurate Coarse Graining of Double-Stranded DNA," *Proceedings of the National Academy of Sciences* 107 (2010): 20340.

48. V. B. Pinheiro and P. Holliger, "The XNA World: Progress towards Replication and Evolution of Synthetic Genetic Polymers," *Current Opinion in Chemical Biology* 16 (2012): 245.

49. E. Westhof, "Water: An Integral Part of Nucleic Acid Structure," *Annual Review of Biophysics and Biophysical Chemistry* 17 (1988): 125.

50. Y. P. Blagoi, O. N. Veselkov, S. N. Volkov, et al., Physical Principles of Molecular Organization and Structural Dynamics of Biopolymers, V. N. Karazin Kharkiv National University, 2011.

51. D. Laage, T. Elsaesser, and J. T. Hynes, "Water Dynamics in the Hydration Shells of Biomolecules," *Chemical Reviews* 117, no. 16 (2017): 10725.

52. V. I. Maleev, M. A. Semenov, A. I. Gasan, and V. A. Kashpur, "Physical Properties of the DNA-Water System," *Biofizika* 38 (1993): 768.

53. W. Saenger, W. N. Hunter, and O. Kennard, "DNA Conformation Is Determined by Economics in the Hydration of Phosphate Groups," *Nature* 324 (1986): 385.

54. N. Lavalle, S. A. Lee, and A. Rupprecht, "Counterion Effects on the Physical Properties and the A to B Transition of Calf-Thymus DNA Films," *Biopolymers* 30, no. 9-10 (1990): 877.

55. G. Albiser, A. Lamiri, and S. Premilat, "The A-B Transition: Temperature and Base Composition Effects on Hydration of DNA," *International Journal of Biological Macromolecules* 28, no. 3 (2001): 199.

56. J. Pilet and J. Brahms, "Investigation of DNA Structural Changes by Infrared Spectroscopy," *Biopolymers* 12 (1973): 387.

57. R. Langridge, D. A. Marvin, W. E. Seeds, et al., "The Molecular Configuration of Deoxyribonucleic Acid," *Journal of Molecular Biology* 2, no. 1 (1960): 38–IN12.

58. E. M. Bradbury, W. C. Price, and G. R. Wilkinson, "Infrared Studies of Molecular Configurations of DNA," *Journal of Molecular Biology* 3 (1961): 301.

59. Y. Nishimura, C. Torigoe, and M. Tsuboi, "Salt Induced B—A Transition of Poly(dG).poly(dC) and the Stabilization of A Form by Its Methylation," *Nucleic Acids Research* 14 (1986): 2737.

60. P. J. Cooper and L. D. Hamilton, "The A-B Conformational Change in the Sodium Salt of DNA," *Journal of Molecular Biology* 16 (1966): 562.

61. T. Weidlich, S. M. Lindsay, and A. Rupprecht, "Counterion Effects on the Structure and Dynamics of Solid DNA," *Physical Review Letters* 61 (1988): 1674.

62. A. K. Singh, C. Wen, S. Cheng, and N. Q. Vinh, "Long-Range DNA-Water Interactions," *Biophysical Journal* 120 (2021): 4966.

63. M. Heyden and D. J. Tobias, "Spatial Dependence of Protein-Water Collective Hydrogen-Bond Dynamics," *Physical Review Letters* 111, no. 21 (2013): 218101.

64. E. A. Perets, D. Konstantinovsky, T. Santiago, et al., "Beyond the "Spine of Hydration": Chiral SFG Spectroscopy Detects DNA First Hydration Shell and Base Pair Structures," *Journal of Chemical Physics* 161 (2024): 95104.

65. G. S. Manning and J. Ray, "*Counterion Condensation Revisited, Journal of Biomolecular Structure and Dynamics*, 16, no. 2 (1998): 461.

66. F. Oosawa, *Polyelectrolytes* (Marcel Dekker, INC, 1971).

67. K. Andresen, R. Das, H. Y. Park, et al., "Spatial Distribution of Competing Ions around DNA in Solution," *Physical Review Letters* 93, no. 24 (2004): 248103.

68. K. Andresen, X. Qiu, S. A. Pabit, et al., "Mono- and Trivalent Ions around DNA: A Small-Angle Scattering Study of Competition and Interactions," *Biophysical Journal* 95, no. 1 (2008): 287.

69. R. Das, T. T. Mills, L. W. Kwok, et al., "Counterion Distribution around DNA Probed by Solution X-Ray Scattering," *Physical Review Letters* 90 (2003): 188103.

70. Y. Bai, M. Greenfeld, K. J. Travers, et al., "Quantitative and Comprehensive Decomposition of the Ion Atmosphere around Nucleic Acids," *Journal of the American Chemical Society* 129, no. 48 (2007): 14981.

71. S. Perepelytsya and O. Zdorevskyi, "Counterion Atmosphere around DNA Double Helix: Trapping of Counterions at the Nanoscale," *Low Temperature Physics* 48 (2022): 293.

72. J. Yoo and A. Aksimentiev, "Competitive Binding of Cations to Duplex DNA Revealed through Molecular Dynamics Simulations," *Journal of Physical Chemistry B* 116 (2012): 12946.

73. F. Mocci and G. Saba, "Molecular Dynamics Simulations of A · T-Rich Oligomers: Sequence-Specific Binding of Na^+ in the Minor Groove of B-DNA," *Biopolymers* 68, no. 4 (2003): 471.

74. X. Shui, L. McFail-Isom, G. G. Hu, and L. D. Williams, "The B-DNA Dodecamer at High Resolution Reveals a Spine of Water on Sodium," *Biochemistry* 37, no. 23 (1998): 8341.

75. Y. Duan, P. Wilkosz, M. Crowley, and J. M. Rosenberg, "Molecular Dynamics Simulation Study of DNA Dodecamer d(CGCGAATTCGCG) in Solution: Conformation and Hydration," *Journal of Molecular Biology* 272 (1997): 553.

76. Y. Yonetani and H. Kono, "Sequence Dependencies of DNA Deformability and Hydration in the Minor Groove," *Biophysical Journal* 97 (2009): 1138.

77. B. Jana, S. Pal, and B. Bagchi, "Enhanced Tetrahedral Ordering of Water Molecules in Minor Grooves of DNA: Relative Role of DNA Rigidity, Nanoconfinement, and Surface Specific Interactions," *Journal of Physical Chemistry B* 114, no. 10 (2010): 3633.

78. V. P. Chuprina, U. Heinemann, A. A. Nurislamov, P. Zielenkiewicz, R. E. Dickerson, and W. Saenger, "Molecular Dynamics Simulation of the Hydration Shell of a B-DNA Decamer Reveals Two Main Types of Minor-Groove Hydration Depending on Groove Width," *Proceedings of the National Academy of Sciences* 88 (1991): 593.

79. H. R. Drew, R. M. Wing, T. Takano, et al., "Structure of a B-DNA Dodecamer: Conformation and Dynamics," *Proceedings of the National Academy of Sciences* 78 (1981): 2179.

80. G. Minasov, V. Tereshko, and M. Egli, "Atomic-Resolution Crystal Structures of B-DNA Reveal Specific Influences of Divalent Metal Ions on Conformation and Packing," *Journal of Molecular Biology* 291, no. 1 (1999): 83.

81. V. P. Denisov, G. Carlström, K. Venu, and B. Halle, "Kinetics of DNA Hydration," *Journal of Molecular Biology* 268 (1997): 118.

82. M. G. Kubinec and D. E. Wemmer, "NMR Evidence for DNA Bound Water in Solution," *Journal of the American Chemical Society* 114, no. 22 (1992): 8739.

83. E. Liepinsh, G. Otting, and K. Wüthrich, "NMR Observation of Individual Molecules of Hydration Water Bound to DNA Duplexes: Direct Evidence for a Spine of Hydration Water Present in Aqueous Solution," *Nucleic Acids Research* 20, no. 24 (1992): 6549.

84. M. L. McDermott, H. Vanselous, S. A. Corcelli, and P. B. Petersen, "DNA's Chiral Spine of Hydration," *ACS Central Science* 3, no. 7 (2017): 708.

85. P. S. Subramanian, G. Ravishanker, and D. L. Beveridge, "Theoretical Considerations on the "Spine of Hydration" in the Minor Groove of d(CGCGAATTCGCG).d(GCGCTTAAGCGC): Monte Carlo Computer Simulation," *Proceedings of the National Academy of Sciences* 85 (1988): 1836.

86. D. J. Floisand and S. A. Corcelli, "Computational Study of Phosphate Vibrations as Reporters of DNA Hydration," *Journal of Physical Chemistry Letters* 6 (2015): 4012.

87. K. E. Furse and S. A. Corcelli, "The Dynamics of Water at DNA Interfaces: Computational Studies of Hoechst 33258 Bound to DNA," *Journal of the American Chemical Society* 130, no. 39 (2008): 13103.

88. A. N. Lane, T. C. Jenkins, and T. A. Frenkiel, "Hydration and Solution Structure of d(CGCAAATTTGCG)2 and Its Complex with Propamidine From NMR and Molecular Modelling," *Biochimica et Biophysica Acta (BBA) - Gene Structure and Expression* 1350, no. 2 (1997): 205.

89. A. T. Phan, J. L. Leroy, and M. Guéron, "Determination of the Residence Time of Water Molecules Hydrating B'- DNA and B-DNA, by One-Dimensional Zero-Enhancement Nuclear Overhauser Effect Spectroscopy," *Journal of Molecular Biology* 286, no. 2 (1999): 505.

90. D. Saha, S. Supekar, and A. Mukherjee, "Distribution of Residence Time of Water around DNA Base Pairs: Governing Factors and the Origin of Heterogeneity," *Journal of Physical Chemistry B* 119 (2015): 11371.

91. S. Pal, P. K. Maiti, and B. Bagchi, "Exploring DNA Groove Water Dynamics through Hydrogen Bond Lifetime and Orientational Relaxation," *Journal of Chemical Physics* 125 (2006): 234903.

92. Y. Yonetani and H. Kono, "What Determines Water-Bridge Lifetimes at the Surface of DNA? Insight From Systematic Molecular Dynamics Analysis of Water Kinetics for Various DNA Sequences," *Biophysical Chemistry* 160 (2012): 54.

93. E. Duboué-Dijon, A. C. Fogarty, J. T. Hynes, and D. Laage, "Dynamical Disorder in the DNA Hydration Shell," *Journal of the American Chemical Society* 138 (2016): 7610.

94. P. Auffinger and E. Westhof, "Water and Ion Binding around RNA and DNA (C, G) Oligomers," *Journal of Molecular Biology* 300, no. 5 (2000): 1113.

95. Y. P. Blagoi, V. L. Galkin, V. L. Gladchenko, S. V. Kornilova, V. A. Sorokin, and A. G. Shkorbatov, *The Complexes of Nucleic Acids and Metals in the Solutions* (Naukova Dumka, 1991).

96. R. K. O. Sigel and H. Sigel, "A Stability Concept for Metal Ion Coordination to Single-Stranded Nucleic Acids and Affinities of Individual Sites," *Accounts of Chemical Research* 43 (2010): 974.

97. V. N. Bartenev, E. Golovamov, K. A. Kapitonova, M. A. Mokulskii, L. I. Volkova, and I. Skuratovskii, "Structure of the B DNA Cationic Shell as Revealed by an X-Ray Diffraction Study of CsDNA," *Journal of Molecular Biology* 169, no. 1 (1983): 217.

98. S. Cruz-León and N. Schwierz, "RNA Captures More Cations than DNA: Insights From Molecular Dynamics Simulations," *Journal of Physical Chemistry B* 126 (2022): 8646.

99. K. D. Collins, "Charge Density-Dependent Strength of Hydration and Biological Structure," *Biophysical Journal* 72 (1997): 65.

100. J. Mähler and I. Persson, A Study of the Hydration of the Alkali Metal Ions in Aqueous Solution," *Inorganic Chemistry* 51, no. 1 (2012): 425.

101. Y. Marcus, "Effect of Ions on the Structure of Water: Structure Making and Breaking," *Chemical Reviews* 109, no. 3 (2009): 1346.

102. Z. Jing, Y. Zhou, T. Yamaguchi, et al., "Hydration of Alkali Metal and Halide Ions From Static and Dynamic Viewpoints," *Journal of Physical Chemistry Letters* 14, no. 27 (2023): 6270.

103. S. Perepelytsya, "Positively and Negatively Hydrated Counterions in Molecular Dynamics Simulations of DNA Double Helix," *Ukrainian Journal of Physics* 65 (2020): 510.

104. A. P. Lyubartsev and A. Laaksonen, "Molecular Dynamics Simulations of DNA in Solution with Different Counter-Ions," *Journal of Biomolecular Structure and Dynamics* 16, no. 3 (1998): 579.

105. F. Pan, C. Roland, and C. Sagui, "Ion Distributions around Left- and Right-Handed DNA and RNA Duplexes: A Comparative Study," *Nucleic Acids Research* 42 (2014): 13981.

106. M. Pasi, J. H. Maddocks, and R. Lavery, "Analyzing Ion Distributions around DNA: Sequence-Dependence of Potassium Ion Distributions From Microsecond Molecular Dynamics," *Nucleic Acids Research* 43 (2015): 2412.

107. P. D. Dans, L. Danilāne, I. Ivani, et al., "Long-Timescale Dynamics of the Drew-Dickerson Dodecamer," *Nucleic Acids Research* 44 (2016): 4052.

108. A. Pérez, F. J. Luque, and M. Orozco, "Dynamics of B-DNA on the Microsecond Time Scale," *Journal of the American Chemical Society* 129 (2007): 14739.

109. V. P. Denisov and B. Halle, "Sequence-Specific Binding of Counterions to B -DNA," *Proceedings of the National Academy of Sciences* 97 (2000): 629.

110. L. V. Dijk, M. L. H. Gruwel, W. Jesse, J. D. Bleijser, and J. C. Leyte, "Sodium Ion and Solvent Nuclear Relaxation Results in Aqueous Solutions of DNA," *Biopolymers* 26 (1987): 261.

111. V. A. Bloomfield, "DNA Condensation," *Current Opinion in Structural Biology* 6, no. 3 (1996): 334.

112. M.-L. Ainalem and T. Nylander, "DNA Condensation Using Cationic Dendrimers—morphology and Supramolecular Structure of Formed Aggregates," *Soft Matter* 7, no. 10 (2011): 4577.

113. A. Estévez-Torres and D. Baigl, "DNA Compaction: Fundamentals and Applications," *Soft Matter* 7 (2011): 6746.

114. M. Takahashi, K. Yoshikawa, V. V. Vasilevskaya, and A. R. Khokhlov, "Discrete CoilGlobule Transition of Single Duplex DNAs Induced by Polyamines," *Journal of Physical Chemistry B* 101 (1997): 9396.

115. K. Yoshikawa, M. Takahashi, V. V. Vasilevskaya, and A. R. Khokhlov, "Large Discrete Transition in a Single DNA Molecule Appears Continuous in the Ensemble," *Physical Review Letters* 76 (1996): 3029.

116. H. Deng and V. A. Bloomfield, "Structural Effects of Cobalt-Amine Compounds on DNA Condensation," *Biophysical Journal* 77 (1999): 1556.

117. C. C. Conwell, I. D. Vilfan, and N. V. Hud, "Controlling the Size of Nanoscale Toroidal DNA Condensates with Static Curvature and Ionic Strength," *Proceedings of the National Academy of Sciences* 100 (2003): 9296.

118. F. Mocci, A. Laaksonen, L. Engelbrecht, T. Vasiliu, and S. Perepelytsya, *DNA-Polyamine Interactions: Insight From Molecular Dynamics Simulations on the Sequence-Specific Binding of Spermidine*, Springer Proceedings in Physics, (Springer International Publishing, 2022) vol. 266, 163–192.

119. T. Vasiliu, F. Mocci, A. Laaksonen, L. D. V. Engelbrecht, and S. Perepelytsya, "Caging Polycations: Effect of Increasing Confinement on the Modes of Interaction of Spermidine^{3+} with DNA Double Helices," *Frontiers in Chemistry* 10 (2022): 836994.

120. S. Perepelytsya, T. Vasiliu, A. Laaksonen, L. D. V. Engelbrecht, G. Brancato, and F. Mocci, "Conformational Flexibility of Spermidine^{3+} Interacting with DNA Double Helix," *Journal of Molecular Liquids* 389 (2023): 122828.

121. S. Perepelytsya, T. Vasiliu, A. Laaksonen, L. D. V. Engelbrecht, and F. Mocci, "Unusual Bending Patterns of Spermidine^{3+} Bound to DNA Double Helix," *Low Temperature Physics* 50 (2024): 204.

122. S. M. Perepelytsya, G. M. Glibitskiy, and S. N. Volkov, "Texture Formation in DNA Films with Alkali Metal Chlorides," *Biopolymers* 99 (2013): 508.

123. J. Pelta, D. Durand, J. Doucet, and F. Livolant, "DNA Mesophases Induced by Spermidine: Structural Properties and Biological Implications," *Biophysical Journal* 71 (1996): 48.

124. G. M. Glibitskiy, "Na-DNA Films with Ions of Metals," *Biophysical Bulletin* 2, no. 21 (2006): 29.

125. B. Sclavi, W. L. Peticolas, and J. W. Powell, "Fractal-Like Patterns in DNA Films, B Form at 0humidity, and Antiheteronomous DNA: An Ir Study," *Biopolymers* 1105 (1994): 34.

126. M. Nakata, G. Zanchetta, B. D. Chapman, et al., "End-to-End Stacking and Liquid Crystal Condensation of 6- to 20-Base Pair DNA Duplexes," *Science* 318 (2007): 1276.

127. C. Maffeo, B. Luan, and A. Aksimentiev, "End-to-End Attraction of Duplex DNA," *Nucleic Acids Research* 40, no. 9 (2012): 3812.

128. J. Duguid, V. Bloomfield, J. Benevides, and G. Thomas, "Raman Spectroscopy of DNA-Metal Complexes. I. Interactions and Conformational Effects of the Divalent Cations: Mg, Ca, Sr, Ba, Mn, Co, Ni, Cu, Pd, and Cd," *Biophysical Journal* 651993): 1916.

129. J. G. Duguid and V. A. Bloomfield, "Aggregation of Melted DNA by Divalent Metal Ion-Mediated Cross-Linking," *Biophysical Journal* 69 (1995): 2642.

130. J. H. Shibata and J. M. Schurr, "A Theory of Aggregation in the Thermal Denaturation Region of Multistrand Biopolymers," *Biopolymers* 20 (1981): 525.

131. C. Ma and V. A. Bloomfield, "Condensation of Supercoiled DNA Induced by MnCl2," *Biophysical Journal* 67, no. 4 (1994): 1678.

132. N. V. Hud and J. Feigon, "Characterization of Divalent Cation Localization in the Minor Groove of the AnTn and TnAn DNA Sequence Elements by 1H NMR Spectroscopy and Manganese(II)," *Biochemistry* 41, no. 31 (2002): 9900.

133. J. C. Sitko, E. M. Mateescu, and H. G. Hansma, "Sequence-Dependent DNA Condensation and the Electrostatic Zipper," *Biophysical Journal* 84 (2003): 419.

134. A. A. Kornyshev and S. Leikin, "Electrostatic Zipper Motif for DNA Aggregation," *Physical Review Letters* 82, no. 20 (1999): 4138.

135. C. M. Muntean, K. Nalpantidis, I. Feldmann, and V. Deckert, "Zn^{2+}–DNA Interactions in Aqueous Systems: A Raman Spectroscopic Study," *Journal of Spectroscopy* 23, no. 3-4 (2009): 155.

136. S. B. Mitta, R. Harpalsinh, J. Kim, H. S. Park, and S. H. Um, Flexible Supercapacitor with a Pure DNA Gel Electrolyte, *Advanced Materials Interfaces* 9, no. 14 (2022): 2200133.

137. S. B. Mitta, J. Kim, H. H. Rana, et al., "A Biospecies-Derived Genomic DNA Hybrid Gel Electrolyte for Electrochemical Energy Storage," *PNAS Nexus* 3, no. 6 (2024): 213.

138. W. Xia, Y. Wang, A. Yang, and G. Yang, "DNA Compaction and Charge Inversion Induced by Organic Monovalent Ions," *Polymers* 9 (2017): 128.

139. K. S. Egorova, A. V. Posvyatenko, S. S. Larin, and V. P. Ananikov, "Ionic Liquids: Prospects for Nucleic Acid Handling and Delivery," *Nucleic Acids Research* 49, no. 3 (2021): 1201.

140. Y.-L. Chen and X.-H. Zhang, "Effects of Imidazolium-Based Ionic Liquids on the Elasticity of DNA Revealed by Magnetic Tweezers," *Journal of Molecular Liquids* 410 (2024): 125646.

141. S. Husale, W. Grange, M. Karle, S. Bürgi, and M. Hegner, "Interaction of Cationic Surfactants with DNA: A Single-Molecule Study," *Nucleic Acids Research* 36, no. 5 (2008): 1443.

142. E. F. Silva, U. M. S. Andrade, K. M. de Oliveira, A. V. N. C. Teixeira, and M. S. Rocha, "Dodecyltrimethylammonium Bromide Surfactant Effects on DNA: Unraveling the Competition between Electrostatic and Hydrophobic Interactions," *Physical Review. E* 102 (2020): 032401.

143. S. Poole, B. McGorman, C. J. Cardin, and A. Kellett, "Recent Progress in Probing Small Molecule Interactions with DNA," *Biophysical Reviews* 17, no. 4 (2025): 1157.

144. C. Lima, G. Almeida, and M. Rocha, "A Cooperative Transition From the Semi-Flexible to the Flexible Regime of Polymer Elasticity: Mitoxantrone-Induced DNA Condensation," *Biochimica et Biophysica Acta (BBA) - General Subjects* 1862, no. 5 (2018): 1107.

145. S. Gupta, N. Tiwari, and M. Munde, "A Comprehensive Biophysical Analysis of the Effect of DNA Binding Drugs on Protamine-Induced DNA Condensation," *Scientific Reports* 9 (2019): 5891.

146. R. Satange, C.-K. Chang, and M.-H. Hou, "A Survey of Recent Unusual High-Resolution DNA Structures Provoked by Mismatches,

Repeats and Ligand Binding," *Nucleic Acids Research* 46, no. 13 (2018): 6416.

147. H. Y. Alniss, H. M. Al-Jubeh, Y. A. Msallam, et al., "Structure-Based Drug Design of DNA Minor Groove Binders and Evaluation of Their Antibacterial and Anticancer Properties," *European Journal of Medicinal Chemistry* 271 (2024): 116440.

148. O. Kulyk, A. Krivoshey, O. Kolosova, et al., "Nucleic Acid-Binding Bis-Acridine Orange Dyes with Improved Properties for Bioimaging and PCR Applications," *Journal of Materials Chemistry. B* 12 (2024): 11968.

149. J. Xu, G. A. Wang, L. Gao, et al., "Enabling Programmable Dynamic DNA Chemistry Using Small-Molecule DNA Binders," *Nature Communications* 14, no. 1 (2023): 4248.

150. J. Ray and G. S. Manning, "An Attractive Force between Two Rodlike Polyions Mediated by the Sharing of Condensed Counterions," *Langmuir : the Acs Journal of Surfaces and Colloids* 10 (1994): 2450.

151. I. Rouzina and V. A. Bloomfield, "Macroion Attraction Due to Electrostatic Correlation between Screening Counterions. 1. Mobile Surface-Adsorbed Ions and Diffuse Ion Cloud," *Journal of Physical Chemistry* 100 (1996): 9977.

152. B. I. Shklovskii, "Wigner Crystal Model of Counterion Induced Bundle Formation of Rodlike Polyelectrolytes," *Physical Review Letters* 82 (1999): 3268.

153. G. S. Manning, "The Molecular Theory of Polyelectrolyte Solutions with Applications to the Electrostatic Properties of Polynucleotides," *Quarterly Reviews of Biophysics* 11, no. 2 (1978): 179.

154. S. M. Perepelytsya and S. N. Volkov, "Ion-Phosphate Mode in the DNA Low-Frequency Spectra," *Ukrainian Journal of Physics* 49, no. 11 (2004): 1072.

155. S. Perepelytsya and S. N. Volkov, "Low-Frequency Vibrations of DNA with Counterions in Cross-Stranded Position," *Ukrainian Journal of Physics* 55 (2010): 1182.

156. S. M. Perepelytsya and S. N. Volkov, "Conformational Vibrations of Ionic Lattice in DNA," *Journal of Molecular Liquids* 164 (2011): 113.

157. S. M. Perepelytsya and S. N. Volkov, "Dynamics of Ion-Phosphate Lattice of DNA in Left-Handed Double Helix Form," *Ukrainian Journal of Physics* 58, no. 6 (2013): 554.

158. S. M. Perepelytsya and S. N. Volkov, "Vibrations of Ordered Counterions around Left- and Right-Handed DNA Double Helixes," *Journal of Physics: Conference Series* 438 (2013): 12013.

159. J. Yoo and A. Aksimentiev, "Improved Parametrization of Li+, Na+, K+, and Mg2+ Ions for All-Atom Molecular Dynamics Simulations of Nucleic Acid Systems," *Journal of Physical Chemistry Letters* 3, no. 1 (2012): 45.

160. J. Yoo and A. Aksimentiev, "The Structure and Intermolecular Forces of DNA Condensates," *Nucleic Acids Research* 44, no. 5 (2016): 2036.

161. C. Saintomé, S. Amrane, J.-L. Mergny, and P. Alberti, "The Exception that Confirms the Rule: A Higher-Order Telomeric G-Quadruplex Structure More Stable in Sodium than in Potassium," *Nucleic Acids Research* 44, no. 6 (2016): 2926.

162. E. Kristoffersen, A. Coletta, L. Lund, B. Schiøtt, and V. Birkedal, "Inhibited Complete Folding of Consecutive Human Telomeric G-Quadruplexes," *Nucleic Acids Research* 51, no. 4 (2023): 1571.

163. I. S. Joung and T. E. Cheatham, "Determination of Alkali and Halide Monovalent Ion Parameters for Use in Explicitly Solvated Biomolecular Simulations," *Journal of Physical Chemistry B* 112 (2008): 9020.

164. P. Li and K. M. J. Merz, "Taking into Account the Ion-Induced Dipole Interaction in the Nonbonded Model of Ions," *Journal of Chemical Theory and Computation* 10, no. 1 (2014): 289.

165. K. Liebl and M. Zacharias, "The Development of Nucleic Acids Force Fields: From an Unchallenged past to a Competitive Future," *Biophysical Journal* 122, no.14 (2023): 2841.

166. A. Warshel and M. Levitt, "Theoretical Studies of Enzymic Reactions: Dielectric, Electrostatic and Steric Stabilization of the Carbonium Ion in the Reaction of Lysozyme," *Journal of Molecular Biology* 103, no. 2 (1976): 227.

167. H. M. Senn and W. Thiel, "QM/MM Methods for Biomolecular Systems," *Angewandte Chemie International Edition* 48, no. 7 (2009): 1198.

168. J. Borggräfe, C. G. W. Gertzen, A. Viegas, H. Gohlke, and M. Etzkorn, "The Architecture of the 10-23 DNAzyme and Its Implications for DNA-Mediated Catalysis," *FEBS Journal* 290, no. 8 (2023): 2011.

169. D. M. York Şölen Ekesan, "Dynamical Ensemble of the Active State and Transition State Mimic for the RNA-Cleaving 8-17 DNAzyme in Solution," *Nucleic Acids Research* 47 (2019): 10282.

170. G. A. Cisneros, L. Perera, M. García-Díaz, K. Bebenek, T. A. Kunkel, and L. G. Pedersen, "Catalytic Mechanism of Human DNA Polymerase Lambda with Mg^{2+} and Mn^{2+} From Ab Initio Quantum Mechanical/ Molecular Mechanical Studies," *DNA Repair* 7, no. 11 (2008): 1824.

171. J. Aranda, M. Terrazas, H. Gómez, N. Villegas, and M. Orozco, "An Artificial DNAzyme RNA Ligase Shows a Reaction Mechanism Resembling that of Cellular Polymerases," *Nature Catalysis* 2, no. 6 (2019): 544.

172. A. P. Lyubartsev and A. Laaksonen, "Calculation of Effective Interaction Potentials From Radial Distribution Functions: A Reverse Monte Carlo Approach," *Physical Review E* 52, no. 4 (1995): 3730.

173. W. G. Noid, "Perspective: Coarse-Grained Models for Biomolecular Systems," *Journal of Chemical Physics* 139, no. 9 (2013): 090901.

174. C. Peter and K. Kremer, "Multiscale Simulation of Soft Matter Systems - From the Atomistic to the Coarse-Grained Level and Back," *Soft Matter* 5 (2009): 4357.

175. A. P. Lyubartsev and L. Nordenskioeld, "Monte Carlo Simulation Study of Ion Distribution and Osmotic Pressure in Hexagonally Oriented DNA," *Journal of Physical Chemistry* 99, no. 25 (1995): 10373.

176. A. P. Lyubartsev and L. Nordenskiöld, "Monte Carlo Simulation Study of DNA Polyelectrolyte Properties in the Presence of Multivalent Polyamine Ions," *Journal of Physical Chemistry B* 101, no. 21 (1997): 4335.

177. N. Korolev, A. P. Lyubartsev, A. Rupprecht, and L. Nordenskiöld, "Competitive Binding of Mg^{2+}, Ca^{2+}, Na^{+}, and K^{+} Ions to DNA in Oriented DNA Fibers: Experimental and Monte Carlo Simulation Results," *Biophysical Journal* 77, no. 5 (1999): 2736.

178. N. Korolev, A. P. Lyubartsev, L. Nordenskiöld, and A. Laaksonen, "Spermine: An "Invisible" Component in the Crystals of B-DNA. A Grand Canonical Monte Carlo and Molecular Dynamics Simulation Study," *Journal of Molecular Biology* 308, no. 5 (2001): 907.

179. N. Korolev, A. P. Lyubartsev, and L. Nordenskiöld, "A Systematic Analysis of Nucleosome Core Particle and Nucleosome-Nucleosome Stacking Structure," *Scientific Reports* 8, no. 1 (2018): 1543.

180. T. Sun, A. Mirzoev, V. Minhas, N. Korolev, A. P. Lyubartsev, and L. Nordenskiöld, "A Multiscale Analysis of DNA Phase Separation: From Atomistic to Mesoscale Level," *Nucleic Acids Research* 47, no. 11 (2019): 5550.

181. K. S. Park and H. G. Park, "Technological Applications Arising From the Interactions of DNA Bases with Metal Ions," *Current Opinion in Biotechnology* 28 (2014): 17.

182. A. Gonzàlez-Rosell, C. Cerretani, P. Mastracco, T. Vosch, and S. M. Copp, "Structure and Luminescence of DNA-Templated Silver Clusters," *Nanoscale Advances* 3, no. 5 (2021): 1230.

183. K. Li, Y. Liu, B. Lou, Y. Tan, L. Chen, and Z. Liu, "DNA-Guided Metallization of Nanomaterials and Their Biomedical Applications," *Molecules* 28, no. 9 (2023): 3922.

184. Q. Sun, X. Xie, Y. Song, and L. Sun, "A Review on Silver-Mediated DNA Base Pairs: Methodology and Application," *Biomaterials Research* 26, no. 1 (2022): 9.

185. S. Atwell, E. Meggers, G. Spraggon, and P. G. Schultz, "Structure of a Copper-Mediated Base Pair in DNA," *Journal of the American Chemical Society* 123, no. 49 (2001): 12364.

186. K. Tanaka, A. Tengeiji, T. Kato, N. Toyama, and M. Shionoya, "A Discrete Self-Assembled Metal Array in Artificial DNA," *Science* 299 (2003): 1212.

187. K. Tanaka, G. H. Clever, Y. Takezawa, et al., "Programmable Self-Assembly of Metal Ions inside Artificial DNA Duplexes," *Nature Nanotechnology* 1 (2006): 190.

188. D. Buceta, N. Busto, G. Barone, et al., "Ag2 and Ag3 Clusters: Synthesis, Characterization, and Interaction with DNA," *Angewandte Chemie International Edition* 54, no. 26 (2015): 7612.

189. J. Kondo, Y. Tada, T. Dairaku, et al., "A Metallo-DNA Nanowire with Uninterrupted One-Dimensional Silver Array," *Nature Chemistry* 9, no. 10 (2017): 956–960.

190. S. Vecchioni, B. Lu, W. Livernois, et al., "Metal-Mediated DNA Nanotechnology in 3D: Structural Library by Templated Diffraction," *Advanced Materials* 35, no. 29 (2023): 2210938.

191. R. Lohikoski, J. Timonen, and A. Laaksonen, "Molecular Dynamics Simulation of Single DNA Stretching Reveals a Novel Structure," *Chemical Physics Letters* 407, no. 1-3 (2005): 23.

192. A. Balaeff, S. L. Craig, and D. N. Beratan, "B-DNA to Zip-DNA: Simulating a DNA Transition to a Novel Structure with Enhanced Charge-Transport Characteristics," *Journal of Physical Chemistry A* 115, no. 34 (2011): 9377.

193. C. Sathe, A. Girdhar, J.-P. Leburton, and K. Schulten, "Electronic Detection of dsDNA Transition From Helical to Zipper Conformation Using Graphene Nanopores," *Nanotechnology* 25 (2014): 445105.

194. C. Bruot, J. L. Palma, L. Xiang, V. Mujica, M. A. Ratner, and N. Tao, "Piezoresistivity in Single DNA Molecules," *Nature Communications* 6, no. 1 (2015): 8032.

195. D. D. Eley and R. B. Leslie, "Conduction in Nucleic Acid Components," *Nature* 197, no. 4870 (1963): 898.

196. H. W. Fink and C. Schönenberger, "Electrical Conduction through DNA Molecules," *Nature* 398, no. 6726 (1999): 407.

197. O. Legrand, D. Côte, and U. Bockelmann, "Single Molecule Study of DNA Conductivity in Aqueous Environment, Physical Review E - Statistical," *Nonlinear, and Soft Matter Physics* 73, no. 3 (2006): 1.

198. R. Zhuravel, H. Huang, G. Polycarpou, et al., "Backbone Charge Transport in Double-Stranded DNA," *Nature Nanotechnology* 15, no. 10 (2020): 836.

199. M. Wiesner, J. Barciszewski, A. Belter, A. Sierakowski, A. Drzazga, and M. K. Chmielewski, "Low Bias Charge Transport in DNA," *Scientific Reports* 14, no. 1 (2024): 22405.

200. H. Zhou, H. Lin, Q. Wang, et al., "Tunneling or Hopping? A Direct Electrochemical Observation of Electron Transfer in DNA," *Analytical Chemistry* 94, no. 44 (2022): 15324–15331.

201. M. Wolter, M. Elstner, U. Kleinekathöfer, and T. Kubař, "Microsecond Simulation of Electron Transfer in DNA: Bottom-Up Parametrization of an Efficient Electron Transfer Model Based on Atomistic Details," *Journal of Physical Chemistry B* 121, no. 3 (2017): 529.

202. M. Mantela, A. Morphis, K. Lambropoulos, C. Simserides, and R. Di Felice, "Effects of Structural Dynamics on Charge Carrier Transfer in B-DNA: A Combined MD and RT-TDDFT Study," *Journal of Physical Chemistry B* 125, no. 16 (2021): 3986.

203. S. Bag, A. Aggarwal, and P. K. Maiti, "Machine Learning Prediction of Electronic Coupling between the Guanine Bases of DNA," *Journal of Physical Chemistry A* 124, no. 38 (2020): 7658.

204. J. Hur, K. Im, S. Hwang, et al., "DNA Hydrogel-Based Supercapacitors Operating in Physiological Fluids," *Scientific Reports* 3, no. 1 (2013): 1282.

205. J. Kumar, F. Ouchen, D. A. Smarra, G. Subramanyam, and J. G. Grote, *DNA Based Electrolyte/Separator for Lithium Battery Application, In Nanobiosystems: Processing, Characterization, and Applications VIII* (SPIE, 2015).

206. S. C. Sutradhar, N. Banik, M. S. Ahmed, H. Jang, K.-W. Nam, and M. Islam, "Applications of Hydrogels for Next-Generation Batteries," *Gels* 11, no. 9 (2025): 757.

207. V. Vandeginste and J. Wang, "A Review of the Synthesis of Biopolymer Hydrogel Electrolytes for Improved Electrode "Electrolyte Interfaces in Zinc-Ion Batteries," *Energies* 17, no. 2 (2024): 310.

208. S. Dalwadi, A. Goel, C. Kapetanakis, D. Salas-de la Cruz, and X. Hu, "The Integration of Biopolymer-Based Materials for Energy Storage Applications: A Review," *International Journal of Molecular Sciences* 24, no. 4 (2023): 3975.

209. E. Lizundia and D. Kundu, "Advances in Natural Biopolymer-Based Electrolytes and Separators for Battery Applications," *Advanced Functional Materials* 31, no. 3 (2021): 2005646.

210. G. Landi, L. La Notte, A. L. Palma, and G. Puglisi, "Electrochemical Performance of Biopolymer-Based Hydrogel Electrolyte for Supercapacitors with Eco-Friendly Binders," *Polymers* 14, no. 20 (2022): 4445.

211. K. Xu, "Electrolytes and Interphases in Li-Ion Batteries and Beyond," *Chemical Reviews* 114, no. 23 (2014): 11503.

212. M. Armand and J.-M. Tarascon, "Building Better Batteries," *Nature* 451, no. 7179 (2008): 652.

213. X. Chen and R. Holze, "Polymer Electrolytes for Supercapacitors," *Polymers* 16, no. 22 (2024): 3164.

214. J. Ding, Y. Yang, J. Poisson, et al., "Recent Advances in Biopolymer-Based Hydrogel Electrolytes for Flexible Supercapacitors," *ACS Energy Letters* 9, no. 4 (2024): 1803.

215. A. T. Guy, T. J. Piggot, and S. Khalid, "Single-Stranded DNA Within Nanopores: Conformational Dynamics and Implications for Sequencing; a Molecular Dynamics Simulation Study," *Biophysical Journal* 103, no. 5 (2012): 1028.

216. M. Mihovilovic, N. Hagerty, and D. Stein, "Statistics of DNA Capture by a Solid-State Nanopore," *Physical Review Letters* 110, no. 2 (2013): 28102.

217. M. Belkin and A. Aksimentiev, "Molecular Dynamics Simulation of DNA Capture and Transport in Heated Nanopores," *ACS Applied Materials & Interfaces* 8 (20 (2016): 12599.

218. N. A. W. Bell, K. Chen, S. Ghosal, M. Ricci, and U. F. Keyser, "Asymmetric Dynamics of DNA Entering and Exiting a Strongly Confining Nanopore," *Nature Communications* 8, no. 1 (2017): 380.

219. N. A. W. Bell and U. F. Keyser, "Nanopores Formed by DNA Origami: A Review," *FEBS Letters* 588, no. 19 (2014): 3564.

220. B. Shen, P. Piskunen, S. Nummelin, Q. Liu, M. A. Kostiainen, and V. Linko, "Advanced DNA Nanopore Technologies," *ACS Applied Bio Materials* 3 (2020): 5606.

221. X. Shi, A.-K. Pumm, C. Maffeo, et al., "A DNA Turbine Powered by a Transmembrane Potential across a Nanopore," *Nature Nanotechnology* 19 (2024): 338.

222. F. Liu, T. Arai, D. Guo, Z. Jiang, L. Zhao, and X. Liu, "Engineering DNA Nanopores: From Structural Evolution to Sensing and Transport," *Materials Today Bio* 34 (2025): 102137.

223. Y. Xing, A. Dorey, L. Jayasinghe, and S. Howorka, "Highly Shape- and Size-Tunable Membrane Nanopores Made with DNA," *Nature Nanotechnology* 17, no. 7 (2022): 708.

224. Z. Peng, S. Kanno, K. Shimba, Y. Miyamoto, and T. Yagi, "Synthetic DNA Nanopores for Direct Molecular Transmission between Lipid Vesicles," *Nanoscale* 16, no. 25 (2024): 12174.

225. Y. He, M. Tsutsui, Y. Zhou, and X.-S. Miao, "Solid-State Nanopore Systems: From Materials to Applications," *NPG Asia Materials* 13, no. 1 (2021): 48.

226. S. Zeng, M. Chinappi, F. Cecconi, T. Odijk, and Z. Zhang, "DNA Compaction and Dynamic Observation in a Nanopore Gated Sub-Attoliter Silicon Nanocavity," *Nanoscale* 14, no. 33 (2022): 12038.

227. J. Feng, K. Liu, R. D. Bulushev, et al., "Identification of Single Nucleotides in MoS2 Nanopores," *Nature Nanotechnology* 10, no. 12 (2015): 1070.

228. B. Yurke, A. J. Turberfield, A. P. Mills, F. C. Simmel, and J. L. Neumann, "A DNA-Fuelled Molecular Machine Made of DNA," *Nature* 406 (2000): 605.

229. B. Yurke and A. P. Mills, Using DNA to Power Nanostructures, *Genetic Programming and Evolvable Machines* 4 (2003): 111.

230. R. Zhang, R. Chen, Y. Ma, J. Liang, S. Ren, and Z. Gao, "Application of DNA Nanotweezers in Biosensing: Nanoarchitectonics and Advanced Challenges," *Biosensors and Bioelectronics* 237 (2023): 115445.

231. C. Ma, S. Li, Y. Zeng, and Y. Lyu, "DNA-Based Molecular Machines: Controlling Mechanisms and Biosensing Applications," *Biosensors* 14, no. 5 (2024): 236.

232. U. Singh, V. Morya, B. Datta, C. Ghoroi, and D. Bhatia, Stimuli Responsive, Programmable DNA Nanodevices for Biomedical Applications, *Frontiers in Chemistry* 9 (2021): 704234.

233. T. E. Ouldridge, A. A. Louis, and J. P. K. Doye, "DNA Nanotweezers Studied with a Coarse-Grained Model of DNA," *Physical Review Letters* 104 (2010): 178101.

234. T. E. Ouldridge, A. A. Louis, and J. P. K. Doye, "Structural, Mechanical, and Thermodynamic Properties of a Coarse-Grained DNA Model," *Journal of Chemical Physics* 134, no. 8 (2011): 085101.

235. S. Dhakal, M. R. Adendorff, M. Liu, H. Yan, M. Bathe, and N. G. Walter, "Rational Design of DNA-Actuated Enzyme Nanoreactors Guided by Single Molecule Analysis," *Nanoscale* 8 (2016): 3125.

236. N. Nguyen, J. J. Birktoft, R. Sha, et al., "The Absence of Tertiary Interactions in a Self-Assembled DNA Crystal Structure," *Journal of Molecular Recognition* 25 (2012): 234.

237. R. S. Sedeh, K. Pan, M. R. Adendorff, O. Hallatschek, K.-J. Bathe, and M. Bathe, "Computing Nonequilibrium Conformational Dynamics of Structured Nucleic Acid Assemblies," *Journal of Chemical Theory and Computation* 12, no. 1 (2016): 261.

238. C. Maffeo, L. Quednau, J. Wilson, and A. Aksimentiev, "DNA Double Helix, a Tiny Electromotor," *Nature Nanotechnology* 18, no. 3 (2023): 238.

239. B. Zhou, Y. Dong, and D. Liu, "Recent Progress in DNA Motor-Based Functional Systems," *ACS Applied Bio Materials* 4, no. 3 (2021): 2251.

240. M. Vogt, J. List, M. Langecker, I. Santiago, F. C. Simmel, and E. Kopperger, "Electrokinetic Torque Generation by DNA Nanorobotic Arms Studied via Single-Molecule Fluctuation Analysis," *Journal of Physical Chemistry B* 127 (2023): 10710.

241. Z. Zhang, L. Wang, and W. Si, "Electroosmotic Flow-Driven DNA-CNT Nanomotor via Tunable Surface-Charged Nanopore Array," *Journal of Physical Chemistry Letters* 15 (2024): 10950.

242. A.-K. Pumm, W. Engelen, E. Kopperger, et al., "A DNA Origami Rotary Ratchet Motor," *Nature* 607 (2022): 492.

243. Y. Zhou, J. Dong, and Q. Wang, "Fabricating Higher-Order Functional DNA Origami Structures to Reveal Biological Processes at Multiple Scales," *NPG Asia Materials* 15 (2023): 25.

244. J. Yoo and A. Aksimentiev, "In Situ Structure and Dynamics of DNA Origami Determined through Molecular Dynamics Simulations," *Proceedings of the National Academy of Sciences* 110 (2013): 20099.

245. J. A. L. Roodhuizen, P. J. T. M. Hendrikx, P. A. J. Hilbers, T. F. A. de Greef, and A. J. Markvoort, "Counterion-Dependent Mechanisms of DNA Origami Nanostructure Stabilization Revealed by Atomistic Molecular Simulation," *ACS Nano* 13, no. 9 (2019): 10798.

246. B. E. K. Snodin, J. S. Schreck, F. Romano, A. A. Louis, and J. P. K. Doye, "Coarse-Grained Modelling of the Structural Properties of DNA Origami," *Nucleic Acids Research* 47 (2019): 1585.

247. P. Šulc, F. Romano, T. E. Ouldridge, L. Rovigatti, J. P. K. Doye, and A. A. Louis, "Sequence-Dependent Thermodynamics of a Coarse-Grained DNA Model," *Journal of Chemical Physics* 137, no. 13 (2012): 135101.

248. B. E. K. Snodin, F. Randisi, M. Mosayebi, et al., "Introducing Improved Structural Properties and Salt Dependence into a Coarse-Grained Model of DNA," *Journal of Chemical Physics* 142, no. 23 (2015): 234901.

249. S. Yang, W. Liu, R. Nixon, and R. Wang, "Metal-Ion Responsive Reversible Assembly of DNA Origami Dimers: G-Quadruplex Induced Intermolecular Interaction," *Nanoscale* 10, no. 8 (2018): 3626.

250. M. Rebič, A. Laaksonen, J. Šponer, J. Uličný, and F. Mocci, "Molecular Dynamics Simulation Study of Parallel Telomeric DNA Quadruplexes at Different Ionic Strengths: Evaluation of Water and Ion Models," *Journal of Physical Chemistry B* 120, no. 30 (2016): 7380.

251. M. Havrila, P. Stadlbauer, B. Islam, M. Otyepka, and J. Šponer, "Effect of Monovalent Ion Parameters on Molecular Dynamics Simulations of G-Quadruplexes," *Journal of Chemical Theory and Computation* 13, no. 8 (2017): 3911.

252. M. Rebič, F. Mocci, A. Laaksonen, and J. Uličný, "Multiscale Simulations of Human Telomeric G-Quadruplex DNA," *Journal of Physical Chemistry B* 119, no. 1 (2015): 105.

253. M. Rebič, F. Mocci, J. Uličný, A. P. Lyubartsev, and A. Laaksonen, "Coarse-Grained Simulation of Rodlike Higher-Order Quadruplex Structures at Different Salt Concentrations," *ACS Omega* 2, no. 2 (2017): 386.

254. A. Naômé, A. Laaksonen, and D. P. Vercauteren, "A Solvent-Mediated Coarse-Grained Model of DNA Derived with the Systematic Newton Inversion Method," *Journal of Chemical Theory and Computation* 10, no. 8 (2014): 3541.

255. N. Li, Y. Gao, F. Qiu, and T. Zhu, "Benchmark Force Fields for the Molecular Dynamic Simulation of G-Quadruplexes," *Molecules* 26 (2021): 17.

256. K. W. Wang, T. Betancourt, and C. K. Hall, "Computational Study of DNA-Cross-Linked Hydrogel Formation for Drug Delivery Applications," *Macromolecules* 51 (2018): 9758.

257. Z. Xing, C. Ness, D. Frenkel, and E. Eiser, "Structural and Linear Elastic Properties of DNA Hydrogels by Coarse-Grained Simulation," *Macromolecules* 52 (2019): 504.

258. K. Jeon, C. Lee, J. Y. Lee, and D.-N. Kim, DNA Hydrogels with Programmable Condensation, Expansion, and Degradation for Molecular Carriers, *ACS Applied Materials & Interfaces*, 16, no. 19 (2024). 24162.

259. J. Bush, C.-H. Hu, and R. Veneziano, "Mechanical Properties of DNA Hydrogels: Towards Highly Programmable Biomaterials," *Applied Sciences* 11, no. 4 (2021): 1885.

260. R. Acharya, S. D. Dutta, H. Mallik, et al., "Physical Stimuli-Responsive DNA Hydrogels: Design, Fabrication Strategies, and Biomedical Applications," *Journal of Nanobiotechnology* 23, no. 1 (2025): 233.

261. R. Wu, W. Li, P. Yang, et al., "DNA Hydrogels and Their Derivatives in Biomedical Engineering Applications," *Journal of Nanobiotechnology* 22 (2024): 518.

262. Y. Li, R. Chen, B. Zhou, Y. Dong, and D. Liu, "Rational Design of DNA Hydrogels Based on Molecular Dynamics of Polymers," *Advanced Materials* 36, no. 7 (2024): 2307129.

263. D. Wang, J. Cui, M. Gan, et al., "Transformation of Biomass DNA into Biodegradable Materials From Gels to Plastics for Reducing Petrochemical Consumption," *Journal of the American Chemical Society* 142 (2020): 10114.

264. L. Song, Y. Zhuge, X. Zuo, M. Li, and F. Wang, "DNA Walkers for Biosensing Development," *Advanced Science* 9, no. 18 (2022): e2200327.

265. B. Shen, L. Li, M. Guo, et al., "Advances in DNA Walking Nanomachine-Based Biosensors," *Interdisciplinary Medicine* 2, no. 1 (2024): e20230046.

266. J. Valero and M. Škugor, "Mechanisms, Methods of Tracking and Applications of DNA Walkers: A Review," *Chemphyschem : A European Journal of Chemical Physics and Physical Chemistry* 21 (2020): 1971.

267. Y. Wang, Y. Wang, S. Liu, et al., "Toehold-Mediated DNA Strand Displacement-Driven Super-Fast Tripedal DNA Walker for Ultrasensitive and Label-Free Electrochemical Detection of Ochratoxin A," *Analytica Chimica Acta* 1143 (2021): 21.

268. Y. Wu, M. Jin, C. Peng, G. A. Wang, and F. Li, "Kinetics and Activation Strategies in Toehold-Mediated and Toehold-Free DNA Strand Displacement," *Biosensors* 15 (2025): 683.

269. T. E. Ouldridge, R. L. Hoare, A. A. Louis, J. P. K. Doye, J. Bath, and A. J. Turberfield, "Optimizing DNA Nanotechnology through Coarse-Grained Modeling: A Two-Footed DNA Walker," *ACS Nano* 7 (2013): 2479.

270. P. Šulc, T. E. Ouldridge, F. Romano, J. P. K. Doye, and A. A. Louis, "Simulating a Burnt-Bridges DNA Motor with a Coarse-Grained DNA Model," *Natural Computing* 13, no. 4 (2014): 535.

271. D. C. Khara, J. S. Schreck, T. E. Tomov, et al., "DNA Bipedal Motor Walking Dynamics: An Experimental and Theoretical Study of the Dependency on Step Size," *Nucleic Acids Research* 46, no. 3 (2018): 1553.

272. S. R. Tee, X. Hu, I. Y. Loh, and Z. Wang, "Mechanosensing Potentials Gate Fuel Consumption in a Bipedal DNA Nanowalker," *Physical Review Applied* 9 (2018): 034025.

273. W. Siti, H. L. Too, T. Anderson, X. R. Liu, I. Y. Loh, and Z. Wang, "Autonomous DNA Molecular Motor Tailor-Designed to Navigate DNA Origami Surface for Fast Complex Motion and Advanced Nanorobotics," *Science Advances* 9 (2023): eadi8444.

274. D. Wang, C. Vietz, T. Schröder, G. Acuna, B. Lalkens, and P. Tinnefeld, "A DNA Walker as a Fluorescence Signal Amplifier," *Nano Letters* 17 (2017): 5368.

275. J. Li, A. Johnson-Buck, Y. R. Yang, W. M. Shih, H. Yan, and N. G. Walter, "Exploring the Speed Limit of Toehold Exchange with a Cartwheeling DNA Acrobat," *Nature Nanotechnology* 13 (2018): 723.

276. J. Mou, H. Zhang, L. Zhang, et al., "Simulation-Guided Rational Design of DNA Walker-Based Theranostic Platform," *Small* 20, no. 33 (2024): e2400963.

277. H. Xu, R. Hou, H. Li, and Z. Wang, "A Unified Model for DNA Bipedal Nanomotors," *Journal of Applied Physics* 128 (2020): 164701.

278. M. O. Ogieva, W. G. Pfeifer, and S. Sensale, "Enhancing the Speed of DNA Walkers through Soft Confinement," *Scientific Reports* 15 (2025): 9450.

279. R. R. Breaker and G. F. Joyce, "A DNA Enzyme that Cleaves RNA," *Chemistry & Biology* 1, no. 4 (1994): 223.

280. S. W. Santoro and G. F. Joyce, "A General Purpose RNA-Cleaving DNAenzyme," *Proceedings of the National Academy of Sciences* 94 (1997): 4262.

281. K. Schlosser and Y. Li, "Biologically Inspired Synthetic Enzymes Made From DNA," *Chemistry & Biology* 16 (2009): 311.

282. D. A. Baum and S. K. Silverman, "Deoxyribozymes: Useful DNA Catalysts In Vitro and In Vivo," *Cellular and Molecular Life Sciences* 65, no. 14 (2008): 2156.

283. J. Li, "In Vitro Selection and Characterization of a Highly Efficient Zn(II)-Dependent RNA-Cleaving Deoxyribozyme," *Nucleic Acids Research* 28, no. 2 (2000): 481.

284. Y. Lu, "New Transition-Metal-Dependent DNAzymes as Efficient Endonucleases and as Selective Metal Biosensors," *Chemistry* 8, no. 20 (2002): 4588.

285. J. Wieruszewska, A. Pawłowicz, E. Połomska, K. Pasternak, Z. Gdaniec, and W. Andrałojć, "The 8-17 DNAzyme Can Operate in a Single Active Structure Regardless of Metal Ion Cofactor," *Nature Communications* 15 (2024): 4218.

286. M. Kenward and K. D. Dorfman, "Coarse-Grained Brownian Dynamics Simulations of the 10-23 DNAzyme," *Biophysical Journal* 97, no. 10 (2009): 2785.

287. A. Ganguly, B. P. Weissman, J. A. Piccirilli, and D. M. York, "Evidence for a Catalytic Strategy to Promote Nucleophile Activation in Metal-Dependent RNA-Cleaving Ribozymes and 8-17 DNAzyme," *ACS Catalysis* 9, no. 12 (2019): 10617.

288. L. Zhang, Z. Zhang, X. Ou, et al., "Simulation-Guided DNAzyme Based Nanomachine Design for Identifying Single Nucleotide Variants," *Sensors and Actuators B: Chemical* 324 (2020): 128719.

289. K. Nguyen, T. N. Malik, and J. C. Chaput, "Chemical Evolution of an Autonomous DNAzyme with Allele-Specific Gene Silencing Activity," *Nature Communications* 14 (2023): 2413.

290. S. K. Amini and P. Bashirbanaem, "Evidences for Reaction Mechanism of 9DB1 DNA Catalyst," *International Journal of Biological Macromolecules* 253, no. Pt 2 (2023): 126710.

291. J. F. Schmuck, J. Borggräfe, and M. Etzkorn, "The Dynamic World of the 8-17 DNAzyme," *Nature Communications* 15 (2024): 5145.